



HOKKAIDO UNIVERSITY

DOCTORAL DISSERTATION

**Study on Inference of Direct/Indirect Interactions Between
Agents from Their Time Series in Complex Biological Systems**
(複雑生物系における時系列データからエージェント間の直接/間接相互作用を推測
する研究)

by

Mohiuddin Md.

Graduate School of Chemical
Sciences and Engineering
Hokkaido University
Japan

September, 2025

Declaration

I hereby declare that the contents of this thesis entitled “*Study on Inference of Direct/Indirect Interactions Between Agents from Their Time Series in Complex Biological Systems*” are entirely my own work, which was carried out under the supervision of **Prof. Tamiki Komatsuzaki** at Molecule & Life Nonlinear Sciences Laboratory (MLNS), Hokkaido University, Japan. I also confirm that no part of this thesis has been previously submitted elsewhere to achieve any other academic qualification. I apologize for any unintentional omissions or errors in judgment that may have occurred.

Mohiuddin Md.

August 25, 2025

Abstract

Systems composed of many interacting agents—such as cells, bacteria, granular rods, active colloids, robotic swimmers, and many others—often exhibit complex collective behaviors. The mechanisms underlying such collective behaviors have been extensively studied both theoretically and experimentally. It is well known that interaction between agents—the way or process through which agents communicate or influence each other’s behaviors—is one of the fundamental drivers of the emergence of collective patterns in a system without explicit external control. Agents may interact with each other through mechanisms such as physical contact, forces (i.e., attraction and repulsion), environmental signals (e.g., light, sound, chemical stimuli), and many other factors.

However, in a system of many interconnected agents, interaction between one agent and another agent may occur directly or indirectly through one or more mediators. For example, in a system composed of only two agents, the interaction is straightforwardly direct. When a system contains more than two agents, the interaction between one agent and another agent may also occur indirectly through a third agent. The compounding of such direct and indirect interactions among agents makes it more difficult to understand the actual relationships or direct interactions between agents in a system. Therefore, to understand the mechanisms underlying collective behaviors, it is essential to understand the interactions—whether direct or indirect—between pairs of individual agents.

Since in a pair of interacting agents one regulates the behavior of another through interaction, there should be a cause-and-effect relationship—that means, one should have causal influence on another at a certain time delay/lag—where the former agent is the cause and the latter agent is the effect. Some approaches such as conditional Granger causality, partial transfer entropy, causation entropy, etc. have already been proposed to investigate whether the causal influence of one agent on another arises from direct or indirect interactions among them. These approaches aim to disentangle direct interaction

from indirect one by conditioning on additional agents of the system (or more generally on some third effect such as chemical stimuli). However, when the total number of agents (n) increases, the total number of combinations—that is, all possible pairs of agents (whose total number is nC_2) has $n - 2$ possible third agents—increases very rapidly ($\propto O(n^3)$), making it more difficult to infer direct or indirect interactions among agents in practice. Therefore, it is highly demanded to develop a simpler yet versatile scheme to uncover direct or indirect interactions between a pair of agents using only their pairwise time series, allowing other agents of the system to be hidden from the analysis.

In this study, I have addressed the question: Given observational tracking data from only a single pair of agents, can one determine whether their interaction is direct or indirect mediated by an unseen third agent? I have proposed an approach based on modified transfer entropy analysis across delay times to detect the presence of a hidden mediator. This approach reveals a distinct signature: direct interactions exhibit a consistently decreasing modified transfer entropy (MT) with increasing delay time (τ), while indirect interactions deviate from this trend.

Intuitively, the plausible reason for the distinct behaviors of MT with increasing τ for direct and indirect interactions can be explained as follows: suppose that the time series of agents X and Y are measured in the unit of their interaction timescale (τ_0), where τ_0 means the time delay or lag between an “action” of one agent and “its impact” on another. When X directly interacts with Y at a timescale τ_0 , MT from X to Y provides the higher influence of X on Y at time delay $\tau = \tau_0$, and then consistently lower influences for the larger values of $\tau (> \tau_0)$, since the larger values of τ correspond to longer time delays in the interaction between X and Y compared to the interaction timescale τ_0 . In contrast, when X indirectly interacts with Y through a mediator, X first influences the mediator at timescale τ_0 and then the mediator influences Y at an additional unit of the timescale τ_0 . Thus, X requires a longer time delay τ than τ_0 to influence Y through a mediator, and hence MT provides the higher value at a longer value of τ than at $\tau = \tau_0$. In this study, two standard mathematical vehicles, namely Vicsek model (VM) and Langevin dynamics (LD), are used to simulate time series data of agents under some schematic interaction networks involving direct and indirect influences. It has also been observed that the original transfer entropy (TE) cannot necessarily infer direct and indirect interactions between a pair of agents X and Y properly, depending

on how much the target agent Y possesses its own memory.

Furthermore, in this study, the typical interaction radius or distance among *D. discoideum* cells has also been investigated by analyzing their tracking data using another information-theoretic approach, such as transfer entropy (TE) as a function of cutoff distance (λ).

Keywords: Collective behavior, Causal influence, Direct-indirect interactions, Transfer entropy, Modified transfer entropy, Modified Vicsek model, Langevin dynamics model, Monotonicity metric map, Interaction radius.

ACKNOWLEDGEMENTS

First of all, I would like to sincerely thank my esteemed supervisor, **Prof. Tamiki Komatsuzaki**, for his unwavering encouragement and excellent guidance during my research journey. Without his insightful suggestions and inspiring ideas, this thesis would not have been possible to accomplish. Dear **Komatsuzaki** Sensei, I am deeply grateful to you for your important role in my academic development.

I am very pleased to be a proud member of this vibrant and collaborative research team. I am deeply grateful to each and every lab member for providing such a welcoming and supportive research environment.

In particular, I am deeply grateful to my mentor **Dr. Sulimon Sattari**, and our team member **Dr. Udoj Sankar Basak** for their encouragement, invaluable scientific discussions, and advice during my research journey.

I also would like to express my sincere gratitude to my examiners, **Prof. Tetsuya Taketsugu**, **Prof. Manabu Tokeshi** and **Prof. Keisuke Takahashi**, for their constructive feedback and insightful discussions. My heartfelt thanks also go to **Prof. Koji Tabata**, **Dr. Jean-Emmanuel Clement**, and **Prof. Yuta Mizuno** for their fruitful discussions, which helped me a lot during my research.

I am also grateful to our dedicated secretary **Matsue Koida** for continuously supporting me in both academic and personal endeavors. I also wish to acknowledge my respected colleague **Prof. Khalifa Mohammad Helal** for his inspiration and continuous mental support.

I also extend my gratitude to the Ministry of Education, Culture, Sports, Science and Technology, Japan (MEXT) for financially supporting me during my study at Hokkaido University in Japan.

Finally, I would like to extend my deepest gratitude to my family members for their unwavering love, patience, and belief in me. Without their support, this journey would have been more challenging.

Above all, I humbly offer my deepest gratitude to the **Almighty** for granting me the strength and perseverance to achieve this significant milestone in my life.

Mohiuddin Md.

August 25, 2025

Contents

1 General introduction	1
1.1 Background	1
1.2 Objectives	6
1.3 Thesis Layout	7
2 An overview of information-theoretic measures	9
2.1 Introduction	9
2.2 Information-theoretic measures	10
2.2.1 Shannon Entropy	10
2.2.2 Joint Entropy	10
2.2.3 Conditional Entropy	11
2.2.4 Mutual Information	12
2.2.5 Time Delayed Mutual Information	13
2.2.6 Transfer Entropy	14
2.2.7 Modified Transfer Entropy	15
2.3 Role of the 1 st term as upper bound of <i>TE</i> and <i>MT</i> measures	16
2.4 Variation in the upper bound of the Eqs. <i>TE</i> and <i>MT</i> with respect to time delay (τ): A binary model analysis	17
2.5 Concluding Remarks	19
3 Application of Modified Vicsek Model	21
3.1 Introduction	21
3.2 Direct and indirect interactions	21
3.3 Modified Vicsek Model	23
3.4 Results and discussion	25

3.4.1	Prediction of direct/indirect interactions in the unidirectional interaction network	26
3.4.2	Monotonicity metric (d_m)	28
3.4.3	Prediction of direct/indirect interactions in the bidirectional interaction network	30
3.5	Concluding Remarks	34
4	Application of Langevin dynamics model	35
4.1	Introduction	35
4.2	Langevin Dynamics (LD) Model	36
4.3	Estimation of timescale (τ_0) from decay rate of autocorrelation function (ACF) via curve fitting	39
4.4	Results and discussion	41
4.4.1	Prediction of direct/indirect interactions for bidirectional interaction networks	41
4.5	Concluding Remarks	45
5	Interactions in Dictyostelium discoideum cells	47
5.1	Introduction	47
5.2	Aggregation of D. discoideum cells via cAMP pulse	48
5.3	Inference of typical interaction distance in D. discoideum cells	49
5.3.1	Transfer entropy (TE) vs cutoff distance (λ) approach	49
5.3.2	Application of TE vs cutoff distance (λ) approach in D. discoideum cells	51
5.3.3	Results and discussion	53
5.4	Concluding Remarks	55
6	General conclusions	57
Appendix A	Appendix	73
A.1	Hypothetical statistical test	73
A.2	Estimation of the degree of monotonicity	75

A.3 Monotonicity metric d_m of $TE(\tau)$ and $MT(\tau)$ values estimated from the trajectories of agents simulated using modified VM under the unidirectional interaction illustrated in Fig. 3.1(Ba)	77
A.4 Monotonicity metric d_m of $MT(\tau)$ values estimated from the trajectories of agents simulated using modified VM under the unidirectional interaction loop illustrated in Fig. 3.1(Bb)	78
A.5 Monotonicity metric d_m of $MT(\tau)$ values estimated from the trajectories of agents simulated using modified VM under the bidirectional interaction illustrated in Fig. 3.1(AB)	81
A.6 Monotonicity metric d_m of $MT(\tau)$ values estimated from the trajectories of agents simulated using LD model under the bidirectional interaction illustrated in Fig. 3.1(AB)	82

List of Figures

1.1	Collective behaviors in living agents	1
1.2	Collective behaviors in granular rods	2
1.3	Collective behaviors in active colloids	2
1.4	A schematic 3-agents-based interaction network involving direct/indirect influences	3
2.1	Behaviors of TE and MT from X to Y in the binary model for $q, p = 0.15, 0.25$ and 0.35	18
3.1	Schematic demonstration of some uni/bidirectional interaction patterns between agents involving direct and indirect influences.	22
3.2	A schematic demonstration of modified VM composed of three agents . .	23
3.3	TE and MT over τ for individual pair of agents shown in Fig. 3.1(Ba) estimated from the modified VM-simulated trajectories at noises $\eta = 0.5\pi, 0.7\pi$ and 0.9π , and coupling strength $w = 0.8$	26
3.4	Variations in the upper bounds of TE and MT as a function of time delay τ	27
3.5	Monotonicity metric d_m of the values of TE and MT over time delays $\tau = 1, 2, 3, 4$ for each individual pair of agents shown in Fig. 3.1(Ba) under the different conditions of modified VM varying noise (η) and coupling strength (w)	29
3.6	Monotonicity metric (d_m) of the values of TE and MT with increasing τ for each individual pair of agents shown in Fig. 3.1(Aa) under different conditions of modified VM varying noise (η) and coupling strength (w) .	31
3.7	Variations in the upper bounds of TE and MT as a function of time delay τ , in case of interactions in Fig. 3.1(Aa), in modified VM at $\eta = 0.5\pi, 0.7\pi$ and 0.9π with different coupling constant w , (a) $w = 0.3$ and (b) $w = 0.8$. .	32

4.1	An illustration of Morse potential function as a function of inter-agent distance r_{ij} , where r_e and ε , respectively, denote the equilibrium distance and potential well depth.	37
4.2	Damped oscillatory and exponential decay patterns of velocity trajectories of agents at the lower and higher thermal energies	40
4.3	TE and MT over time delay τ for LD-simulated velocity trajectories with $k_B T = 1.0, 1.4$, and 1.8 , and friction coefficient $\gamma = 0.4$	42
4.4	Variations in the upper bounds of TE and MT as a function of time delay τ obtained from the LD-simulated trajectories of interactions in Fig. 3.1(Aa) for $k_B T = 1.0, 1.4$, and 1.8 , and $\gamma = 0.4$, respectively.	43
4.5	Monotonicity metric map of the TE and MT values for pairs of agents of interactions shown in Fig. 3.1(Aa) in LD simulations as a function of $k_B T$ and γ	44
5.1	Life cycle of <i>D. discoideum</i> cells	48
5.2	Aggregation of <i>D. discoideum</i> cells	49
5.3	cAMP secretion of <i>D. discoideum</i> cells	49
5.4	Diagram of cutoff distance scheme	50
5.5	Graphical representation of the application of TE vs cutoff distance (λ) approach	52
5.6	Demonstration of cAMP waves of <i>D. discoideum</i> cells at three distinct time points during the observation period	53
5.7	TE and gradient of TE vs cutoff distance λ between the consecutive images at three different time stages of wave development	54
S1	The hypothetical tests of statistical significance between $MT(3)$ and $MT(4)$ of the MT (with time delay $3\tau_0$ and $4\tau_0$) from X to Z in interactions of Fig. 3.1(Ba) in the modified VM	74
S2	Examples of the time delay (τ) sequence and the number of writes of the MT values $MT(\tau)$ in the modified VM in Figs. 3.5 and S3	76

S3	Monotonicity metric map (d_m) of TE and MT values estimated from the trajectories of agents using modified VM varying noise level η and coupling strength w (discussed in the main text Fig. 3.5) without applying hypothetical test	77
S4	Monotonicity metric map d_m of the MT values between a pair of agents depicted in Fig. 3.1(Bb) at different conditions of the modified VM varying noise (η) and coupling strength (w)	79
S5	Monotonicity metric map of CMT values across τ for all pairs of agents shown in Fig. 3.1(Bb) obtained from modified VM simulations as a function of noise η and coupling strength w	80
S6	Demonstration of the causal relationship between agents in the unidirectional interaction loop shown in Fig. 3.1(Bb)	81
S7	Monotonicity metric map of MT values for direct pairs 1-2, 1-4 and 5-6 and indirect pairs 1-5, 2-6 and 3-5 of interactions in Fig. 3.1(AB) in the modified VM as a function of η and w	82
S8	Monotonicity metric map of the TE and MT values for pairs of agents of interactions shown in Fig. 1(AB) in LD simulations as a function of $k_B T$ and γ	83

List of Tables

4.1 Estimation of timescale τ_0 using curve fitting approach	41
---	----

List of Symbols

Information theory

X, Y	Stochastic/random variables
t	time
X_t	Outcome of X at time t
Y_t	Outcome of Y at time t
$p(\cdot)$	Probability function
$p(\cdot, \cdot)$	Joint probability function
$p(\cdot \cdot)$	Conditional probability function
τ	Time delay/lag
$H(\cdot)$	Shannon entropy
$H(\cdot, \cdot)$	Joint entropy
$H(\cdot \cdot)$	Conditional entropy

Modified Vicsek model

N	Number of agents
i, j	Indices of agents
Δt	Observational time step
\bar{r}_i^t	Position of agent i at time t
\bar{v}_i^t	Velocity of agent i at time t
$\theta_i(t)$	Orientation of agent i at time t
τ_0	Interaction timescale
R	Interaction radius
\mathbf{w}	Interaction matrix
$\Delta\theta_i$	Thermal noise in the orientation of agent i

Langevin dynamics model

N	Number of agents
i	Index of an agent
Δt	Observational time step
L	Length of simulation box
\vec{r}_i	Position of agent i
\vec{v}_i	Velocity of agent i
$v_{x,i}, v_{y,i}$	Velocity components of agent i along x - and y -axis
x_i, y_i	Coordinates of agent i along x - and y -axes
m_i	Mass of agent i
\vec{a}_i	Acceleration of agent i
\vec{F}_i	Potential force acting on agent i
\vec{i}, \vec{j}	Unit vectors to represent the axes of the simulation box
r_{ij}	Distance between agents i and j
U	Morse potential energy function
ϵ_{ij}	Potential well depth/dissociation energy of agents i and j
α	Width of the potential
$\vec{\xi}_i$	random force i
r_e	Equilibrium distance between agents
k_B	Boltzmann constant
T	Temperature
γ	Friction/drag coefficient
$\delta_{i,j}$	Kronecker δ function
$\delta(t - t')$	Direct δ function of two distinct time instances t and t'
τ_0	Interaction timescale

List of Abbreviations

VM	Vicsek model
LD	Langevin dynamics
MI	Mutual information
TDMI	Time-delayed mutual information
TE	Transfer entropy
MT	Modified transfer entropy
ACF	Autocorrelation function
HOOMD-blue	Highly optimized object-oriented many-particle dynamics-blue
D. discoideum cells	Dictyostelium discoideum cells

Chapter 1

General introduction

1.1 Background

Systems composed of many entities or agents (i.e., molecules, cells, and organisms) often exhibit collective behavior or movement that cannot be attributed to individuals alone. This scenario is observed in natural systems of living agents, ranging from multicellular organisms at the macroscopic level to unicellular organisms at the microscopic level, such as fish schools [1,2], bird flocks[3–5], insect swarms [6], bacterial colonies [7,8], cell dynamics in cancer growth and wound healing [9,10].

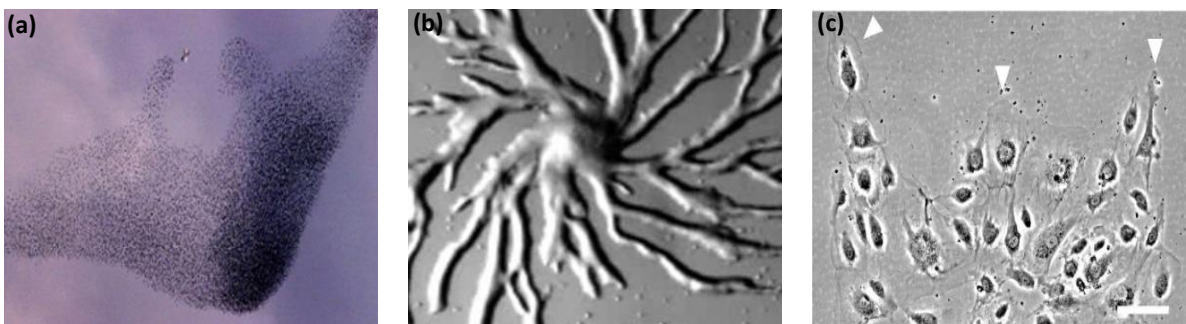


Figure 1.1: Examples of collective behavior in (a) bird flock (starling) [11], (b) *Dictyostelium discoideum* cells [12], and (c) endothelial cells during wound healing [10].

For example, in a large flock of starlings, birds move collectively when they are being hunted by aerial predators (peregrine falcon) (Fig. 1.1 (a)). During starvation, *Dictyostelium discoideum* cells emit cyclic adenosine monophosphate (cAMP) signals. In response, nearby cells detect the source of cAMP signals and collectively move toward the source, initiating the aggregation process to form a multicellular fruiting body (Fig.

1.1 (b)). In the wound repair process, it is observed that endothelial cells often proliferate and collectively migrate to the center of the wound as groups or large sheets [10] (Fig. 1.1 (c)).

However, collective behavior is observed not only in biological systems, but also in some chemical and physical systems composed of nonliving agents. Examples include granular rods placed on a vibrating surface [13], active liquid crystals [14], synthetic colloidal particles in liquid [15–17], unicellular microswimmers [18], and many more.

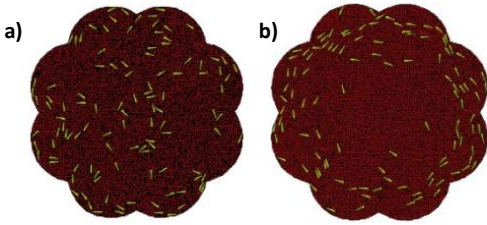


Figure 1.2: Collective behavior among granular rods on a vibrating surface. (a) Disordered phase, where rods move in all direction in a disordered way. (b) Ordered phase, where all rods align and move in the same direction in a coordinated manner [13].

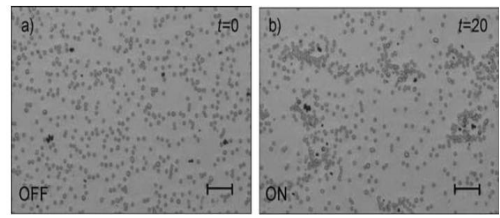


Figure 1.3: Collective behavior among AgCl (darker objects) and silica (light gray objects) colloids in deionized water[17]: (a) Before UV light is applied. (b) Upon UV illumination, after 20 seconds, silica particles migrate and surround the AgCl particles.

It is observed that the granular rods on a vibrating surface switch from a disordered phase (Fig. 1.2 (a)) to an ordered phase by aligning their orientations and velocities (Fig. 1.2 (b)) through a friction mechanism due to vibrational energy [13]. Upon UV illumination, collective behavior is also observed among AgCl and silica particles in water. The silver chloride (AgCl) particles release HCl molecules into the water under UV illumination. The silica particles respond to the HCl molecules emitted by the AgCl particles and migrate toward them collectively (Fig. 1.3 (b)) [17].

As the systems of both living and nonliving agents emerge collective behavior, researchers from different fields such as biology, physics, chemistry, and engineering think that the underlying mechanisms of collective behavior in biological systems can be understood based on the dynamics of the agents of collective behavior in non-biological systems. Understanding how individual agents lead the formation of collective behavior can provide insight into the processes of cancer growth and wound healing. Therefore, understanding the role of individual agents in the collective patterns and structures of a system is one of the intriguing topics of ongoing research. It is well known that one

of the fundamental drivers of collective patterns in both biological and non-biological systems is the interaction between agents by which the action of an agent is influenced by the action of another agent [5,11,12,19–25]. Interaction between agents may occur through some mechanisms such as physical contact, visual cues, medium-based signals (light, sound), and chemical stimuli (chemotaxis) [11,15,17,26]. However, in most cases, agents cannot interact with each other over an infinite distance. Therefore, it is naturally assumed that the interaction between agents is inherently local [27–30]. Since agents' interaction is constrained to their local vicinity, a common question naturally arises: *How does a collective pattern at the global level emerge from the interactions of individual agents at the local level?*

For a system composed of only two agents, the interaction between agents is straightforwardly direct. However, when there are many agents in a system, interaction can typically occur in the following ways: directly between a pair of agents and indirectly between a pair of agents through one or more mediators [31,32]. In this case, agents can influence each other through direct and indirect interactions, leading to collective behavior in a system of many agents [33,34]. Therefore, inferring direct and indirect interactions between a pair of agents in a system is crucial to explain the mechanisms of collective behavior. Now, consider a simple example for direct and indirect interactions in a group of three agents such as X , Y , and Z :

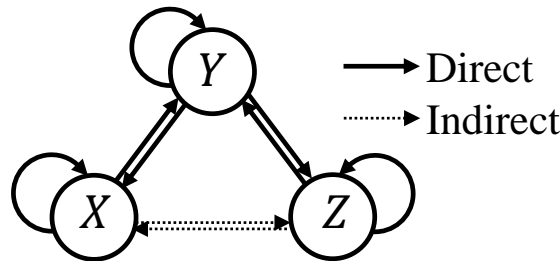


Figure 1.4: Schematic interaction network involving direct and indirect interactions among agents X , Y and Z .

Here, agent X acts based on its own and Y 's past states, agent Y acts based on the past states of all agents, and agent Z acts based on its own and Y 's past states. There is no direct relation between X and Z . Due to the intermediary role of Y , an indirect influence is expected between X and Z . The definition of direct and indirect interactions is as follows:

- **Direct interaction:** The interaction between two agents in the absence of any mediator is a direct interaction. For example, $X \leftrightarrow Y$ and $Y \leftrightarrow Z$ represent the direct interactions between agents in pairs $X-Y$ and $Y-Z$, respectively (Fig. 1.4, solid lines).
- **Indirect interaction:** The interaction between two agents through one or more mediators is an indirect interaction. For example, the dashed lines (Fig. 1.4 represent indirect interactions from X to Z , and Z to X through mediator Y .

Since an agent's behavior depends on the behavior of another in a pair of interacting agents such as $X-Y$, there should exist "cause" (X) and "effect" (Y) relationship (that is, causation or causal influence) between a physical quantity of an agent and that of another. One might mistakenly analogue the terms "correlation" and "causation". However, in fact, these are not the same. Now, let us discuss these two quantities more straightforwardly. Correlation simply means the association or statistical relationship among two variables, which can even be observed between irrelevant variables. As an example, correlation is observed between variables "robberies" and "ice cream sales". Now, the question is: *Does this correlation imply that eating ice cream encourages people to commit robberies?* The answer may be "not", because the actual cause is something else, such as the weather. In summer, both ice cream sales and robberies increase due to weather, leading to this correlation between them. Therefore, this correlation—which is observed just because both selling ice cream and committing robberies increase together—does not imply that the changes in one variable cause the changes in another variable. In contrast, causation means the relationship between two variables, where changes in one variable cause changes in another. For example, there is a correlation between smokers and lung cancer patients. It has been found that tobacco smoking is responsible for developing lung cancer, and smokers are more likely to be infected by lung cancer compared to non-smokers [35,36]. In this case, the correlation between smokers and lung cancer patients, which arises because smoking causes lung cancer, indicates the causation or causal influence of one variable on another.

One may seek the answer to the question of how to evaluate the causal influence between two variables. Typically, a variable behaves in response to the actions of another variable when there is an interaction between them; otherwise, both behave independently. If the behaviors of the variables are represented as time series, then it can be

possible to evaluate whether one has causal influence on another or not. Norbert Wiener (in 1956) first introduced the idea of quantifying causal influence between variables from their time series. It was hypothesized that if information about the past states of one variable is useful to predict the other variable, then the first variable (cause) has a causal effect on the second variable (effect) [27,37,38]. This statement is known as Wiener's principle of causality. This principle was later formalized by Granger [27,37] as follows: Assume there are two variables $X = \{\dots, X_{t-1}, X_t, X_{t+1}, \dots\}$ and $Y = \{\dots, Y_{t-1}, Y_t, Y_{t+1}, \dots\}$, and one aims to infer the future state Y_{t+1} of Y . Inference can be done using the following two ways: Using only Y 's past information, or using both X 's and Y 's past information. If the second approach can predict Y_{t+1} more accurately compared to the first one, then one can say that the past state of X conveys the information about Y_{t+1} that is not conveyed by the past state of Y alone. Therefore, X is said to be a Granger cause (G-cause) of Y . This approach was widely used to estimate the causal influence between variables of dynamical systems in different fields, such as economics and finance [39,40], social science [41], physics [42], bio-informatics [43], and many more. The drawback of this approach is that it assumes that the dependencies between agents in a system are linear. However, in natural systems, agents can also have non-linear dependencies. Granger's approach fails to capture the effects of non-linear dependencies between agents in a system [44]. To overcome the challenge in Granger causality (GC) approach regarding the non-linear dependencies of agents, T. Schreiber [45] later formalized Wiener's principle in terms of an information-theoretic metric known as transfer entropy (TE), a probability distribution-based approach that can capture both linear and non-linear relationships between agents in a system. The basic idea of TE is that if a variable Y is changed in response to the action of the past state of another variable X at a time delay τ , then TE from X to Y at delay τ measures how much the current state of X (X_t) can predict the future state of Y ($Y_{t+\tau}$), beyond what Y 's own current state Y_t can predict. It has been widely applied to estimate the causal influence between agents in complex systems of many scientific fields, such as biology [46,47], neuroscience [48], chemical analysis [49], economics [50,51], music [52], epidemiology [53,54], and many more.

Based on the seminal studies of GC and TE methods, various approaches have been developed to measure whether the causal influence between two agents in a complex system originates from either direct interaction or indirect interaction. Examples in-

clude conditional Granger causality [42,55,56], global Granger causality [57], partial cross-mapping [32], partial transfer entropy [58,59], direct transfer entropy [60], and causation entropy [61–63]. These methods aim to distinguish direct and indirect causal influences between a pair of agents by conditioning on the information of the remaining agents in a system. However, with increasing the number of agents (n) in a system, the number of possible combinations—that is, the number of all possible pairs of agents (which is nC_2) each with $n - 2$ possible additional agents—also increases very rapidly ($\propto O(n^3)$), making it more challenging to predict direct and indirect interactions between a pair of agents in practice. Recently, Sipahi et al.[64] proposed a method based on time-delayed transfer entropy to infer direct and indirect influences among agents in a system. Instead of tackling the combinatorial issue, they constructed network’s adjacency matrix \mathbf{A}_τ for each time delay τ based on the causal influences estimated for all pairs of agents. Subsequently, they conducted a systematic comparison between the adjacency matrix \mathbf{A}_τ for each value of $\tau > 0$ and the corresponding $(\tau + 1)$ times of the adjacency matrix \mathbf{A}_0 obtained at delay time $\tau = 0$ (that is, $(\mathbf{A}_0)^{\tau+1}$) for a predefined mismatch threshold between these matrices. This framework requires the trajectories of all agents in a system to determine whether the link is direct or indirect between a pair of agents. Therefore, it is highly desirable to establish a simpler, yet versatile framework to infer direct and indirect interactions between a pair of agents using solely their own pairwise time series data, while keeping the information of remaining agents in the system hidden from the analysis.

1.2 Objectives

As the influence between agents cannot occur instantaneously, some time delay is typically considered when characterizing the influence among agents [45,65]. Intuitively, the influence between a pair of agents is expected to decrease with respect to a time delay in the unit of timescale of interaction of the agents when the interaction is direct. In this study, considering this statement as a working hypothesis, the answer to the question of “*Can one identify direct or indirect interactions between a pair of agents only from their pairwise time series data?*” has been investigated. Here, a modified transfer entropy (MT) [66] based framework is proposed to estimate causal influence as a function of time

delay (τ) between a pair of agents solely from their own pairwise time series data simulated using two distinct mathematical models, such as the modified Vicsek model (VM) [67], and the Langevin dynamics model (LD) [68]. Both models are widely used in the studies of collective patterns observed in many physical and stochastic systems [69–75]. The basic concept of modified transfer entropy (MT) is that when an agent X influences another agent Y at a delay time τ , MT from X to Y with respect to τ measures how much the current state X_t (of X) can infer the future state $Y_{t+\tau}$ (of Y), beyond what can be inferred by the immediate past state $Y_{t+\tau-1}$ of $Y_{t+\tau}$. The intuitive explanation of the working hypothesis is as follows: Suppose that the time series of agents X and Y are recorded in units of the timescale of interaction of them. If there is a direct interaction of X with Y at delay time $\tau = 1$, then the MT from X to Y measures the maximum influence of X on Y at delay time $\tau = 1$, and then the estimated influence consistently decreases as $\tau (> 1)$ increases. This is because the larger values of τ correspond to longer delays in the interaction between X and Y rather than the interaction time delay (i.e., $\tau = 1$). In contrast, if there is an indirect interaction of X with Y through a mediator, X first influences the mediator at some delay time and then the mediator influences Y at an additional delay time. Therefore, X needs a longer value of τ than the interaction time delay $\tau = 1$ to influence Y through a mediator. In this case, the MT measures a greater influence at the longer value of τ than at the time delay $\tau = 1$. Furthermore, in this study, it is also investigated that the original transfer entropy (TE) cannot always reliably disentangle direct and indirect interactions between a pair of agents X_t and $Y_{t+\tau}$, depending on the amount of memory retained by the target agent Y in its own process Y_t .

1.3 Thesis Layout

This thesis is organized into the following chapters:

- Chapter 2 describes some information-theoretic quantities that are used to determine the causal influence between agents in this study. Section 2.2 focuses on the mathematical formulations and explanations of these quantities, ranging from Shannon entropy to transfer entropy (TE) including a modified version of TE known as modified transfer entropy (MT). Section 2.3 provides a plausible rationale

for the first terms of TE and MT as the upper bound of causal influence. Section 2.4 presents the variations in the upper bounds of TE and MT over time delay based on a simple binary model.

- Chapter 3 discusses a modified Vicsek model (VM) and the application of the proposed approach to predict direct/indirect interactions between agents using only their time series data without knowing the interaction ground truth of agents.
- Chapter 4 presents the Langevin dynamics model (LD) and the application of the proposed approach to predict direct/indirect interactions between agents using only their time series data without knowing the ground truth of interactions of agents. Section 4.3 describes the estimation of the interaction timescale (τ_0) of agents by fitting a curve to the autocorrelation data of their trajectories.
- Chapter 5 describes the inference of the interaction distance (R) between *D. discoideum* cells by analyzing their experimental data using an information-theoretic approach such as transfer entropy (TE) with respect to a cutoff distance variable (λ).
- Chapter 6 presents a summary of the findings of this study along with a brief discussion of some possible directions for future research.

Chapter 2

An overview of information-theoretic measures

2.1 Introduction

The dynamics of agents in a complex system are usually shaped based on both linear and non-linear relationships of agents. Traditional approaches, such as Cross-correlation [76,77] and Granger causality [78,79] mainly work based on the assumption that the relationships between agents are linear. Therefore, these approaches fail to capture the causal effects appeared due to non-linear relationships. In contrast, the information-theoretic approaches perform based on the probability distributions that are capable to capture causal effects of both linear and non-linear relationships among agents. This chapter presents some key information-theoretic measures necessary to quantify causal influence by analyzing the time series data of agents in a system.

Suppose $X = \{..., X_{t-1}, X_t, X_{t+1}, ...\}$ and $Y = \{..., Y_{t-1}, Y_t, Y_{t+1}, ...\}$ are two random variables (or time series observations of two agents) with probability mass functions $p(X_t) = \text{Prob}(X = X_t)$ and $p(Y_t) = \text{Prob}(Y = Y_t)$, respectively. Now, let us discuss the information-theoretic measures based on the contexts of these variables:

2.2 Information-theoretic measures

2.2.1 Shannon Entropy

The *Shannon entropy* (or, entropy) is the most basic information-theoretic measure. It represents the average uncertainty of the possible outcomes of a random variable. If X is a random variable, then the *Shannon entropy* (denoted by $H(X)$) has the following form [80,81]:

$$H(X) = - \sum_{X_t \in X} p(X_t) \log_2 p(X_t) \quad (2.1)$$

where $p(X_t)$ represents the probability of the outcome of X at time t . Since $p(X_t)$ varies within the range $[0, 1]$, $H(X)$ always provides a non-negative value (i.e., $H(X) \geq 0$) and varies from 0 to $\log_2(M)$, where M denotes the number of types of outcomes in X . When the possible outcomes of X are equally likely, $H(X)$ provides the highest value, that is, $H(X) = \log_2(M)$. For the situation in which a single outcome is highly probable compared to the others, $H(X) = 0$. Furthermore, since the term $\log_2 p(X_t)$ is undefined when $p(X_t) = 0$, the convention $0\log_2 0 = 0$ is typically considered in Eq.2.1, which can also be justified by continuity as $x\log x=0$ as $x \rightarrow \infty$.

2.2.2 Joint Entropy

It has already been discussed that the entropy can provide the average uncertainty of the outcomes of a single random variable. In general, there is no major difference between the concepts of entropy and joint entropy. Joint entropy is just an extension of the entropy that deals with multiple random variables and provides the average uncertainty of the outcomes of variables based on their joint probability distribution. More precisely, suppose that X and Y are two random variables, $p(X_t)$ and $p(Y_t)$ are their marginal probabilities, and $p(X_t, Y_t)$ is their joint probability. Then, the joint entropy (denoted by $H(X, Y)$) has the following form [80,81]:

$$H(X, Y) = - \sum_{X_t \in X, Y_t \in Y} p(X_t, Y_t) \log_2 p(X_t, Y_t). \quad (2.2)$$

The joint entropy always provides a non-negative value and satisfies the symmetric property, that is, $H(X, Y) = H(Y, X)$. If there is no relationship or dependency between X

and Y , that is, if $p(x,y) = p(x)p(y)$, then the joint entropy is simply the sum of the individual entropies, that is, $H(X,Y) = H(X) + H(Y)$. Conversely, when there is any relationship or statistical dependency, then $H(X,Y)$ becomes smaller than the combined amount of individual entropies $H(X)$ and $H(Y)$, that is, $H(X,Y) < H(X) + H(Y)$.

2.2.3 Conditional Entropy

Conditional entropy provides insight into whether a random variable has dependency on another random variable or not. If X and Y are two random variables, then the entropy of Y conditioned on X (denoted by $H(Y|X)$)—which quantifies the remaining uncertainty or unpredictability about Y when the information or knowledge of X is known—is defined as follows [80,81]:

$$\begin{aligned} H(Y|X) &= \sum_{X_t \in X} p(X_t)H(Y|X = X_t), \\ &= -\sum_{X_t \in X} p(X_t) \sum_{Y_t \in Y} p(Y_t|X_t) \log_2 p(Y_t|X_t), \\ &= -\sum_{X_t \in X} \sum_{Y_t \in Y} p(X_t, Y_t) \log_2 p(Y_t|X_t), \\ &= -\sum_{X_t \in X, Y_t \in Y} p(X_t, Y_t) \log_2 \frac{p(X_t, Y_t)}{p(X_t)}. \end{aligned} \quad (2.3)$$

It can also be expressed in terms of $H(X,Y)$ and $H(X)$ as follows:

$$\begin{aligned} H(Y|X) &= -\sum_{X_t, Y_t} p(X_t, Y_t) \log_2 p(X_t, Y_t) + \sum_{X_t, Y_t} p(X_t, Y_t) \log_2 p(X_t) \\ &= H(X,Y) - H(X). \end{aligned} \quad (2.4)$$

Similarly, the entropy of X conditioned on Y (denoted by $H(X|Y)$) is defined as follows:

$$\begin{aligned} H(X|Y) &= -\sum_{X_t \in X, Y_t \in Y} p(X_t, Y_t) \log_2 \frac{p(X_t, Y_t)}{p(Y_t)} \\ &= -\sum_{X_t, Y_t} p(X_t, Y_t) \log_2 p(X_t, Y_t) + \sum_{X_t, Y_t} p(X_t, Y_t) \log_2 p(Y_t) \\ &= H(X,Y) - H(Y). \end{aligned} \quad (2.5)$$

When the variable Y has any dependency on the variable X , then $H(Y|X) < H(Y)$. Otherwise, $H(Y|X) = H(Y)$. Furthermore, Eqs. 2.4 and 2.5 clearly show that the conditional entropy does not satisfy the symmetric property, that is, $H(Y|X) \neq H(X|Y)$. Now, for a case of three variables such as X , Y and Z , the entropy of Y conditioned on both X and Z is reduced to the following form [82]:

$$H(Y|X, Z) = - \sum_{X_t \in X, Y_t \in Y, Z_t \in Z} p(X_t, Y_t, Z_t) \log_2 \frac{p(X_t, Y_t, Z_t)}{p(X_t, Z_t)}, \quad (2.6)$$

where the summation runs over all possible outcomes of X , Y , and Z . The Eq. 2.6 quantifies the remaining uncertainty about Y when the information or knowledge of both X and Z is known.

2.2.4 Mutual Information

Mutual information (MI) is one of the information-theoretic measures that provides insight into mutual dependency between two random variables. If X and Y are two random variables, then mutual information (denoted by $I(X, Y)$) measures the amount of information mutually shared between X and Y , which is defined by the following formula [80,81,83]:

$$I(X; Y) = \sum_{X_t \in X, Y_t \in Y} p(X_t, Y_t) \log_2 \frac{p(X_t, Y_t)}{p(X_t)p(Y_t)}, \quad (2.7)$$

where $p(X_t)$, $p(Y_t)$, and $p(X_t, Y_t)$ represent the marginal and joint probabilities, respectively. If the joint probability $p(X_t, Y_t)$ is equal to the product of the marginal probabilities $p(X_t)$ and $p(Y_t)$, that is, $p(X_t, Y_t) = p(X_t)p(Y_t)$, then $I(X; Y) = 0$, which means that X and Y are independent and do not share any information. In contrast, when the joint probability $p(X_t, Y_t)$ is different from the product of the marginal probabilities $p(X_t)$ and $p(Y_t)$, that is, $p(X_t, Y_t) \neq p(X_t)p(Y_t)$, then $I(X; Y) > 0$, which means that there is a dependency between X and Y , and they can share information with each other. The MI can also be written in terms of entropy, conditional entropy, and joint entropy. The Eq. 2.7 can be expressed as:

$$I(X; Y) = \sum_{X_t, Y_t} p(X_t, Y_t) \log_2 p(X_t, Y_t) - \sum_{X_t, Y_t} p(X_t, Y_t) \log_2 [p(X_t)p(Y_t)]. \quad (2.8)$$

Using Eq. 2.2 in the first term, Eq. 2.8 reduces it to the following form:

$$\begin{aligned} I(X; Y) &= - \sum_{X_t, Y_t} p(X_t, Y_t) \log_2 p(X_t) - \sum_{X_t, Y_t} p(X_t, Y_t) \log_2 p(Y_t) - H(X, Y), \\ &= - \sum_{X_t} p(X_t) \log_2 p(X_t) - \sum_{Y_t} p(Y_t) \log_2 p(Y_t) - H(X, Y), \\ &= H(X) + H(Y) - H(X, Y). \end{aligned} \quad (2.9)$$

Eqs. 2.5 and 2.9 provide the following relation:

$$I(X; Y) = H(X) - H(X|Y). \quad (2.10)$$

Similarly, the following relation is obtained from Eqs. 2.4 and 2.9 :

$$\begin{aligned} I(X; Y) &= H(Y) - H(Y|X) \\ &= I(Y; X). \end{aligned} \quad (2.11)$$

From Eq. 2.11, it is clearly observed that the mutual information $I(\cdot ; \cdot)$ is inherently symmetric. It does not provide insight into the direction of interaction between the variables or the direction of information flow between the variables.

2.2.5 Time Delayed Mutual Information

When information is transferred between two variables, a finite time period (i.e., time delay) is required to pass information from one variable to another [65]. An information-theoretic approach with respect to time delay may provide insight into which variable shares information with other. Therefore, mutual information (MI) was modified by introducing a time delay parameter τ , which is referred to as time delayed mutual information (TDMI). If X and Y are two stochastic variables and τ is a time delay required to pass information from X to Y , then the TDMI between X and Y shifted by τ (i.e., $Y_{t+\tau}$) has the following form [84,85]:

$$I(X; Y, \tau) = \sum_{X_t \in X, Y_{t+\tau} \in Y} p(X_t, Y_{t+\tau}) \log_2 \frac{p(X_t, Y_{t+\tau})}{p(X_t)p(Y_{t+\tau})}. \quad (2.12)$$

Similarly, if information is passed from Y to X with a time delay τ , then the TDMI between Y and X shifted by τ (i.e., $X_{t+\tau}$) can be expressed as follows:

$$I(X; Y, \tau) = \sum_{X_{t+\tau} \in X, Y_t \in Y} p(X_{t+\tau}, Y_t) \log_2 \frac{p(X_{t+\tau}, Y_t)}{p(X_{t+\tau})p(Y_t)}. \quad (2.13)$$

If Eq. 2.12 provides a positive value for a time delay τ , then one can say that X shares information with Y at a time delay τ [44]. In other words, it can be said that X influences Y after a delay time τ . However, despite its ability to quantify the influences of both linear and non-linear interactions between two stochastic variables, a subtle drawback is that it can provide a positive value even for two completely independent variables [67]. In particular, when variables contain their own histories, it can provide a positive value for two independent variables due to their common history or common external driving effects [27,82]. Therefore, TDMI can lead to false inference about which one of the two variables influences the other.

2.2.6 Transfer Entropy

To overcome the limitation of TDMI, Thomas Schreiber introduced a well-known information-theoretic metric known as transfer entropy (TE)[45]. The basic concept of TE is that if a random variable X influences another random variable Y , then TE from X to Y quantifies the reduction of uncertainty about the future state Y_{t+1} of Y when the information of both current states X_t of X and Y_t of Y is known, compared to when only the information of the current state Y_t of Y is known. The transfer entropy (TE) from a variable X to another variable Y (denoted by $\mathcal{T}_{X \rightarrow Y}$) has the following form:

$$\begin{aligned} \mathcal{T}_{X \rightarrow Y} &= I(Y_{t+1}; X_t | Y_t) \\ &= H(Y_{t+1}|Y_t) - H(Y_{t+1}|Y_t, X_t) \\ &= - \sum_{Y_{t+1}, Y_t} p(Y_{t+1}, Y_t) \log_2 \frac{p(Y_{t+1}, Y_t)}{p(Y_t)} + \sum_{Y_{t+1}, Y_t, X_t} p(Y_{t+1}, Y_t, X_t) \log_2 \frac{p(Y_{t+1}, Y_t, X_t)}{p(Y_t, X_t)} \\ &= \sum_{Y_{t+1}, Y_t, X_t} p(Y_{t+1}, Y_t, X_t) \log_2 \frac{p(Y_{t+1}, Y_t, X_t)p(Y_t)}{p(Y_t, X_t)p(Y_{t+1}, Y_t)} \end{aligned} \quad (2.14)$$

where X_t represents the current state of X ; Y_t and Y_{t+1} denote the current and future states of Y , respectively. As with other information-theoretic measures, TE also always

provides a non-negative value, that is, $\mathcal{T}_{X \rightarrow Y} \geq 0$. The nonzero value of TE from X to Y (i.e., $\mathcal{T}_{X \rightarrow Y} > 0$) implies that X influences Y . To estimate the influence of one variable on another not only on the immediate future state (the state at delay time = 1), but also on the future states beyond the immediate one (the states at time delays > 1), Bauer et al. [49] introduced a time delay parameter τ as a prediction window and revised the standard TE equation (Eq.2.14) as follows:

$$\begin{aligned}\mathcal{T}_{X \rightarrow Y}(\tau) &= H(Y_{t+\tau}|Y_t) - H(Y_{t+\tau}|Y_t, X_t) \\ &= \sum_{Y_{t+\tau}, Y_t, X_t} p(Y_{t+\tau}, Y_t, X_t) \log_2 \frac{p(Y_{t+\tau}, Y_t, X_t)p(Y_t)}{p(Y_t, X_t)p(Y_{t+\tau}, Y_t)}.\end{aligned}\quad (2.15)$$

From Eq. 2.15, it is clearly obvious that $\mathcal{T}_{X \rightarrow Y}$ relies not only on the parameter τ , but on the conditional entropies $H(Y_{t+\tau}|Y_t)$ and $H(Y_{t+\tau}|Y_t, X_t)$. The quantity $H(Y_{t+\tau}|Y_t)$ that represents the upper bound (or ‘support’) of the estimation of causal influence using TE (in Eq. 2.15) can change with respect to τ . In particular, when Y possesses more memory, $H(Y_{t+\tau}|Y_t)$ varies much more prominently over τ (Fig. 2.1 (c), dashed lines). In such a case, the variation in $H(Y_{t+\tau}|Y_t)$ with increasing τ can cause an erroneous evaluation of causal influence over τ using TE (Fig. 2.1 (a), blue and orange lines).

2.2.7 Modified Transfer Entropy

The limitation buried in the Eq. (2.15) of standard TE in estimating the optimal time delay of causal influence was discussed by Wibral et al. [65] and Shu et al. [66]. Then, to overcome the challenge in TE , Shu et al. [66] introduced a modified equation of the standard TE (in Eq. (2.15)). The modified transfer entropy (MT) equation to measure the causal influence of X on Y with time delay τ has the following form:

$$\begin{aligned}\mathcal{MT}_{X \rightarrow Y}(\tau) &= H(Y_{t+\tau}|Y_{t+\tau-1}) - H(Y_{t+\tau}|Y_{t+\tau-1}, X_t) \\ &= \sum_{Y_{t+\tau}, Y_{t+\tau-1} \in Y; X_t \in X} p(Y_{t+\tau}, Y_{t+\tau-1}, X_t) \log_2 \frac{p(Y_{t+\tau}, Y_{t+\tau-1}, X_t)p(Y_{t+\tau-1})}{p(Y_{t+\tau-1}, X_t)p(Y_{t+\tau}, Y_{t+\tau-1})},\end{aligned}\quad (2.16)$$

where the current state Y_t of Y is substituted by the immediate prior state of the predicted state $Y_{t+\tau}$ of Y , i.e., $Y_{t+\tau-1}$, which guarantees that the conditional entropy $H(Y_{t+\tau}|Y_{t+\tau-1})$ does not vary over τ , as long as the variable Y is stationary (Fig. 2.1 (d), dashed lines).

As the upper bound of MT in estimating causal influence does not vary over τ and the τ -dependence on MT only comes from the time gap of X and Y , the estimation of causal influence between a pair of agents using MT (in Eq. 2.16) as a function of τ could be more reliable than the standard TE .

2.3 Role of the 1st term as upper bound of TE and MT measures

The 1st terms, $H(Y_{t+\tau}|Y_t)$ of TE and $H(Y_{t+\tau}|Y_{t+\tau-1})$ of MT in Eqs. 2.15 and 2.16, are conditioned on only a single variable Y , a target variable to be predicted. In contrast, the 2nd terms— $H(Y_{t+\tau}|Y_t, X_t)$ of TE and $H(Y_{t+\tau}|Y_{t+\tau-1}, X_t)$ of MT —are conditioned on two variables, especially Y_t and X_t in the case of $H(Y_{t+\tau}|Y_t, X_t)$, and $Y_{t+\tau-1}$ and X_t in the case of $H(Y_{t+\tau}|Y_{t+\tau-1}, X_t)$. As one of the fundamental properties of conditional entropy (whose value is always nonnegative) is that conditioning on more variables provides an uncertainty amount less than or equal to those of conditioned on fewer variables [81]. This leads to the following inequalities:

$$H(Y_{t+\tau}|Y_t) \geq H(Y_{t+\tau}|Y_t, X_t) \geq 0 \quad \text{and} \quad H(Y_{t+\tau}|Y_{t+\tau-1}) \geq H(Y_{t+\tau}|Y_{t+\tau-1}, X_t) \geq 0$$

The difference between 1st and 2nd terms defines TE and MT , making TE and MT always non-negative:

$$T_{X \rightarrow Y} \geq 0 \quad \text{and} \quad MT_{X \rightarrow Y} \geq 0,$$

where the equality comes from the case that any additional information about X_t does not help to predict the future of $Y_{t+\tau}$ on the top of Y_t for TE and $Y_{t+\tau-1}$ for MT . Since TE and MT are calculated by subtracting the 2nd term from the corresponding 1st term, their values cannot exceed the values of their 1st term. Therefore, the 1st terms serve as the upper bounds for TE and MT :

$$H(Y_{t+\tau}|Y_t) \geq T_{X \rightarrow Y} \quad \text{and} \quad H(Y_{t+\tau}|Y_{t+\tau-1}) \geq MT_{X \rightarrow Y}.$$

2.4 Variation in the upper bound of the Eqs. TE and MT with respect to time delay (τ): A binary model analysis

Suppose that the causal influence of a random variable X on another random variable Y is examined by observing their time traces at every intrinsic interaction time τ_0 (≥ 1) (which does not refer to the timescale of observation). When considering the effect of the value of $\tau (= n\tau_0)$ ($n = 0, 1, 2, \dots$) in the computation of TE in Eq. 2.15, one may imagine that TE reaches its maximum value when $\tau \simeq \tau_0$. However, it has been observed that the causal influence estimated using TE does not reach its maximum at $\tau = \tau_0$ in some cases. To examine the mechanism, let us consider a simple binary model comprising two stochastic processes X and Y ($\in [0, 1]$) under the following dynamics:

$$X_{t+1} = \begin{cases} X_t & \text{with probability } 1 - q \\ \text{FCT} & \text{with probability } q \end{cases}$$

$$Y_{t+\tau_0} = \begin{cases} Y_{t+\tau_0-1} & \text{with probability } 1 - p \\ X_t & \text{with probability } p \end{cases}$$

where $q, p \in [0, 1]$, FCT represents a Bernoulli process (similar to the possible outcomes of a fair coin toss). The parameter q denotes the probability of randomly generating the state X_{t+1} , while $1 - q$ signifies the probability of the state X_{t+1} depending on its immediate prior state X_t . Similarly, for generating $Y_{t+\tau_0}$, p and $1 - p$ indicate the probabilities of the state $Y_{t+\tau_0}$ depending on state X_t and on its immediate prior state $Y_{t+\tau_0-1}$, respectively. The lower the values of the parameters p and q , the greater the dependency on the memory of the variables Y and X . Setting $\tau_0 = 1$ and varying $q, p \in [0.1, 1]$, the configurations of X and Y are observed up to time steps 1×10^5 . Since X affects the dynamics of Y with a time delay of $\tau_0 = 1$, one may expect that $T_{X \rightarrow Y}$ over τ will reach maximum at the time delay of $\tau = \tau_0 = 1$, and then gradually decrease as the time delay τ increases. However, this is generally not the case. TE from X to Y does not show the peak at delay $\tau = 1$ when X and Y are more dependent on their memories, i.e, when p and q are small. For example, $T_{X \rightarrow Y}$ reaches maximum at $\tau = 4$ and 2 when $q, p = 0.15$ and 0.25 ,

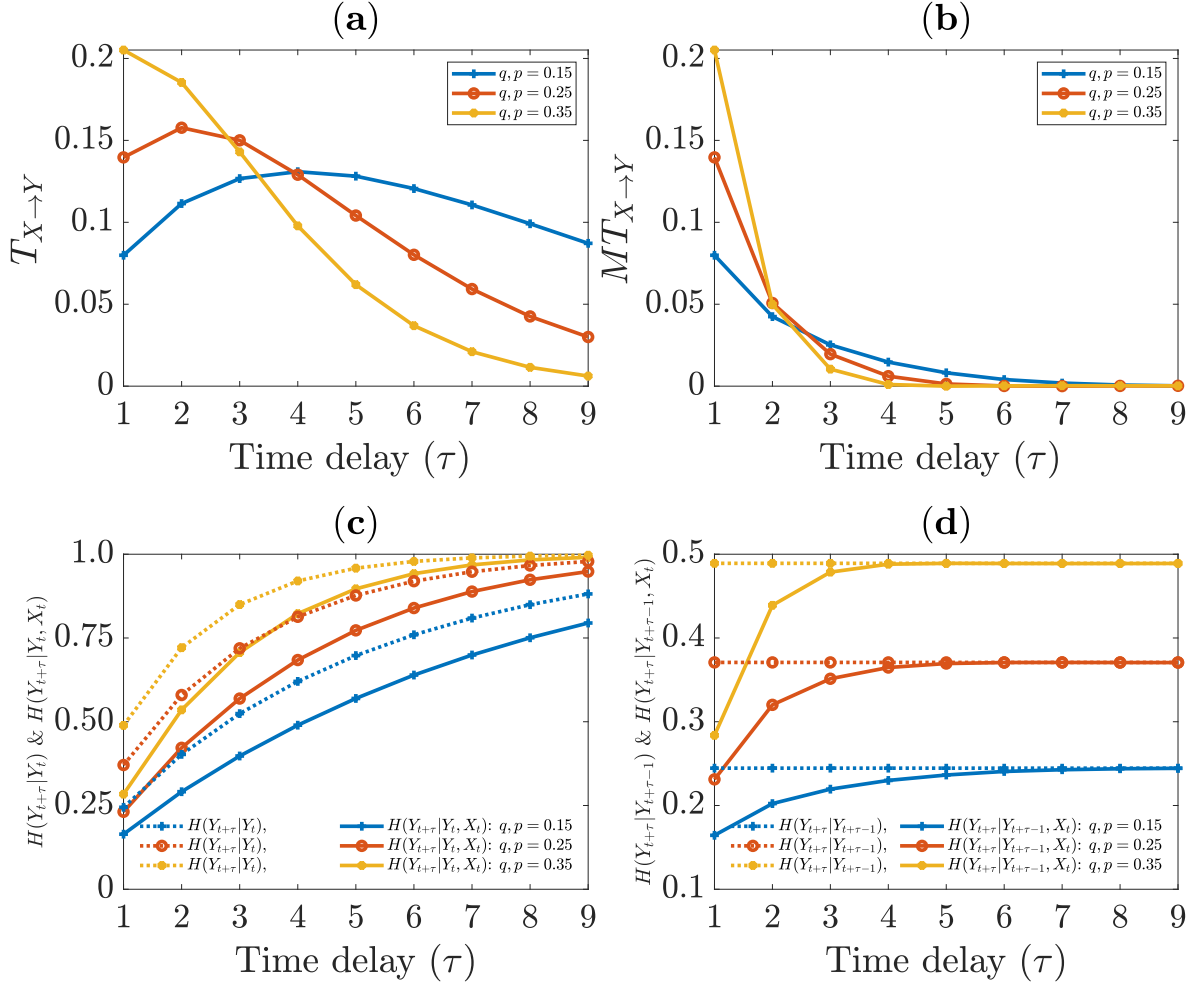


Figure 2.1: Behaviors of TE and MT from X to Y in the binary model for $q, p = 0.15, 0.25$ and 0.35 . (a) $T_{X \rightarrow Y}$ over τ , (b) $M T_{X \rightarrow Y}$ over τ , (c) the 1st (i.e., the upper bound) and 2nd terms of $T_{X \rightarrow Y}$, and (d) the 1st (i.e., the upper bound) and 2nd terms of $M T_{X \rightarrow Y}$. Note that $T_{X \rightarrow Y}$ varies prominently with τ based on the values of p and q , exhibiting a peak at time delay $\tau = 4$ and 2 when X and Y depend on more memory when $q, p = 0.15$ and 0.25 , respectively. As the dependency on memory decreases, i.e., when $q, p = 0.35$, the peak shifts to the interaction time scale $\tau = 1$. In turn, the largest value of $M T_{X \rightarrow Y}$ appears consistently at the interaction time scale $\tau = 1$, regardless of the level of memory dependency. The τ dependency of the upper bound $H(Y_{t+\tau}|Y_t)$ of $T_{X \rightarrow Y}$ becomes weaken or flatten as the values of p and q increase, while the upper bound $H(Y_{t+\tau}|Y_{t+\tau-1})$ of $M T_{X \rightarrow Y}$ remains constant with τ for all combinations of p and q . Note that the 2nd terms, $H(Y_{t+\tau}|Y_t, X_t)$ of $T_{X \rightarrow Y}$ and $H(Y_{t+\tau}|Y_{t+\tau-1}, X_t)$ of $M T_{X \rightarrow Y}$ monotonically increase with τ for any values of p and q .

respectively (Fig. 2.1 (a), blue and orange lines). However, as the memory dependency decreases, that is, as q, p increases to 0.35, $T_{X \rightarrow Y}$ shows the maximum at the interaction time delay $\tau = 1$ (Fig. 2.1 (a), yellow line).

This is interpreted as follows: The second terms $H(Y_{t+\tau}|Y_t, X_t)$ and $H(Y_{t+\tau}|Y_{t+\tau-1}, X_t)$ of TE and MT (see Eqs. 2.15 and 2.16) increase monotonically as a function of τ since the uncertainty about $Y_{t+\tau}$ after knowing Y_t and X_t , and $Y_{t+\tau-1}$ and X_t increases (recall that X interacts directly with Y). In this case, if the upper bounds of TE and MT , $H(Y_{t+\tau}|Y_t)$ and $H(Y_{t+\tau}|Y_{t+\tau-1})$, are (approximately) independent of τ , the measure $T_{X \rightarrow Y}$ and $MT_{X \rightarrow Y}$ exhibit a monotonic decreasing order with increasing time delay τ . When q and p are small, X and Y mainly depend on their own immediate past states. In this regime, X changes little due to random factors (e.g., a fair coin toss), and Y is weakly influenced by X . As q and p increase, X behaves more randomly, and Y becomes more responsive to the prior state of X . Thus, for small q and p , both variables retain more memory of past configurations. This gives rise to greater variability in the upper bound $H(Y_{t+\tau}|Y_t)$ of $T_{X \rightarrow Y}$ with respect to τ (Fig. 2.1 (c), dashed lines). These memory effects may cause the peak of $T_{X \rightarrow Y}$ to appear with longer delays, masking the interaction timescale at $\tau = 1$. In contrast, the metric MT provides the highest causal influence of X on Y at time delay $\tau = 1$ for any values of q and p (Fig. 2.1 (b)). Here, the upper bound $H(Y_{t+\tau}|Y_{t+\tau-1})$ remains constant across τ (Fig. 2.1 (d), dashed lines). Therefore, MT 's τ -dependence reflects only the causal time lag from X to directly interacting Y , which makes it have the highest value at $\tau = \tau_0 = 1$ and decreases for larger τ .

2.5 Concluding Remarks

It is observed that the standard transfer entropy (TE) may sometimes fail to accurately estimate the causal influence with the agents' interaction time delay. However, the modified transfer entropy (MT) can always quantify the maximum causal influence at interaction time delay between agents, as expected. When two agents interact directly, it shows a logically expected descending trend in its values as the time delay increases. Therefore, in this study, to discern direct and indirect influences between each individual pair of agents solely using their own pairwise time series observation, the metric (MT) as a function of a time delay τ in units of agents' interaction time delay is used to estimate

causal influence.

Chapter 3

Application of Modified Vicsek Model

3.1 Introduction

The Vicsek model [86] serves as a standard mathematical vehicle, which is widely used in the study of collective patterns in many physical and stochastic systems such as bird flocks [87–89], fish schools [90,91], insect swarms [92–94], etc. In the original VM [86], it is assumed that all agents have the same influence on each other. Since in this study, the main focus is to disentangle direct and indirect interactions between pairs of agents, I let some pairs of agents interact directly with each other, and some pairs of agents interact indirectly through one or more mediators in the system. In the simulation, the pairs of agents that interact directly and indirectly are known, which helps to evaluate the performance of the proposed approach in identifying pairs of agents that interact directly and indirectly.

3.2 Direct and indirect interactions

The interaction between agents in complex systems refers to the way or process by which agents, such as birds in a flock, cells in a wound healing, robots in a swarm, influence each other's behavior. It is one of the fundamental drivers of the emergence of collective behavior in complex systems [67]. It may occur through mechanisms such as physical contact of agents, forces (e.g., attraction or repulsion), environmental signals (e.g., chemical

stimuli, light, or sound), and so on. Agents share or transfer information from one to another through interaction, causing some changes in their behavior. However, in a system, agents can share information both directly and indirectly. In a system consisting of only two agents, the transfer of information from one agent to another is straightforwardly direct. But in a system composed of many interconnected agents, information can also be transferred from one agent to another indirectly through one or more mediators [32,60]. Thus, agents cascade information from their local to global scales through both direct and indirect interactions, leading to emergent phenomena in complex systems. More specifically, direct and indirect interactions can be defined in the following way:

- **Direct interaction:** The interaction between two distinct agents without any mediator in the interaction pathway is defined as direct interaction. For example, the interactions from X to Y ($X \rightarrow Y$), and Y to Z ($Y \rightarrow Z$) [Fig. 3.1(Ba)] are direct interactions.
- **Indirect interaction:** The interaction between two distinct agents through one or more mediators (i.e., through another third agent or third effect such as chemical signal) is defined as an indirect interaction. For example, the interaction of X with Z ($X \rightarrow Z$) through the mediator Y [Fig. 3.1(Ba)] is an indirect interaction.

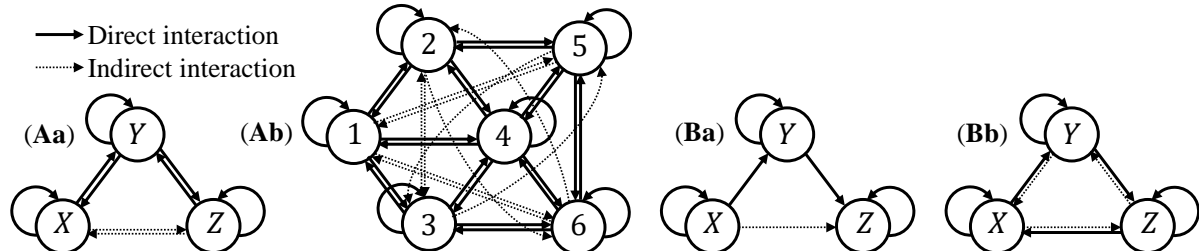


Figure 3.1. Schematic demonstration of some uni/bidirectional interaction patterns between agents involving direct and indirect influences.

In this study, to analyze direct and indirect influences between each individual pair of agents in a system, I have considered a set of schematic unidirectional (Ba and Bb) and bidirectional (Aa and Ab) interaction networks for systems consisting of three and six agents, as illustrated in Fig. 3.1, where the solid, dashed and circular arrows correspond to the direct interaction from one agent to another agent, the indirect interaction from one agent to another agent through one or more mediators, and the interactions of each

agent with itself, respectively. The circles represent the agents. More precisely, the solid arrows directed from X to Y , Y to X , Y to Z , and Z to Y indicate direct interactions (in Fig. 3.1(Aa)), while the dashed arrows directed from X to Z , and Z to X , represent indirect interactions through mediator Y . The interactions of each agent with itself (X to X , Y to Y , and Z to Z) are represented by circular arrows.

3.3 Modified Vicsek Model

To investigate direct and indirect interactions between each individual pair of agents within a given system, a modified form of the original Vicsek model (VM) has been studied [86]. I have considered a system containing N agents moving within a 2-dimensional

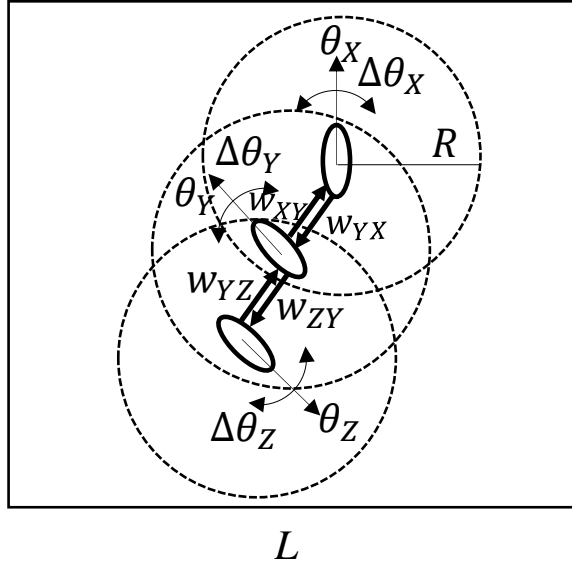


Figure 3.2. Schematic demonstration of modified VM for a system of agents shown in Fig.3.1(Aa) within a 2-dimensional square of area L^2 . The agents X , Y , and Z are indicated by ovals; θ_X , θ_Y , and θ_Z denote their directions of motion; $\Delta\theta_X$, $\Delta\theta_Y$, and $\Delta\theta_Z$ represent thermal noises, respectively. The circular regions of distance R refer to the interaction zones of agents. In this configuration, X and Y influences one another whenever located within each other's interaction zones; similarly, Y and Z influences one another. However, there is no direct interaction between agents X and Z . Due to the intermediary role of the agent Y , an indirect influence from X to Z is expected.

simulation box of area L^2 arb. square units. The initial positions and orientations of all agents are placed randomly within the box at time $t = 0$. The simulation is performed with periodic boundary conditions, ensuring that agents leaving from one edge of the simulation box reappear through the opposite edge. In this simulation, it is considered

that all agents travel at a uniform speed $|\vec{v}_i| = v_0$, and the locations are updated at each time interval Δt as defined in the following way:

$$\vec{r}_i(t + \Delta t) = \vec{r}_i(t) + \vec{v}_i(t)\Delta t, \quad (3.1)$$

where \vec{r}_i and \vec{v}_i , respectively, indicate the location and velocity of agent i at time t . Since each agent moves at a uniform speed, the changes occur solely in the orientation $\theta_i(t)$, which is computed by the following equation:

$$\theta_i(t + \Delta t) = \langle \theta(t) \rangle_{R, \mathbf{w}, \vec{r}_i(t)} + \Delta\theta_i, \quad (3.2)$$

where θ_i denotes the direction of motion of agent i at time t . The quantity $\langle \theta(t) \rangle_{R, \mathbf{w}, \vec{r}_i(t)}$ denotes the weighted average of the neighbors' directions of motion located inside the circle of distance R along with the agent i itself, which is calculated in the following form:

$$\langle \theta(t) \rangle_{R, \mathbf{w}, \vec{r}_i(t)} = \arctan \left[\frac{\sum_j w_{ij} \sin \theta_j(t)}{\sum_j w_{ij} \cos \theta_j(t)} \right],$$

where the sum \sum' accounts for all neighbors j of the agent i that satisfy $|\vec{r}_j - \vec{r}_i| \leq R$. The parameter \mathbf{w} refers to an interaction matrix, where the element $w_{ij} \geq 0$ denotes the coupling strength between agents i and j [67]. In particular, if j has influence on i , then $w_{ij} > 0$. Otherwise, if there is no influence, $w_{ij} = 0$. The self-interaction strength of the agent i is defined as unity, i.e., $w_{ii} = 1$. The term $\Delta\theta_i$ incorporates stochasticity or randomness in the system that follows the uniform distribution within the range $[-\frac{\eta}{2}, \frac{\eta}{2}]$, where η refers to “thermal noise” [67].

In order to mimic the direct and indirect influences between agents in a given interaction network, these relationships are incorporated into the interaction matrix \mathbf{w} to determine how the orientation of an agent at time $t + \Delta t$ depends on the orientations of others at time t . Fig. 3.2 exemplifies the interaction matrix \mathbf{w} in the case of the bidirectional interaction network of Fig. 3.1(Aa). In this interaction network, if two agents are within the interaction range of each other R , their orientations mutually influence each other, and the corresponding off-diagonal weights w_{ij} and w_{ji} are greater than zero. The agent X updates its future state $\theta_X(t + \Delta t)$ based on current states $\theta_X(t)$ and $\theta_Y(t)$ with $w_{XX} = 1$, $w_{XY} > 0$, $w_{XZ} = 0$. The agent Y updates its future state $\theta_Y(t + \Delta t)$ based

on current states $\theta_X(t)$, $\theta_Y(t)$, and $\theta_Z(t)$ with $w_{YY} = 1$, $w_{YX} > 0$, $w_{YZ} > 0$. Similarly, agent Z updates its future state $\theta_Z(t + \Delta t)$ based on current states $\theta_Z(t)$ and $\theta_Y(t)$ with $w_{ZZ} = 1$, $w_{ZX} = 0$, $w_{ZY} > 0$. Likewise, the interaction matrix \mathbf{w} can be modified for the other interaction networks as shown in Fig. 3.1(Ab-Bb). The value of w_{ij} is varied equally within the interval $[0.1, 1]$ for each pair of agents that interact directly. We perform 20 sets of observations using a simulation box of size $L = 10$, an interaction radius of $R = 3$, and a constant speed of $v_0 = 0.3$ arb. units [67]. In this model, the simulation time step Δt indicates the timescale of interaction τ_0 of agents (that is, $\tau_0 = \Delta t = 1$). To evaluate probability distributions required for estimating causal influence using TE and MT , the time series of the directions of motion of agents (θ 's) varying within the interval $[0, 2\pi)$ are partitioned into six uniform bins, and each bin is represented by a unique symbol according to the symbolization method described in Ref. [76]. The remaining uncertainty of possible outcomes in a partitioned time series, measured by Eq. 2.3 based on the probability distributions of 6 distinct symbols (or states), ranges from 0 to $\log_2(6) \approx 2.585$ bits. Thus, in a case where the current state X_t (of X) can completely mitigate the uncertainty about the future state $Y_{t+\tau}$ of Y at a delay time τ , the TE and MT from X to Y can quantify the theoretical maximum value $\log_2(6) \approx 2.585$ bits. The discretization approach leads to smaller TE and MT values in the cases where the ability of X_t to predict $Y_{t+\tau}$ decreases, and eventually both measures tend to zero when X_t cannot infer $Y_{t+\tau}$. In this analysis, the initial 5% of the trajectory time steps is discarded to avoid the risk of possible bias caused by the initial conditions[61].

3.4 Results and discussion

This section presents the inference of direct and indirect interactions between pairs of agents in the schematic interaction networks depicted in Fig. 3.1, based on the causal influence estimated by transfer entropy (TE) and modified transfer entropy (MT) over time delay τ solely from their pairwise time series data. The time series are simulated using the modified VM by varying the values of thermal noise (η) and coupling strength (w).

3.4.1 Prediction of direct/indirect interactions in the unidirectional interaction network

Let us first investigate the inference of direct and indirect influences in each individual pair of agents of the unidirectional interaction network shown in Fig. 3.1(Ba). The working hypothesis of this study is: If an agent X interacts directly with another agent Y at an interaction time delay τ_0 , then the influence of X on Y should decrease monotonically as the time delay τ increases in units of the interaction timescale τ_0 (i.e., $\tau = k\tau_0$, $k \in \mathbb{N}^+$). In other words, the current state X_t (of X) is expected to have more influence on the immediate future state of Y (i.e., $Y_{t+\tau_0}$) than on further future states (i.e., $Y_{t+k\tau_0}$ for $k (> 1)$).

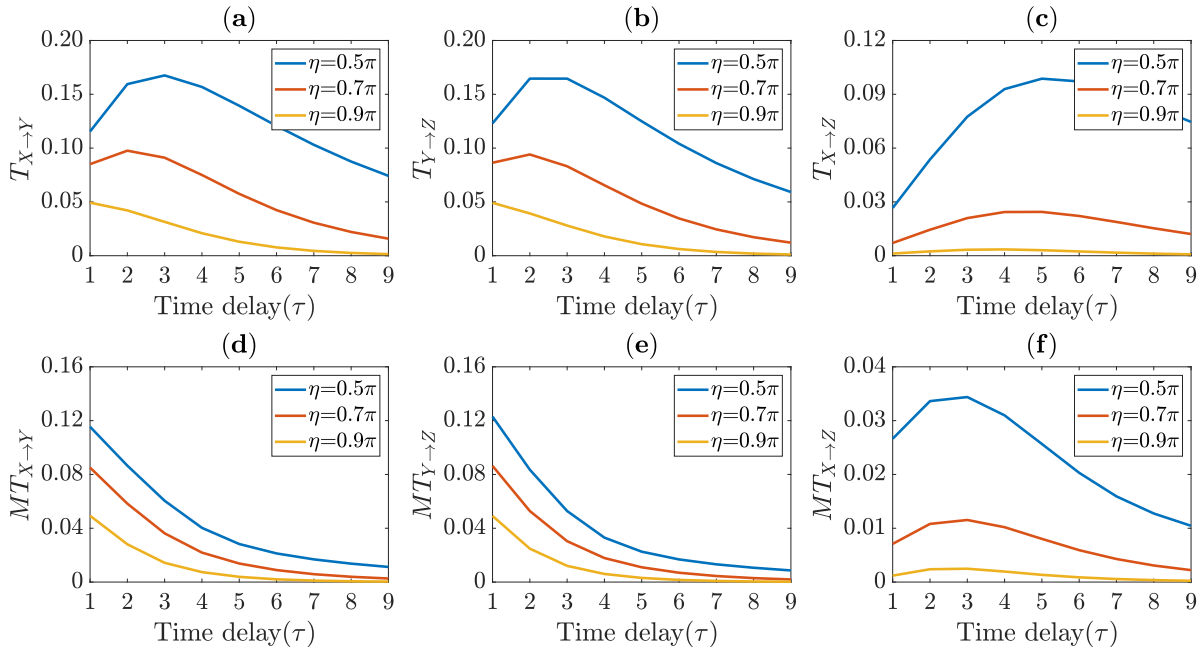


Figure 3.3. TE and MT over τ for individual pair of agents shown in Fig. 3.1(Ba) estimated from the modified VM-simulated trajectories at noises $\eta = 0.5\pi, 0.7\pi$ and 0.9π , and coupling strength $w = 0.8$. (a)-(c) show TE for directly interacting pairs $X-Y$, $Y-Z$ and indirectly interacting pair $X-Z$, respectively. (d)-(f) demonstrate MT for pairs $X-Y$, $Y-Z$ and $X-Z$, respectively. For directly interacting pairs $X-Y$ and $Y-Z$, MT decreases monotonically, although MT shows a nonmonotonic order for the indirectly interacting pair $X-Z$ at all noise levels, as anticipated. However, TE whose maximum value is dependent on the delay time τ exhibits complicated behavior inconsistent with the hypothesis.

Figure 3.3 demonstrates the behaviors of TE and MT over time delay τ for pairs $X-Y$, $Y-Z$ (where agents interact directly) and for pair $X-Z$ (where agents interact indirectly through Y) estimated from the trajectories of modified VM at noises $\eta = 0.5\pi, 0.7\pi$ and

0.9π , and coupling strength $w = 0.8$. It is observed that TE for pairs $X-Y$ and $Y-Z$ does not exhibit a monotonic decreasing order as τ increases when noise is small (i.e., $\eta = 0.5\pi$ and 0.7π). However, with increasing noise level (i.e., $\eta = 0.9\pi$), it exhibits a monotonic decreasing order with increasing τ (Figs. 3.3(a)-(b)). On the other hand, the metric MT shows a monotonic decreasing order with increasing τ for pairs $X-Y$ and $Y-Z$ at all noise levels (Figs. 3.3(d)-(e)). For the pair $X-Z$, it does not show a monotonic decreasing order with increasing τ at all noise levels (Fig. 3.3(f)). This is explained as follows (see also Section 2.4 based on a simple binary model): recall that, for pair $X-Y$, the first terms $H(Y_{t+\tau}|Y_t)$ in TE (Eq. 2.15) and $H(Y_{t+\tau}|Y_{t+\tau-1})$ in MT (Eq. 2.16) are the upper bounds of the measurements of causal influence of X on Y using these information-theoretic measures, respectively (see Section 2.3 for a detailed explanation of the upper bound). Figure 3.4 illustrates the upper bounds over time delay τ for noises $\eta = 0.5\pi, 0.7\pi$ and 0.9π . One can see that the upper bound $H(Y_{t+\tau}|Y_{t+\tau-1})$ in $MT_{X \rightarrow Y}$ does not change

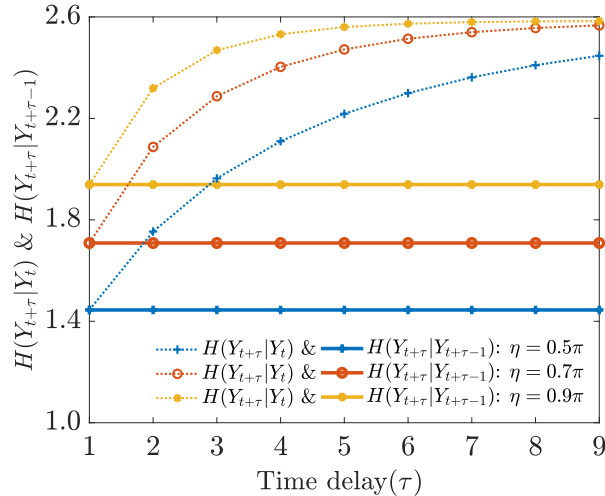


Figure 3.4. Illustration of the upper bounds of TE and MT over time delay τ in estimating the influence from agent X to agent Y at noises $\eta = 0.5\pi, 0.7\pi$ and 0.9π , and coupling strength $w = 0.8$, respectively. TE 's upper bound $H(Y_{t+\tau}|Y_t)$ shows τ -dependence and the dependency becomes more pronounced with decreasing noise η . In contrast, MT 's upper bound $H(Y_{t+\tau}|Y_{t+\tau-1})$ does not change with respect to τ at any noises.

as a function of time delay τ irrespective of η , which implies that the τ dependency of $MT_{X \rightarrow Y}$ originates only from the second term $H(Y_{t+\tau}|Y_{t+\tau-1}, X_t)$ in Eq. 2.16 which increases monotonically over τ for a pair of agents that interact directly. In contrast, the upper bound $H(Y_{t+\tau}|Y_t)$ in $T_{X \rightarrow Y}$ changes over τ , and more importantly, the τ -dependence becomes more pronounced with decreasing noise from $\eta = 0.9\pi$ to 0.5π . The

weaker τ -dependence of the upper bound $H(Y_{t+\tau}|Y_t)$ with increasing noise η indicates that the τ -dependence of $T_{X \rightarrow Y}$ largely arises from the second term $H(Y_{t+\tau}|Y_t, X_t)$ in Eq. 2.15, which monotonically increases with respect to τ . In this condition, if the upper bounds of information-theoretic measures do not (approximately) depend on τ , $T_{X \rightarrow Y}$ at $\eta = 0.9\pi$ and $MT_{X \rightarrow Y}$ at all noises exhibit a monotonically decreasing order with increasing τ . The reduction in noise η results in a greater variation in the upper bound $H(Y_{t+\tau}|Y_t)$ of $T_{X \rightarrow Y}$ over time delay τ , which complicates the τ dependency of $T_{X \rightarrow Y}$. The memory effect (= large τ dependency on the term $H(Y_{t+\tau}|Y_t)$ of TE) may lead to the highest value of $T_{X \rightarrow Y}$ with longer delays (see also Fig. 2.1 (a)). In contrast, the MT metric provides the highest influence from X to Y when time delay $\tau = 1$ for any noise level. Since there is no direct interaction between X and Z , X first affects Y and Y then affects Z , the information is first transferred from X to Y at a delay time τ and then transferred from Y to Z with an extra unit of τ . More precisely, X 's current state X_t affects Y 's future state Y_{t+1} , which then affects Z 's future state Z_{t+2} . As a result, X can predict more about Z for time delays $\tau > 1$ than the delay $\tau = 1$, resulting in a nonmonotonic order with increasing τ in the values of $T_{X \rightarrow Z}$ and $MT_{X \rightarrow Z}$.

3.4.2 Monotonicity metric (d_m)

To examine monotonic/nonmonotonic orders of the values of TE and MT with increasing τ in units of the timescale of interaction τ_0 , that is, $\tau = \tau_0, 2\tau_0, \dots, n\tau_0$, for each individual pair of agents under different conditions in the modified VM varying noise η and coupling strength w , I introduce a monotonicity metric map d_m , which is defined as follows:

$$d_m = \frac{N_{\max} - N_r}{N_{\max}},$$

where $d_m \in [0, 1]$ represents the degree of monotonic decreasing order of the values within a set of TE or MT values, $N_{\max} = n$ is the maximum number of times the values of a set of n elements can be moved from their current positions to their correct positions (or, in short, the maximum number of writes) when arranging in an ascending or a descending order, and N_r is the number of required writes for a set of values of TE or MT to reorder in a monotonically decreasing order. The number of required writes is determined using the cycle sort algorithm [95]. In other words, the number of required writes N_r can be

calculated by counting the number of components at incorrect positions in the given sequence. Figure 3.5 illustrates monotonic and nonmonotonic behaviors of the values of

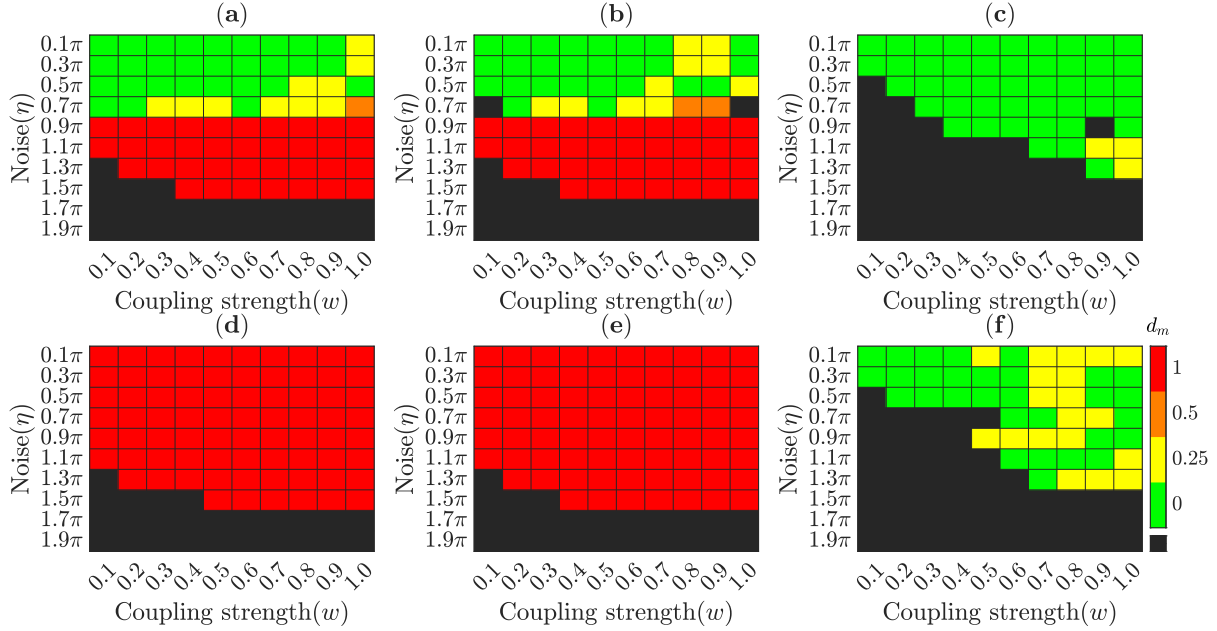


Figure 3.5. Monotonicity metric d_m of the values of TE and MT over time delays $\tau = 1, 2, 3, 4$ for each individual pair of agents shown in Fig. 3.1(Ba) under the different conditions of modified VM varying noise (η) and coupling strength (w). Here, color represents the value of d_m ; red means a monotonically decreasing order (where no write is needed to reorder the values, i.e., $d_m = 1$ with $N_r = 0$), orange denotes a nonmonotonic order (where some writes are needed to reorder the values, i.e., $d_m = 0.5$ with $N_r = 2$), yellow denotes a nonmonotonic order of $d_m = 0.25$ with $N_r = 3$, and green represents a nonmonotonic order of $d_m = 0$ with $N_r = 4$. Black represents the statistically insignificant differences of TE (or, MT) values over consecutive time delays using a hypothetical statistical test (see supplementary appendix A.1). **(a)-(c)** illustrate TE for pairs $X-Y$, $Y-Z$, and $X-Z$, respectively. **(d)-(f)** exhibit MT for pairs $X-Y$, $Y-Z$, and $X-Z$, respectively. For pairs $X-Y$ and $Y-Z$ (where agents interact directly), MT decreases monotonically (red) with increasing τ for all noises η , although it shows nonmonotonic orders for the pair $X-Z$ (where agents interact indirectly) at all noises η . In contrast, TE decreases monotonically (red) only at the noise $\eta(\geq 0.9\pi)$, with decreasing the noise $\eta(\leq 0.7\pi)$, the order deviates into nonmonotonic trends (orange, yellow, green colors) (see also the corresponding map d_m excluding hypothetical statistical test in supplementary Fig. S3).

TE and MT over time delays $\tau = 1, 2, 3$, and 4 (Here, $\tau_0 = 1$) for pairs $X-Y$, $Y-Z$, and $X-Z$ varying noise $\eta \in [0.1\pi, 1.9\pi]$, and coupling strength $w \in [0.1, 1.0]$. The colors represent the values of d_m when the differences between the values of MT (or TE) over consecutive time delays τ (as an example, $MT(\tau = 1) - MT(\tau = 2)$) are statistically significant using a hypothetical statistical test [67,96] (see supplementary Fig. S1 for details of the hypothetical test) and are black whenever the values are not statistically different. The red color refers to the case $d_m = 1$ which indicates that the MT (or TE) values decrease

monotonically over τ , that is, $MT(1) > MT(2) > MT(3) > MT(4)$, where no write is needed to reorder the values from their original order to a monotonically decreasing order. The color varies to orange, yellow and green for different values of $0 \leq d_m < 1$ in Fig. 3.5 which means that the MT (or TE) values are in some nonmonotonic orders, some writes are required to reorder the values to a monotonically decreasing order over τ . The black denotes the statistically insignificant differences between the values of MT (or TE) over consecutive time delays τ (in Fig. 3.5), which are observed mostly at higher noises. At higher noises, the motion of agents is mostly governed by noise, leading to their random movements over time. Agents have very little influence on each other under these conditions. Therefore, both TE and MT estimate very small values that are not significantly different for consecutive time delays τ . Furthermore, in this analysis, the discussion of noise $\eta = 0$ and also for very lower cases is ignored. Since agents' motions are almost aligned at noise level $\eta = 0$ and very few variations are observed in the motion for very small noises, the estimated TE and MT values are not statistically meaningful.

3.4.3 Prediction of direct/indirect interactions in the bidirectional interaction network

Now, let us see how the proposed approach works for the case of bidirectional interactions. I examine the behaviors of the values of TE and MT with increasing τ for each individual pair of agents of the bidirectional interactions shown in Fig. 3.1 (Aa) under different conditions of modified VM varying η and w . Figure 3.6 shows the monotonicity metric d_m of the values of TE and MT with increasing τ by varying the values of parameters η and w . Figure 3.6 demonstrates an almost similar trend as described in Fig. 3.5 for the case of unidirectional interactions. The difference observed between these two figures is that TE also exhibits a monotonically decreasing trend over τ for pairs $X-Y$ and $Y-Z$ at low noises η when the coupling strength is strong, while the trend was found nonmonotonic at smaller coupling strengths (Figs. 3.6(a)-(b)). In these bidirectional interactions, X updates its future state based on the current states of itself and Y , Y updates its future state based on the current states of all agents, and Z updates its future state based on the current states of itself and Y . Therefore, when the coupling strength is very small, agents' motions are mostly governed by their own current states, whereas at large coupling strength, their motions mainly rely on the motions of their neighbors.

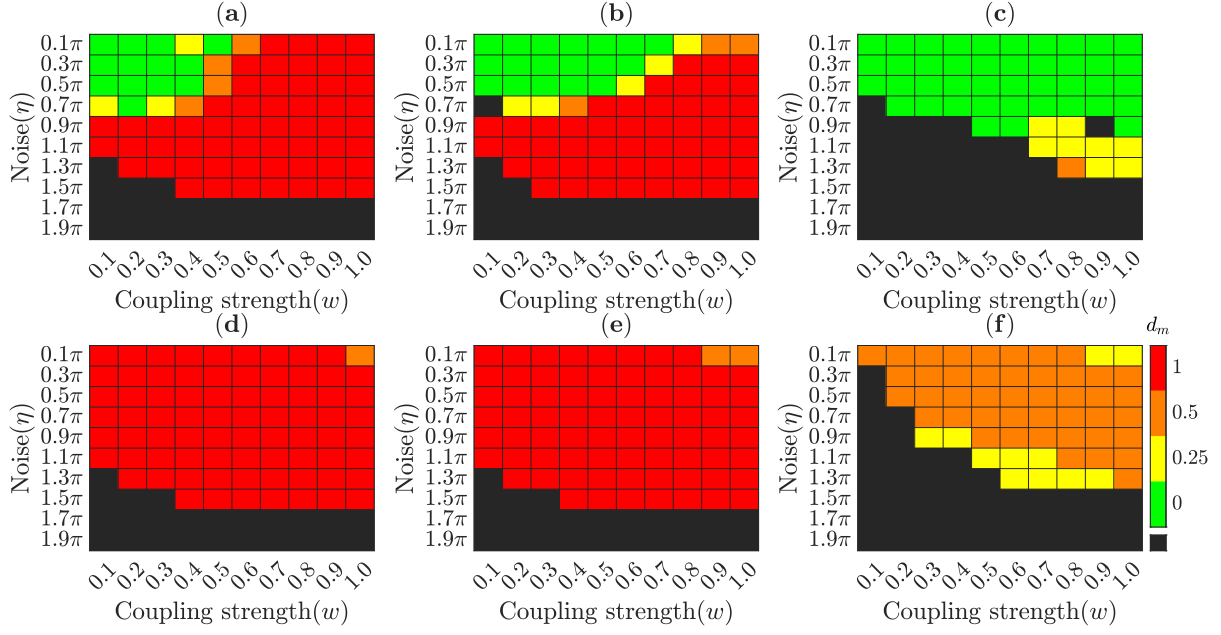


Figure 3.6. Monotonicity metric (d_m) of the values of TE and MT with increasing τ for each individual pair of agents shown in Fig. 3.1(Aa) under different conditions of modified VM varying noise (η) and coupling strength (w). **(a)-(c)** show TE for pairs $X-Y$, $Y-Z$ and $X-Z$, respectively. **(d)-(f)** present MT for pairs $X-Y$, $Y-Z$ and $X-Z$, respectively. For pairs $X-Y$ and $Y-Z$, MT decreases monotonically at all noises η including some deviations (i.e., nonmonotonicity ‘orange’ color) at the lowest noise $\eta = 0.1\pi$ when the coupling strength is very strong, i.e., $w = 0.9$ and 1.0 . However, the expected nonmonotonic trends are found in the values of MT at all noises η for the pair $X-Z$, where agents interact indirectly. On the other hand, depending on noise levels η , TE violates the working hypothesis and exhibits nonmonotonic orders for pairs $X-Y$ and $Y-Z$, where agents interact directly.

As illustrated in Fig. 3.7, the term $H(Y_{t+\tau}|Y_t)$ varies more significantly with τ when the coupling strength is small ($w = 0.3$), compared to the coupling strength ($w = 0.8$), as desired. This leads to a nonmonotonic trend in the values of TE over τ , while for the case of the large coupling strength this variation is not pronounced as much as it is for the small coupling strength, leading to a monotonically decreasing trend over τ (also, $T_{Y \rightarrow Z}$ also shows similar phenomena as τ increases as $T_{X \rightarrow Y}$). It may also be noted that a small nonmonotonic pattern indicated by orange color (where only two ‘writes or changes’ are needed to reorder the values to a monotonic sequence) for pairs $X-Y$ and $Y-Z$ using MT over τ at the lowest noise level when coupling strength is very strong (Figs. 3.6(d)-(e)). As in such cases, agents’ motions are less stochastic because of very small noise (η) compared to the coupling strength(w), agents may have a feedback effect in their dynamics: for instance, in pair $X-Y$, due to negligible random movements, X and Y affect the motions of each other over time by a back-and-forth mechanism, i.e.,

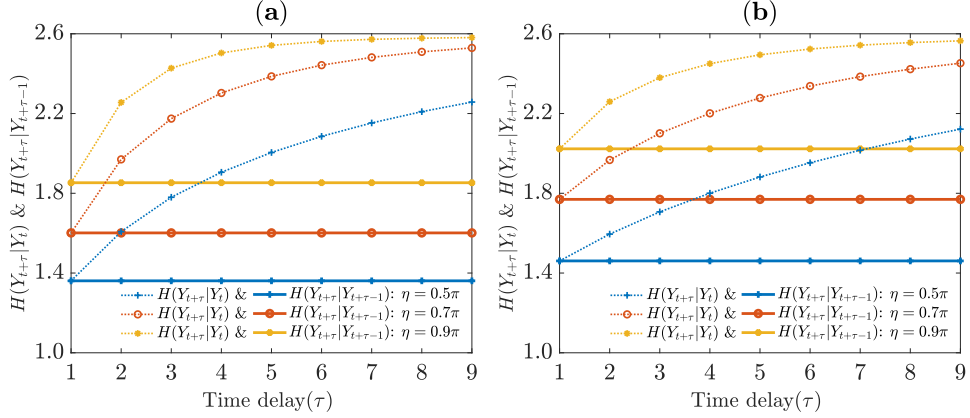


Figure 3.7. Illustration of the upper bounds of TE and MT over time delay τ in quantifying the influence from agent X to agent Y shown in Fig. 3.1(Aa) in the modified VM at noises $\eta = 0.5\pi, 0.7\pi$ and 0.9π with distinct coupling strengths w , (a) $w = 0.3$ and (b) $w = 0.8$. TE 's upper bound $H(Y_{t+\tau}|Y_t)$ (dashed lines) shows more prominent τ -dependence at small coupling strength $w = 0.3$ than the large coupling strength $w = 0.8$. However, MT 's upper bound $H(Y_{t+\tau}|Y_{t+\tau-1})$ (solid lines) does not show τ -dependence for any cases.

$X_t \rightarrow Y_{t+1} \rightarrow X_{t+2} \rightarrow Y_{t+3} \rightarrow \dots$, etc. Therefore, for lower noise levels, the existence of such a back-and-forth mechanism for the case of bidirectional interactions may complicate the prediction of direct/indirect interactions between individual pair of agents. However, for the case of bidirectional interactions, it is observed that the metric MT over time delay τ can distinguish directly interacting pairs $X-Y$ and $Y-Z$ and indirectly interacting pair $X-Z$ more efficiently than the metric TE .

The monotonic and nonmonotonic behaviors of MT over time delay τ to predict direct/indirect interactions have also been examined for a unidirectional interaction loop (Fig. 3.1(Bb)) and for a more complex bidirectional interaction (Fig. 3.1(AB)), which are available in the supplementary appendices A.4 and A.5, respectively. The only difference in the unidirectional interaction loop shown in Fig. 3.1(Bb) from the unidirectional interaction shown in Fig. 3.1(Ba) is that Z also influences X . In this case, X and Z can also act as mediators. Therefore, despite the indirect influence from X to Z through Y that exists in both Figs. 3.1(Ba) and (Bb), the indirect influences from Z to Y through X and from Y to X through Z are also anticipated. In this study, the monotonically decreasing trend is observed in the values of $MT_{X \rightarrow Y}$, $MT_{Y \rightarrow Z}$ and $MT_{Z \rightarrow X}$ with increasing τ for the path $X \rightarrow Y \rightarrow Z \rightarrow X$ (solid arrows in Fig. 3.1(Bb)) (see supplementary Figs. S4(a)-(c)). In contrast, for the opposite path, i.e., $X \rightarrow Z \rightarrow Y \rightarrow X$ (dashed arrows in Fig. 3.1(Bb)), as an overall scenarios, the nonmonotonic trends are observed in

the values of $MT_{Y \rightarrow X}$, $MT_{Z \rightarrow Y}$, and $MT_{X \rightarrow Z}$ as τ increases. However, it is also noticed that there exist some deviations at low noises η when the coupling strength is weak, i.e., $w = 0.1$ and 0.2 , where the monotonically decreasing order is observed for indirect interactions (see supplementary Figs. S4(d)-(f)). This can be interpreted by considering more conditions on the prior state of the predicted agent in the measurement using the metric MT (see for details in the supplementary appendix A.4). In summary, the motion of X mostly depends on its own past state along with some effect of Z when the coupling strength is small, since Z influences X . That is, when determining the remaining uncertainty of $Z_{t+\tau}$ based on the information of X_t in addition to that of $Z_{t+\tau-\tau_0}$ using $MT_{X \rightarrow Z}$, X_t carries some small amounts of past information about Z , i.e., $Z_{t+\tau-2\tau_0}$. Considering the condition on $Z_{t+\tau-2\tau_0}$ when estimating $MT_{X \rightarrow Z}$ restricts X_t from providing additional information about $Z_{t+\tau-2\tau_0}$, which leads to a nonmonotonic order with respect to τ , as described in the supplementary Fig. S5.

For bidirectional interactions in Fig. 3.1(Ab), as almost similar results are noticed for all directly and indirectly interacting pairs, the scenarios for some directly interacting pairs 1-2, 1-4, and 5-6, and for some indirectly interacting pairs 1-5, 2-6, and 3-5 are presented in supplementary Fig. S7. It is observed that MT values exhibit nonmonotonic orders with increasing τ at all noises and coupling strengths, as desired, for all indirectly interacting pairs including those pairs not illustrated (e.g., supplementary Figs. S7(d)-(f)). In turn, the monotonic decreasing order is noticed for all direct pairs (including those pairs not illustrated) at almost all noises and coupling strengths. Similar to the analysis for the interaction presented in Fig. 1(Aa) using modified VM at small noises with strong coupling strength, the same nonmonotonic trends (indicated by orange) are observed for pairs 1-2 and 5-6 (see supplementary Figs. S7(a)-(c)). However, it is also observed that MT decreases monotonically with increasing τ for pair 1-4, even in such conditions (e.g., supplementary Fig. S7(b)). As agent 4 interacts with more agents, its motion depends on the motions of more agents through more back-and-forth mechanisms compared to all other agents. Therefore, the interactions of agent 4 with more agents, possibly, add more variability in its motion, which makes the process of agent 4 more stochastic, leading to a monotonically decreasing trend in the values of $MT_{1 \rightarrow 4}$ with increasing τ (also in MT from all other directly interacting agents to agent 4 (not illustrated)).

3.5 Concluding Remarks

This chapter presents the behaviors of TE and MT metrics in predicting directly and indirectly interacting individual pair of agents solely from their own pairwise time series observations. The time series of agents are simulated for different schematic uni/bidirectional interaction networks (Fig. 3.1) under different conditions of modified VM by varying noise (η) and coupling strength (w).

For unidirectional interactions, it is observed that the metric MT consistently exhibits a monotonically decreasing order as τ increases when agents interact directly, regardless of noise levels η , while it shows the nonmonotonic orders for the case of indirect interaction. In contrast, TE shows a monotonic decreasing order with increasing τ for direct interaction only at moderate to higher noise levels η .

For bidirectional interaction, MT also shows a monotonic decreasing order for direct interaction, and nonmonotonic orders for indirect interaction. However, some exceptions are noticed—that is, small nonmonotonicity (where two changes are required to rearrange into a monotonic decreasing sequence)—at the conditions of lower noises η with coupling strength w . In contrast, TE shows the results almost similar to the results in the case of unidirectional interaction.

Therefore, it can be concluded that the metric MT over time delay τ can identify direct and indirect interactions between each individual pair of agents solely from their pairwise time series more efficiently than the metric TE .

Chapter 4

Application of Langevin dynamics model

4.1 Introduction

In the Vicsek model, it is considered that agents move at a uniform speed in a system, and the directions of agents' motions are updated over time based on the average of the directions of their neighbors' motions within a certain interaction distance. However, in real-world systems like bird flocks, fish schools, and cell dynamics, agents do not always move at a uniform speed, and their motions may also be controlled by forces such as attraction and repulsion. This chapter describes a standard mathematical vehicle, namely the Langevin dynamics model (LD), in which agents move at variable speeds and interact with each other based on attraction and repulsion forces. In this model, direct and indirect influences are introduced between agents in a system by controlling the potential well (ϵ) in the Morse potential energy function. Here, I set the potential well to be non-zero (that is, $\epsilon \neq 0$) for some pairs of agents so that they can attract and repel each other (which are considered as directly interacting pairs) and set it to be zero (that is, $\epsilon = 0$) for some pairs of agents so that they do not attract and repel each other (which are considered as indirectly interacting pairs). In this simulation, all pairs of agents that interact directly and indirectly are known, which helps to assess the efficacy of the proposed approach in predicting directly and indirectly interacting pairs of agents solely from their pairwise tracking data.

4.2 Langevin Dynamics (LD) Model

The LD simulation is performed for a given system of N agents interacting both directly and indirectly within a square simulation box of length L (arb. units) in two dimensions under periodic boundary conditions. The velocity of an agent i —expressed as $\vec{v}_i = (v_{x,i}, v_{y,i})$, where $v_{x,i}$ and $v_{y,i}$ indicate its components along the x and y axes, respectively—is recorded over the simulation time interval Δt according to the under-damped Langevin equation defined by the following form [68]:

$$m_i \vec{a}_i = \vec{F}_i - \gamma \vec{v}_i + \vec{\xi}_i(t), \quad (4.1)$$

where m_i and \vec{a}_i indicate the mass and acceleration of agent i , respectively. The variable \vec{F}_i represents the force acting on the agent i , which is obtained from the Morse potential energy function $U(\{\vec{r}_i\})$ due to the interaction between agents:

$$U(\{\vec{r}_i\}) = \sum_{i>j} \varepsilon_{ij} [e^{-2\alpha(r_{ij}-r_e)} - 2e^{-\alpha(r_{ij}-r_e)}].$$

Here, $r_{ij} = |\vec{r}_i - \vec{r}_j|$ represents the distance between the positions of agents i and j , where $\vec{r}_i = x_i \vec{i} + y_i \vec{j}$ and $\vec{r}_j = x_j \vec{i} + y_j \vec{j}$ are the position vectors (\vec{i} and \vec{j} denote the unit vectors for indicating the axes of the simulation box), respectively. The parameter ε_{ij} known as the depth of the potential well, which represents the energy necessary to separate agents i and j , or equivalently, the interaction strength of i and j . The parameters α and r_e denote the potential width (a decrease in α increases the potential width) and the equilibrium distance at which the agents are balanced, respectively. For simplicity, it is assumed that all agents have a constant mass $m_i = m$. The force \vec{F}_i is defined by

$$\vec{F}_i = -\nabla U(\{\vec{r}_i\}) = -\frac{\partial U}{\partial x_i} \vec{i} - \frac{\partial U}{\partial y_i} \vec{j},$$

where γ denotes the drag or friction coefficient, which characterizes the strength of dissipative forces exerted on agents as they move through a medium. The term $\vec{\xi}_i(t)$ represents a stochastic force, whose values follow a Gaussian distribution with the following properties: the average of the values is zero and the values at two different time instances are completely uncorrelated, such as:

$$\langle \vec{\xi}_i \rangle = 0,$$

and

$$\langle \vec{\xi}_i(t) \vec{\xi}_j(t') \rangle = 2\gamma k_B T \delta_{i,j} \delta(t - t'),$$

where the parameters k_B , T , and δ in $\delta_{i,j}$ and $\delta(t - t')$ represent Boltzmann's constant, system temperature, and Kronecker and Dirac δ -functions, respectively.

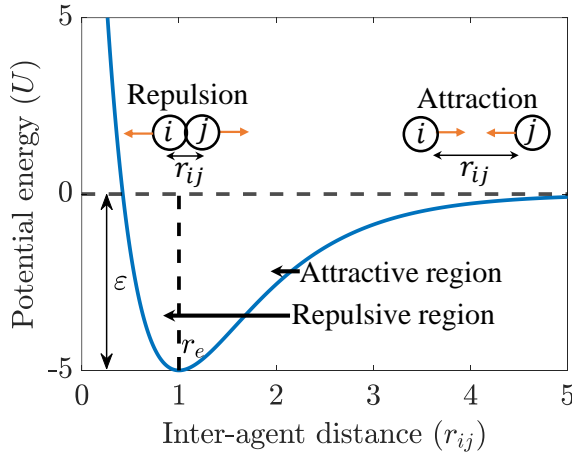


Figure 4.1. An illustration of Morse potential function as a function of inter-agent distance r_{ij} , where $r_e = 1$ and $\varepsilon = 5$, respectively, denote the equilibrium distance and potential well depth. The attractive and repulsive regions are highlighted in the figure. In the attractive region, the distance between agents i and j is greater than r_e , i.e., $r_{ij} > r_e$, and there is a pair potential force $\vec{F} = -\nabla U(\{\vec{r}_i\}) < 0$, which pulls agents close to each other. Conversely, in the repulsive region, the distance is $r_{ij} < r_e$ with a pair potential force $\vec{F} = -\nabla U(\{\vec{r}_i\}) > 0$, which pushes the agents apart.

In this model, the direct and indirect influences between agents in a system—as exemplified in Fig. 3.1(Aa)—are integrated into the agents' dynamics in the following manner: In pairs of agents (X, Y) and (Y, Z), agents affect each other's velocities through the attraction and repulsion forces with potential $\varepsilon = 5$. The velocities \vec{v}_X , \vec{v}_Y and \vec{v}_Z of agents X , Y and Z are updated over time through the interaction between X and Y ($\varepsilon_{XY} = \varepsilon_{YX} = \varepsilon$); Y and X and Z ($\varepsilon_{XY} = \varepsilon_{YX} = \varepsilon_{YZ} = \varepsilon_{ZY} = \varepsilon$); Z and Y ($\varepsilon_{YZ} = \varepsilon_{ZY} = \varepsilon$), respectively. The potential well ε_{ij} is zero for all other interactions, excluding self-interactions. In this simulation, the simulation time step Δt is set to 0.1 to observe the evolution of the velocity trajectories over time. This simulation time step corresponds to approximately 17 times shorter than the characteristic oscillation $T_{\text{osc}} (= 1.66)$ near the minimum of the potential located at r_e . In this study, a total of

20 sets of LD simulation are performed, each is continued up to 1×10^7 time steps to ensure statistical reliability and adequate sampling of the system behavior. The simulations are performed using a Python package known as Highly Optimized Object-oriented Many-particle Dynamics-Blue Edition (HOOMD-blue)[68] for the following parameter values: simulation box length $L = 10$ arb. unit, thermal energy $k_B T \in [0.2, 3.8]$, friction coefficient $\gamma \in [0.332m/T_{\text{osc}}, 3.32m/T_{\text{osc}}]$, mass $m = 1$, equilibrium distance $r_e = 1$ and potential width $\alpha = 1.2$. The initial positions $\vec{r}_i(0)$ of the agents are distributed uniformly within the interval $[-\frac{L}{2}, \frac{L}{2}]$. To increase computational efficiency without compromising the physical accuracy of the system, a cutoff radius $r_{\text{cut}} (\simeq L/2)$ is employed in the simulation beyond that the rate of change of potential with respect to inter-agents distance varies negligibly, allowing long-range interactions to be excluded from the force calculations without significant loss of fidelity. In this analysis, the initial 5% of the trajectory time steps is discarded to avoid the risk of possible bias caused by the initial conditions.

In this model, the time step of observing the velocity trajectories (i.e., simulation time interval Δt) does not necessarily represent the interaction timescale (τ_0)—that is, time delay between an “action” of an agent and its observable “effect” on other—of agents in a system. Therefore, to estimate the influence of one agent on another agent using information-theoretic measures TE and MT , one firstly need to define the appropriate interaction timescale τ_0 —expressed in terms of the simulation time interval Δt —in similar to embedology to reconstruct the underlying state structure from trajectories [97]. The interaction timescale τ_0 is estimated from the decay rate of the autocorrelation function (ACF) of the agents’ velocity trajectories obtained by curve fitting [98–100]. In this simulation, due to the uniform friction coefficient (γ) along the x and y axes, the ACF curves for the components $v_{x,i}$ and $v_{y,i}$ of the agent i decline in the same way, resulting in a unique time constant $\hat{\tau}_i (= \hat{\tau}_{x,i} = \hat{\tau}_{y,i})$, where $\hat{\tau}_{x,i}$ and $\hat{\tau}_{y,i}$ indicate the time constants of $v_{x,i}$ and $v_{y,i}$, respectively. However, in general, the interaction timescales $\hat{\tau}_i$ of individual agents in a system may differ due to the asymmetry in their interaction networks. For example, as illustrated in Fig. 3.1(Aa), Y interacts with both X and Z , while X and Z interact solely with Y . This asymmetry experiences a different time constant $\hat{\tau}_Y$ for agent Y than the time constants $\hat{\tau}_X$ and $\hat{\tau}_Z$ of agents X and Z , respectively (see Fig. 4.2). In this study, to define a unified timescale for the system, the average of the individual time

constants $\hat{\tau}_X$, $\hat{\tau}_Y$, and $\hat{\tau}_Z$ is taken as the interaction timescale τ_0 , which is then used as a time interval for resampling the velocity components $v_{x,i}$ and $v_{y,i}$ to quantify the causal influence between agents:

$$v_{x,i}(t), v_{x,i}(t + \tau_0), v_{x,i}(t + 2\tau_0), v_{x,i}(t + 3\tau_0), \dots$$

and

$$v_{y,i}(t), v_{y,i}(t + \tau_0), v_{y,i}(t + 2\tau_0), v_{y,i}(t + 3\tau_0), \dots$$

That is, the resampled velocity components $\bar{v}_{\xi,i}$ are denoted by $\bar{v}_{\xi,i}(k) = v_{\xi,i}(t + \tau_0(k-1))$, where $\xi = x, y$ and $k \in \mathbb{N}^+$. For the estimation of information-theoretic measures, the resampled velocities $\bar{v}_{\xi,i}$ are discretized into a finite number of bins for each direction ξ (four bins are considered in this study), which corresponds to dividing the values of every $(\bar{v}_{x,i}, \bar{v}_{y,i})$ into 4×4 grids. The grid sizes are constructed to confirm that every grid element contains an equal number of data points. To estimate the probability distributions required for *TE* and *MT*, each of the 16 grids is then uniquely assigned with a symbol from 1 to 16.

4.3 Estimation of timescale (τ_0) from decay rate of autocorrelation function (ACF) via curve fitting

Autocorrelation usually quantifies the extent to which the values in a time series are related to the values in its shifted form by a certain time delay. The typical timescale of a time series denoted by $\hat{\tau}$ —the time delay at which the autocorrelation of the time series significantly reduces—can be estimated from the decay rate of its autocorrelation function [98–100]. For a stationary time series $X = \{\dots, X_{t-1}, X_t, X_{t+1}, \dots\}$, the autocorrelation function (ACF) at a given time lag Δt quantifies the linear relationship between the values X_t and $X_{t+\Delta t}$ as follows:

$$ACF(\Delta t) = \frac{\sum_{t=1}^{n-\Delta t} (X_t - \mu)(X_{t+\Delta t} - \mu)}{\sum_{t=1}^n (X_t - \mu)^2}, \quad (4.2)$$

where μ is the mean of all values of X . In this analysis, using Eq. 4.2, the ACF curves of the velocity components $v_{x,i}$ and $v_{y,i}$ of the agent i are determined from their trajectories

simulated under the interactions illustrated in Fig. 3.1(Aa) varying the thermal energy $k_B T$ within the range [0.2,3.8] and the friction coefficient γ within the range [0.2,2]. Since the friction coefficient γ is uniform in both x and y axes and there is no external field that makes the space asymmetric, the ACF curves for both $v_{x,i}$ and $v_{y,i}$ exhibit similar profiles that decay at the same rate. Moreover, the ACF curves show a damped oscillatory pattern at lower values of $k_B T$ and an exponential decay pattern at higher values of $k_B T$. The possible reason for observing these patterns is the predominance of potential and

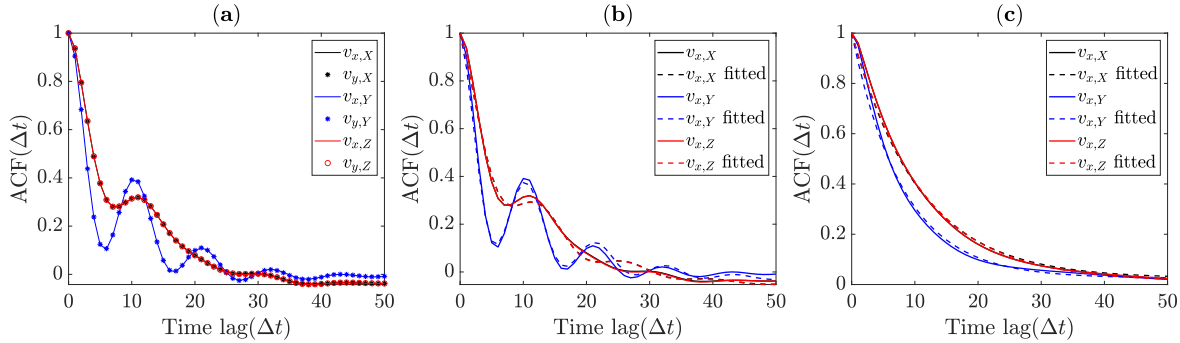


Figure 4.2. (a) Identical ACF curves of velocity components $v_{x,i}$ and $v_{y,i}$ over time lag Δt , where subscript i denotes the agents X (black), Y (blue), and Z (red). (b)-(c) $v_{x,i}$ (solid lines) and fitted curves (dotted lines) at $k_B T = 0.2$, $\gamma = 0.6$ (a damped oscillatory pattern), and at $k_B T = 1.8$, $\gamma = 0.6$ (an exponential decay pattern), respectively.

stochastic (thermal) forces at lower and higher values of $k_B T$, respectively. Therefore, to determine the decay rates of ACF curves for all $k_B T$ and γ values, a damped sinusoidal function (which can capture both damped oscillatory and exponential decay patterns) of the following form is fitted with ACF curves using a non-linear least squares curve fitting method (a built-in function available in MATLAB's Optimization Toolbox):

$$f(t) = \frac{e^{-\gamma_d t}(A + \cos \omega t) + \phi}{1 + A + \phi}, \quad (4.3)$$

where γ_d , A , ω , and ϕ represent the decay rate, amplitude, angular frequency of oscillation, and an offset, respectively. The function (Eq. 4.3) is fitted with the ACF data of $v_{x,i}$ and $v_{y,i}$ for a given system of agents illustrated in Fig. 3.1(Aa). Figure 4.2 displays the ACF curves of $v_{x,i}$ and $v_{y,i}$ at $k_B T = 0.2$, $\gamma = 0.6$, and at $k_B T = 1.8$, $\gamma = 0.6$, respectively. The time constant $\hat{\tau}_i$, defined by $\hat{\tau}_i (= \hat{\tau}_{x,i} = \hat{\tau}_{y,i} = 1/\gamma_{d,i})$, is estimated from the decay rate of the ACF curve of agent i 's trajectory, where $\gamma_{d,i}$ represents the decay rate of the trajectory. As shown in Figs. 4.2(b-c), the ACF of the velocity component $v_{x,Y}$ of agent Y exhibits a distinct decay behavior compared to those of agents X and Z

(i.e., $v_{x,X}$ and $v_{x,Z}$), leading to a distinct time constant $\hat{\tau}_Y$ than the time constants $\hat{\tau}_X$ of X and $\hat{\tau}_Z$ of Z (which are identical). In this analysis, to define a unified timescale for all agents in a given system for the sake of further analysis, the average of the individual time constants $\hat{\tau}_X$, $\hat{\tau}_Y$, and $\hat{\tau}_Z$ are considered as the timescale τ_0 (see Table 4.1), which is then used as a time interval for resampling the velocity trajectories to estimate the influence between a pair of agents in the main text.

Table 4.1: Illustration of the estimation of timescale τ_0 in units of simulation time interval (Δt) obtained from the average of typical time constants of individual agents X , Y and Z shown in Fig. 3.1(Aa) for some values of $k_B T$ and γ , where the function in Eq. 4.3 is fitted with the ACF data with an initial guess of parameters $\gamma_d = 0.5$, $A = 1$, $\omega = 2\pi/10$, and $\phi = 0$.

$(k_B T, \gamma)$	X 's timescale($\hat{\tau}_X$)	Y 's timescale($\hat{\tau}_Y$)	Z 's timescale($\hat{\tau}_Z$)	τ_0
(0.2, 0.2)	17.35	15.56	17.21	≈ 16
(0.6, 0.4)	7.82	6.99	8.14	≈ 8
(1.4, 0.6)	9.48	8.29	9.10	≈ 9
(2.2, 0.8)	9.83	7.92	9.56	≈ 9
(3.4, 1.8)	6.33	6.05	6.30	≈ 6

4.4 Results and discussion

This section describes the behaviors of TE and MT over time delay τ in units of the interaction timescale τ_0 for each individual pair of agents illustrated in Figs. 3.1(Aa and Ab) under different conditions of LD simulations varying thermal energy ($k_B T$) and friction coefficient (γ).

4.4.1 Prediction of direct/indirect interactions for bidirectional interaction networks

To examine the generality of the proposed approach, the inference of direct/indirect interactions between a pair of agents buried in the LD-simulated velocity trajectories of agents shown in Figs. 3.1(Aa and Ab) is investigated, where each agent moves under a bidirectional effect in their dynamics. As in this model, the simulation time step (Δt) does not necessarily represent the interaction timescale (τ_0), the value of τ_0 is estimated based on the rate of decay of the ACF curve obtained by using a curve fitting approach

(see section 4.3). Due to the variations in the number of connectives between agents in a given system, the individual agents' interaction timescales may differ from agent to agent. In this analysis, the average of the timescales of individual agents is taken as the interaction timescale τ_0 to estimate the influence of one agent on another agent.

Figure 4.3 demonstrates the behaviors of TE and MT over time delay τ ($= k\tau_0$) from $k = 1$ to 9 for pairs $X-Y$ and $Y-Z$ (where agents interact directly), and for pair $X-Z$ (where agents interact indirectly) at thermal noises $k_B T = 1.0, 1.4, 1.8$ and friction coefficient $\gamma = 0.4$. It is observed that both TE and MT exhibit a monotonically decreasing order with respect to τ for pairs $X-Y$ and $Y-Z$ (Figs. 4.3(a-b) and (d-e)), and nonmonotonic orders for pair $X-Z$ (Figs. 4.3(c) and (f)). In the pairs of agents $X-Y$

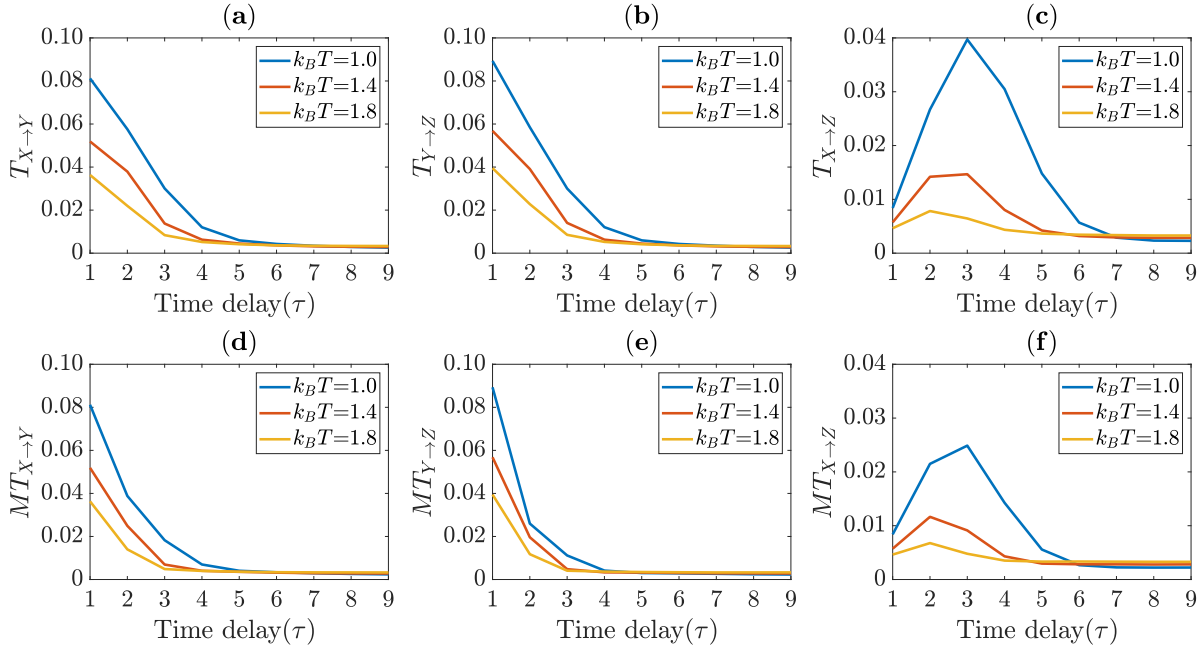


Figure 4.3. TE and MT over τ for LD-simulated velocity trajectories of agents shown in Fig. 3.1(Aa) at thermal noises $k_B T = 1.0, 1.4$, and 1.8 , and friction coefficient $\gamma = 0.4$. (a)-(c) present TE for pairs $X-Y$, $Y-Z$ and $X-Z$, respectively. (d)-(f) show MT for pairs $X-Y$, $Y-Z$ and $X-Z$, respectively. For pairs $X-Y$ and $Y-Z$ (where agents interact directly), both metrics TE and MT show a monotonically decreasing order at all thermal noises $k_B T$. However, for the pair $X-Z$ (where agents interact indirectly), both metrics show nonmonotonic orders at all thermal noises, respectively.

and $Y-Z$, the movements of agents are governed by the attraction and repulsion forces of the potential well. The agents move close to each other because of the attraction force, while the repulsion force pushes the agents away from each other. The interaction timescale τ_0 is observed to be $8\Delta t$, $10\Delta t$, and $12\Delta t$ at thermal noises $k_B T = 1.0, 1.4$, and 1.8 , respectively. At a time delay $\tau = 1 \cdot \tau_0$, the current state X_t (of X) can infer

the future state $Y_{t+1-\tau_0}$ (of Y) more than it can infer the states for longer delay times $\tau (= k\tau_0)$ ($k \geq 1$). With increasing τ , the capacity of the current state X_t to predict the future state $Y_{t+\tau}$ decreases, leading to a monotonically decreasing order in both $T_{X \rightarrow Y}$ and $MT_{X \rightarrow Y}$ as a function of τ . A key finding is that, unlike the modified VM, the upper bound of $T_{X \rightarrow Y}$ —that is, $H(Y_{t+\tau}|Y_t)$ —does not show noticeable variations with time delay τ (see Fig. 4.4, note the very narrow scale changes in the vertical axis), which results in a monotonically decreasing order in the values of $T_{X \rightarrow Y}$ over time delay τ . Similarly, $T_{Y \rightarrow Z}$ and $MT_{Y \rightarrow Z}$ also exhibit a monotonically decreasing order over time delay τ . In contrast, for the indirectly interacting pair $X-Z$, agents neither attract nor repel owing to a flat potential. As a result, X does not directly influence Z at delay time $\tau = \tau_0$. However, since X can attract and repel Y in pair $X-Y$, and Y can attract and repel Z in pair $Y-Z$, so X can indirectly influence Z at delay times $\tau = k\tau_0$ with $k \geq 1$ through the interaction chain $X_t \rightarrow Y_{t+1} \rightarrow Z_{t+2}$, leading to a higher capacity of X to predict Z at delay time with $k > 1$ than with $k = 1$. As a result, both $T_{X \rightarrow Z}$ and $MT_{X \rightarrow Z}$ exhibit nonmonotonic orders with respect to τ . Furthermore, both TE and MT also decline as

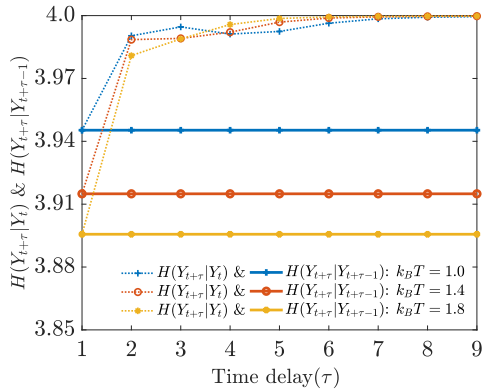


Figure 4.4. Illustration of the upper bounds of TE and MT over time delay τ in estimating the influence of agent X on agent Y from the LD-simulated velocity trajectories under the interactions illustrated in Fig. 3.1(Aa) for $k_B T = 1.0, 1.4$, and 1.8 , and $\gamma = 0.4$, respectively. MT 's upper bound $H(Y_{t+\tau}|Y_{t+\tau-1})$ does not change with respect to τ (solid lines), whereas TE 's upper bound $H(Y_{t+\tau}|Y_t)$ shows τ -dependence (dashed lines), but very slightly relative to the scale of the vertical axis.

thermal noise $k_B T$ increases. At low to moderate values of $k_B T$, agents undergo minor displacements and tend to remain within the potential well for longer periods. In such cases, due to attraction and repulsion forces, inter-agent collisions occur more frequently, which produces reliable statistics of interacting agents that are less affected by stochastic thermal noises given off by the medium. On the other hand, higher values of $k_B T$ inten-

sify the collisions of agents with the external medium (γ), leading to larger displacements and enabling agents to escape from the potential well. As a result, agents move more randomly over time, leading to comparatively lower TE and MT values at the higher levels of $k_B T$. The monotonicity metric map in Fig. 4.5 demonstrates monotonic and

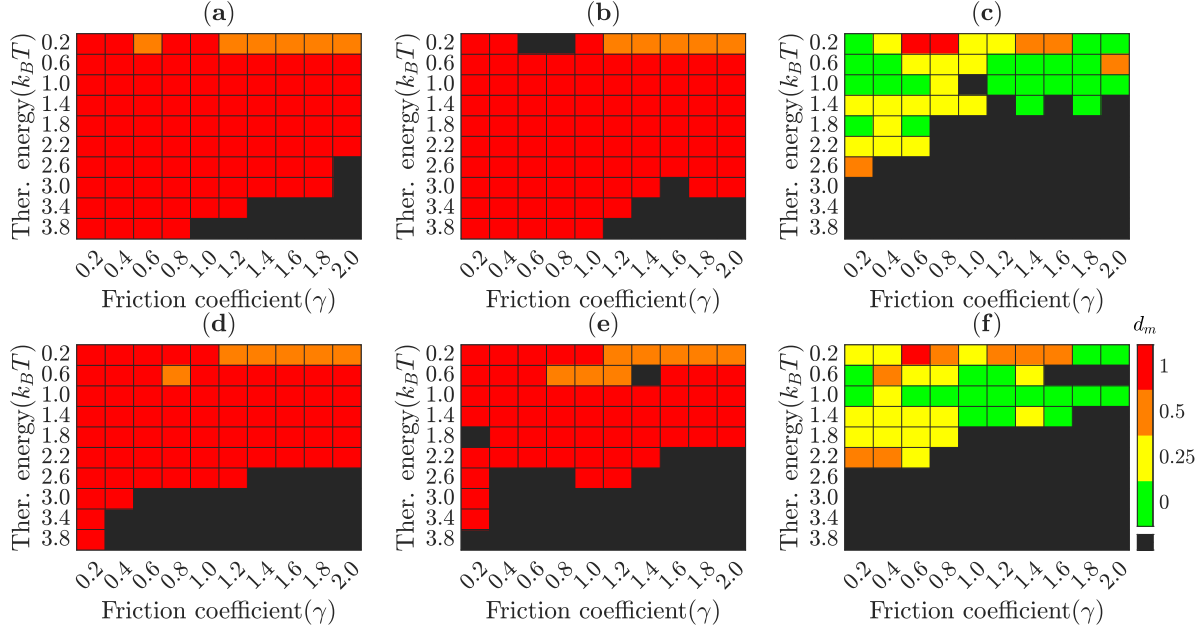


Figure 4.5. Monotonicity metric d_m of the values of TE and MT over τ for each individual pair of agents illustrated in Fig. 3.1(Aa) under different conditions of LD simulations varying $k_B T$ and γ . (a)-(c) illustrate TE for pairs $X-Y$, $Y-Z$, and $X-Z$, respectively. (d)-(f) show MT for pairs $X-Y$, $Y-Z$, and $X-Z$, respectively. Both measures show a monotonically decreasing order for pairs $X-Y$ and $Y-Z$, and nonmonotonic orders for the pair $X-Z$, including some exceptions—nonmonotonicity ‘orange’ color when agents interact directly and monotonicity ‘red’ when agents interact indirectly—at the lower levels of $k_B T$.

nonmonotonic behaviors of the values of TE and MT over $\tau = \tau_0, 2\tau_0, 3\tau_0$, and $4\tau_0$ for pairs of agents directly and indirectly interacting shown in Fig. 3.1(Aa), varying thermal noise $k_B T \in [0.2, 3.8]$, and friction coefficient $\gamma \in [0.2, 2]$. The black regions denote the statistically insignificant differences in the values of TE (and also MT) over consecutive time delay τ . At higher levels of $k_B T$, the stochastic force dominates the movements of agents, and higher friction γ accelerates energy dissipation and reduces the agents’ dependence on their past states. In these cases, agents have less effect on each other’s motion, resulting in relatively smaller TE and MT values, with changes in τ showing no statistically significant differences.

However, Figure 4.5 also displays a small nonmonotonic order for directly interacting pairs (orange color in Figs. 4.5(a-b) and (d-e)) and a monotonic decreasing order for indi-

rectly interacting pairs (red color) in Fig. 4.5(c) and (f)) at very low levels of $k_B T$ relative to the potential well depth ($\varepsilon = 5$). Since the movements of agents are less influenced by random force when the value of $k_B T$ is low, they are probably confined more times inside the potential well, which produces the oscillatory dynamics of the agents. In these cases, oscillatory phenomena may affect the movements of agents through a back-and-forth mechanism. For instance, in the pair $X-Y$, the less stochastic movements in their dynamics allow X and Y to influence each other's motion over time via a strong bidirectional interaction like a feedback process, that is, $X_t \rightarrow Y_{t+\tau_0} \rightarrow X_{t+2\tau_0} \rightarrow Y_{t+3\tau_0} \rightarrow \dots$, etc. Therefore, at lower levels of $k_B T$, the presence of this type of strong bidirectional interactions makes it more difficult to predict the influence of one agent on another using information-theoretic measures TE and MT over time delay τ . Furthermore, direct/indirect interactions for each individual pair of agents are also inferred using TE and MT over time delay τ under different conditions of the LD simulations for a case of more complex bidirectional interaction shown in Fig. 3.1(Ab), which are presented in the supplementary Appendix A.6.

4.5 Concluding Remarks

In this chapter, to examine the generality of the proposed hypothesis, the behaviors of TE and MT in predicting direct/indirect interactions between a pair of agents solely from their pairwise time series observations are investigated for different conditions of LD simulations by varying thermal noise $k_B T$ and friction coefficient γ .

It is observed that both metrics TE and MT show a monotonically decreasing order with increasing τ when agents interact directly and nonmonotonic orders when agents interact indirectly through a mediator. However, some exceptions are noticed—that is, nonmonotonicity for direct interaction and monotonicity for indirect interaction—at the lower level of $k_B T$. Similar exceptions were also found in modified VM for bidirectional interaction at lower noise levels (η) with strong coupling strength (w) due to the possible feedback effect in the agents' movements. In the LD model, the exceptions at the lowest thermal noise ($k_B T$) are observed, perhaps, because of a such feedback effect. Since at the lowest thermal energy ($k_B T$), agents likely spend more time inside the potential well (in this study, $\epsilon = 5$) and behave as oscillators.

However, it is noticed that the metric MT shows fewer exceptions compared to the metric TE . Therefore, it can be concluded that MT over time delay τ can be a more robust indicator to distinguish direct/indirect interactions between a pair of agents only from their pairwise time series data.

Chapter 5

Interactions in *Dictyostelium discoideum* cells

5.1 Introduction

Dictyostelium discoideum is a species of “social amoeba” [101,102]. It grows from a unicellular to a multicellular structure mainly through two distinct phases: the vegetative and the social (or development). In the vegetative phase, *D. discoideum* cells live as single cells that feed on bacteria through phagocytosis and divide rapidly by binary fission every several hours. The cells then enter a social phase triggered by a period of starvation, during which the individual cells aggregate to generate a multicellular organism [103,104]. *D. discoideum* cells usually communicate with each other via a chemoattractant called cyclic adenosine monophosphate (cAMP). In the social phase, during starvation, a few cells emit cAMP pulses to send signals to nearby cells [106,107]. In response, nearby cells move towards the source of the emitted cAMP pulses by releasing additional cAMP pulses. Over time, more and more nearby cells start to release cAMP pulses and move toward the highly concentrated cAMP region, resulting in a collective wave pattern of cAMP pulses. Therefore, an intriguing question is that: *How far can a cell influence another cell through the cAMP pulse?*

In this chapter, I would like to address this question by analyzing the **AMATERUS** imaging data of *D. discoideum* cells using an information-theoretic scheme called “transfer entropy (TE) with respect to a cutoff distance variable (λ)” [76,108].

*I would like to express my sincere appreciation to Prof. Kazuki Horikawa of Tokushima

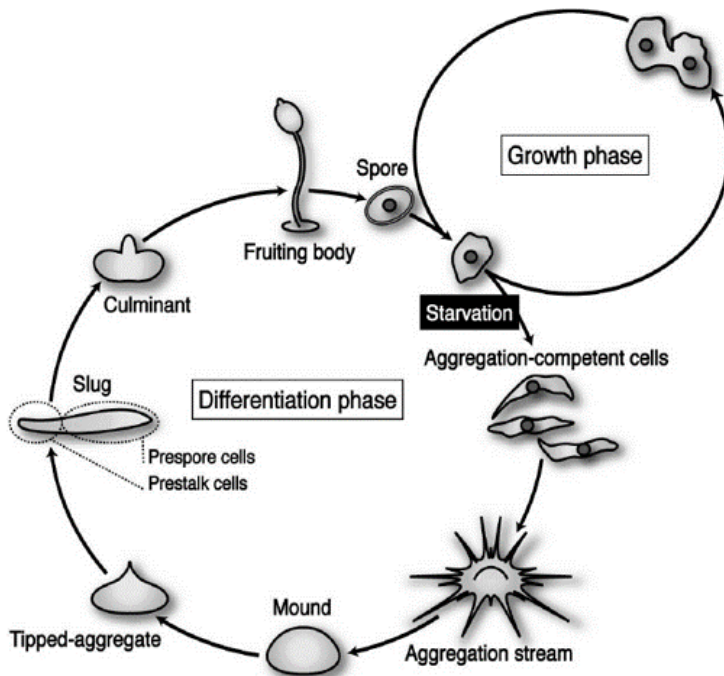


Figure 5.1. Life cycle of *D. discoideum* cells [105].

*University for sharing the imaging data of *D. discoideum* cells.*

5.2 Aggregation of *D. discoideum* cells via cAMP pulse

During the life cycle of *D. discoideum* cells, they initially move almost freely as unicellular organisms. Upon nutrient depletion, the aggregation process starts and forms a multicellular organism [109]. This transition from a unicellular to a multicellular state typically occurs over a period of approximately 24 hours after the onset of starvation [101]. Figure 5.2 illustrates the aggregation process of *D. discoideum* cells for three distinct time periods.

It is well known that cells aggregate through a mechanism known as ‘chemotaxis’, that is, the displacement of an organism caused by a chemoattractant called cAMP [106,107]. This attractant is generated and periodically emitted by cells during starvation [110]. When a cell detects external cAMP, it moves toward the source of cAMP and emits an additional cAMP spike simultaneously. Consequently, this behavior amplifies local differences in cell density, leading to aggregation [110]. Figure 5.3 illustrates the cAMP spikes of *D. discoideum* cells for three different time periods.

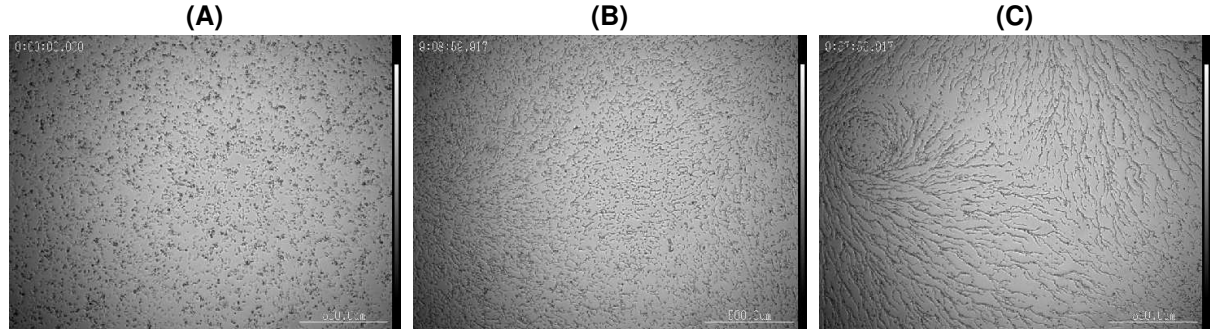


Figure 5.2. Aggregation of *D. discoideum* cells for three distinct time intervals. (A) Cells migrate independently. (B) Cells are trying to gather. (C) Finally, cells are gathering in a common place [27].

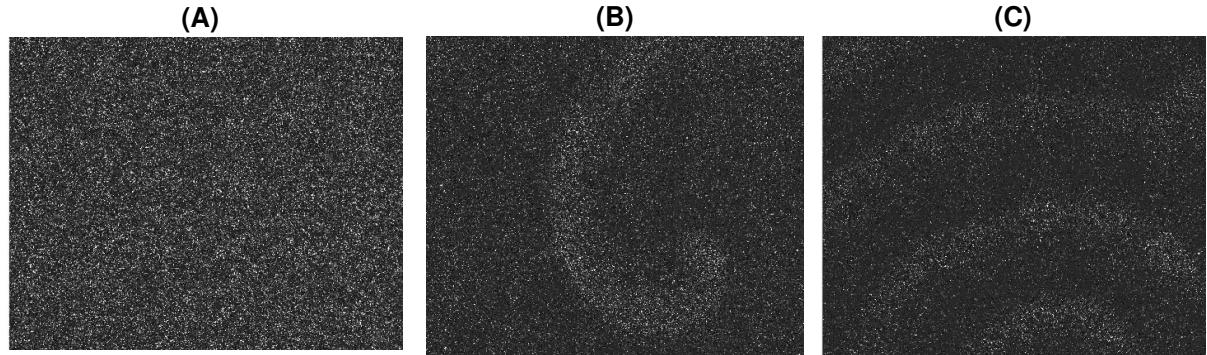


Figure 5.3. cAMP pulse of *D. discoideum* cells for three distinct time intervals [27].

5.3 Inference of typical interaction distance in *D. discoideum* cells

This section describes the application of an information-theoretic approach, that is, transfer entropy (TE) with respect to a cutoff distance variable (λ), to infer the underlying typical interaction distance in *D. discoideum* cells when a cAMP spiral wave is developed.

5.3.1 Transfer entropy (TE) vs cutoff distance (λ) approach

In real-world systems such as bird flocks [87–89], fish schools [90,91], cell dynamics [7–10], and many others, the typical interaction distance of agents is unknown. Therefore, how the interaction distance of agents in a system can be inferred using only their observed time series is an intriguing topic of study. Basak et al. [76] proposed an information theoretic approach as a function of the cutoff distance variable (λ) to infer the interaction distance solely based on the observed time series of agent in a system. They analyzed time series of agents simulated using the modified Vicsek model (VM) for a known inter-

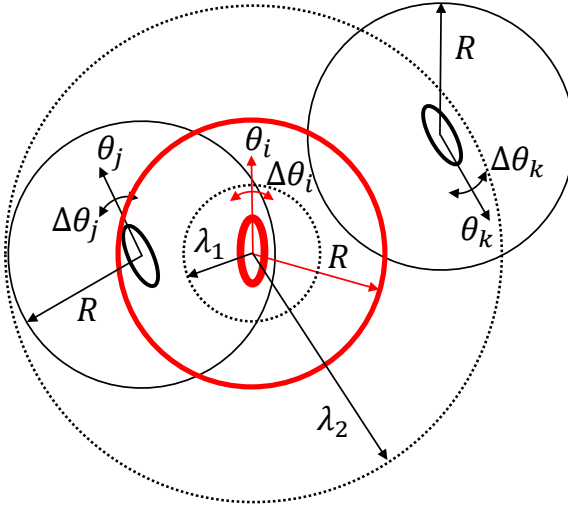


Figure 5.4. A schematic representation of cutoff distance scheme [76]. Red oval denotes an influential agent, while black ovals indicate nearby follower agents. The orientations of agents at time t are represented by θ_i , θ_j and θ_k . The parameters $\Delta\theta_i$, $\Delta\theta_j$ and $\Delta\theta_k$ denote thermal noises of individual agents. The circles indicate the interaction regions of distance R of the agents. Here, λ_1 and λ_2 represent two distinct values of the cutoff distance variable λ .

action distance (R) based on the assumption that agents interact only if their distances are less than R . Then, to predict the interaction distance R only from the time series of agents, they introduced the idea of cutoff distance variable λ in the information-theoretic measure TE [76]. The cutoff distance means the distance up to which the nearby agents' information is taken into account to quantify the influence one agent on another agent. More precisely, TE from the time series of one agent to that of another agent is computed from the probability distributions evaluated only at the time points t at which the distances between the agents are within the cutoff distance λ . For a given cutoff distance λ , TE from an agent X to another agent Y is defined as follows [76]:

$$TE_{X \rightarrow Y}(\lambda) = \sum_{y_{t+\tau}, y_t, x_t} p(y_{t+\tau}, y_t, x_t | d \leq \lambda) \times \log_2 \left(\frac{p(y_{t+\tau} | y_t, x_t, d \leq \lambda)}{p(y_{t+\tau} | y_t, d \leq \lambda)} \right) \quad (5.1)$$

where, x_t , y_t , and $d = |\vec{r}_X^t - \vec{r}_Y^t|$ indicate the orientation of agents X and Y at time t , and the distance between agents X and Y at time t , respectively. In order to predict the interaction distance (R) using Eq. 5.1, TE form one agent to another agent is estimated by varying λ from small to large values.

In Fig. 5.4, the nearby agents (black ovals) are influenced by the influential agent (red oval) once they enter its interaction zone (red circle). The strength of this influence should logically decrease as the distance between the influential agent and its neighbors increases. Therefore, if the value of the cutoff distance λ goes beyond the value of interaction distance R , the estimated value of $TE_{X \rightarrow Y}(\lambda)$ will decrease. The reason is that the calculation of TE includes both interacting and non-interacting agents, which tends to “dilute” the overall influence between genuinely interacting agents. In addition, beyond R , the magnitude of the negative gradient of TE with respect to λ varies over λ , and gradually decreases as λ increases. Since the influential agent influences a nearby agent located within its interaction distance R , TE is expected to exhibit a finite value with some fluctuations for $\lambda \leq R$.

5.3.2 Application of TE vs cutoff distance (λ) approach in D. discoideum cells

In *D. discoideum* cells, it would be better if the trajectory of an individual cell could be observed over time, similar to the simulation data presented by Basak et al. [76]. However, it is a very difficult task. So, as an alternative approach to analyze *D. discoideum* cells, an image of the cells (Fig. 5.2) is first divided into a set of grids and then transformed into a binary image (Fig. 5.3), where white represents the cells that emit cAMP and black indicates the cells that do not emit cAMP. Now, let us discuss the application of the TE vs cutoff distance (λ) approach in more detail based on the graphical representation shown below:

Suppose X_t represents the set of all grids in the image at time t , the center of the circle of cutoff distance λ is denoted by x (Fig. 5.5(b)). The set of all the remaining grids within the circle except the center is defined by Y_t and each element is represented by y . Similarly, in the delayed image at time $t + \tau$, the set of all remaining grids within the same circle except the center is denoted as $Y_{t+\tau}$ and each element is represented by y' (Fig. 5.5(c)). Since, at time t , both the center of the circle and another element within the circle emit cAMP, the corresponding values of x and y are both 1 in the table (indicated by arrows in Fig. 5.5(a)). As in the delayed image, the corresponding grid for y does not emit cAMP, so the value of y' is 0 in the table (also indicated by an arrow in Fig. 5.5(a)). This is the way in which the numbers of all possible outcomes of the table (Fig. 5.5(a))

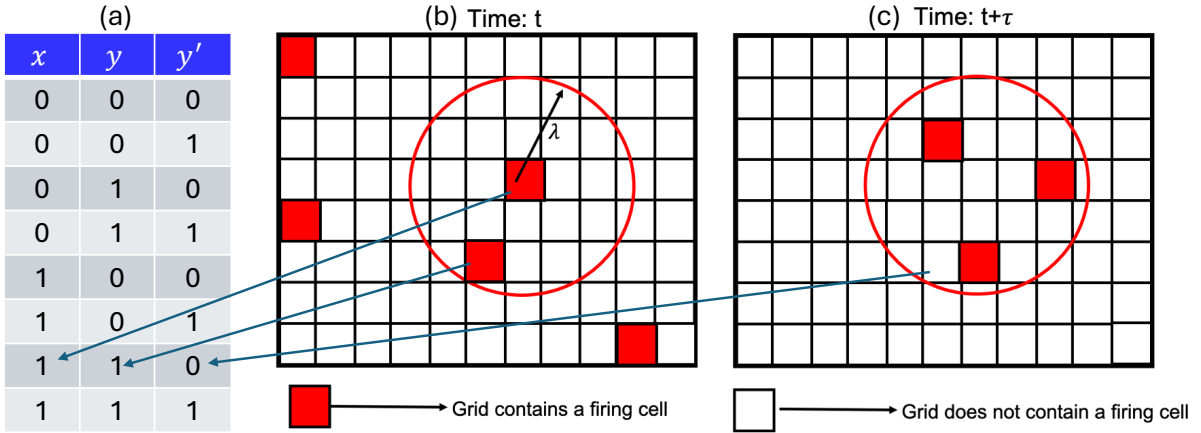


Figure 5.5. Graphical representation of the application of TE vs cutoff distance (λ) approach between the images of *D. discoideum* cells at time t and $t + \tau$. (a) shows the possible outcomes or firing frequencies of the triplets (x, y, y') between the images. (b) Image at time t , where red indicates the firing cells and white indicates the non firing cells. (c) Image at the delayed time $t + \tau$.

are counted only for the circle of cutoff distance λ for all grids of the images. Then the joint probabilities of the possible outcomes, i.e., $p(x, y, y')$ are estimated based on the number of possible outcomes. In the case of *D. discoideum* cells, the approach based on TE vs cutoff distance (λ) between the images at time t and $t + \tau$ is defined as follows:

$$TE_{X_t \rightarrow Y_{t+\tau}}(\tau, d < \lambda, t) = H(Y_{t+\tau}|Y_t, d < \lambda, t) - H(Y_{t+\tau}|Y_t, X_t, d < \lambda, t). \quad (5.2)$$

Here, the quantity $H(Y_{t+\tau}|Y_t, X_t, d < \lambda, t)$, i.e., the conditional entropy of $Y_{t+\tau}$ when the information of Y_t and X_t at time t is given if the distance $d(x, y)$ is less than the cutoff distance λ , where $x \in X_t$ and $y \in Y_t$, is defined by,

$$H(Y_{t+\tau}|Y_t, X_t, d < \lambda, t) = - \sum_{x \in X_t} \sum_{\substack{y \in Y_t \\ (=X_t/x, d(x,y) < \lambda)}} \sum_{\substack{y' \in Y_{t+\tau} \\ (=X_{t+\tau}/x, d(y',y) = 0)}} p(y', y, x|t) \times \log_2 \left(\frac{p(y', y, x|t)}{p(y, x|t)} \right) \quad (5.3)$$

Then, using Eq. 5.2, TE from the image at time t to the delayed image at time $t + \tau$ is computed only for the circle of distance λ based on Eq. 5.3. The same procedure is repeated to systematically estimate the TE between the images varying the size of λ from small to large values. The results obtained by applying the above approach in the early phase to fully developed cAMP spiral wave phases of *D. discoideum* cells are illustrated

in Fig. 5.7.

5.3.3 Results and discussion

A total of 1,190 images of *D. discoideum* cells were systematically recorded at every 30-second time interval during the observation period. It was noticed that the cAMP wave started to emerge around image number 400 and then the wave progressed over time. Figure 5.6 demonstrates the cAMP wave patterns in *D. discoideum* cells at three distinct time points throughout the observation period.

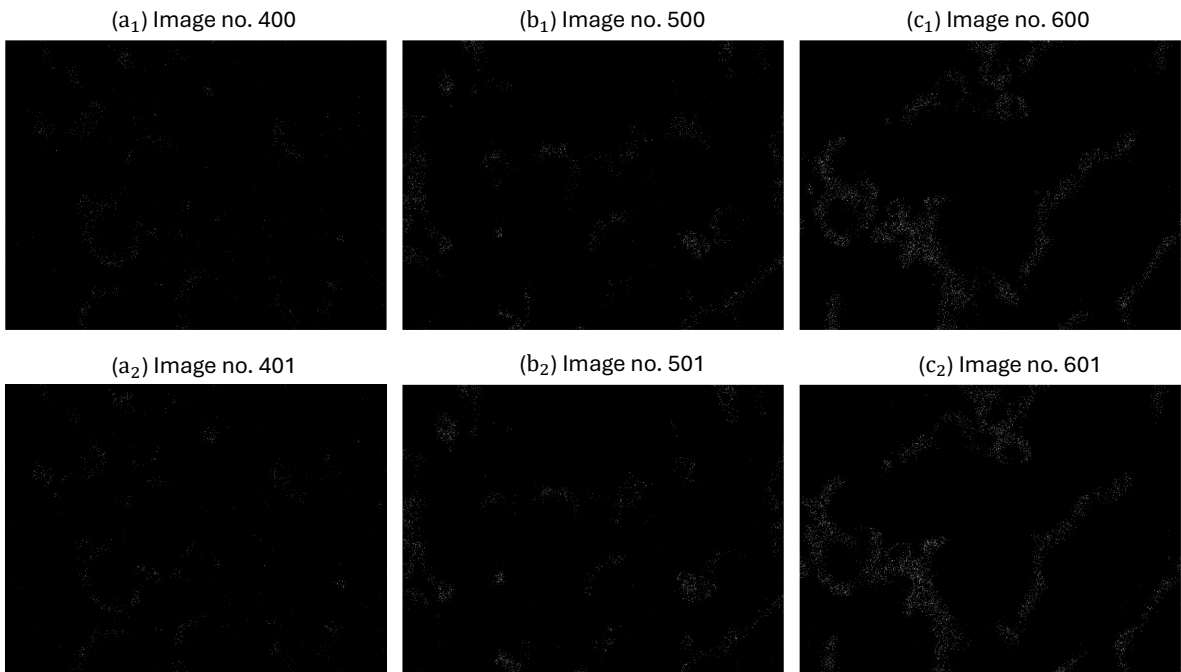


Figure 5.6. Demonstration of cAMP wave patterns in *D. discoideum* cells at three distinct time stages during the observation period. (a₁ & a₂) show the waves for two consecutive images at the initial phase of wave formation. (b₁ & b₂) depict the waves for two consecutive images during the intermediate phase of wave development. (c₁ & c₂) present the waves for two consecutive images at the fully developed phase of wave.

In this analysis, the TE vs cutoff distance λ approach is applied between these consecutive image pairs (specifically, $TE_{400 \rightarrow 401}(\lambda)$, $TE_{500 \rightarrow 501}(\lambda)$, and $TE_{600 \rightarrow 601}(\lambda)$) to infer the interaction distance (R) between *D. discoideum* cells at these distinct time stages of wave progression. Figure 5.7 demonstrates the results of TE vs λ and its gradient with respect to λ for images a₁ to a₂ (blue), images b₁ to b₂ (orange), and images c₁ to c₂ (red). It is observed that TE monotonically decreases with increasing λ for images of the early phase (Fig. 5.7(a), blue), whereas it exhibits a plateau for the images when time goes

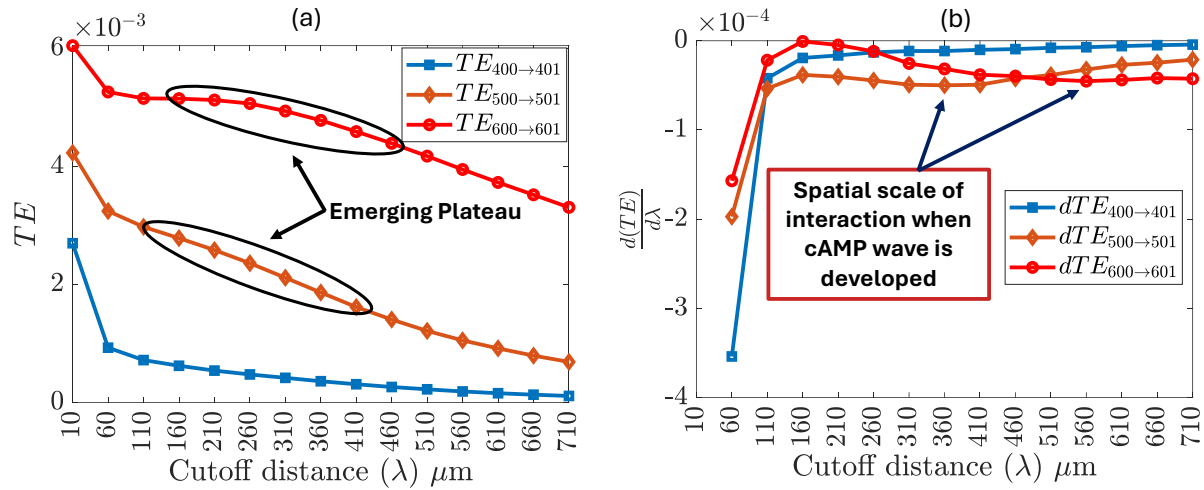


Figure 5.7. (a) TE vs cutoff distance λ and (b) gradient of TE with respect to λ are shown for consecutive image pairs at three distinct time points of cAMP wave progression. At the early stage of wave formation (i.e., images a_1 to a_2), the TE vs λ relationship does not show any plateau. However, when time goes on from early stage to fully wave development stages (i.e., images b_1 to b_2 , and images c_1 to c_2), TE vs λ exhibits a plateau. The derivative of TE also shows this behavior (i.e., a local minima) near the distance $\lambda = 360 \mu\text{m}$ for images b_1 to b_2 , and near the distance $\lambda = 560 \mu\text{m}$ for images c_1 to c_2 , which may be the possible spatial scale of interaction at these time points of wave development. Notably, in the early phase, there is no local minima in the derivative of TE .

on to wave development stages (i.e., images b_1 to b_2 , and images c_1 to c_2) (Fig. 5.7(a)), orange and red, respectively). The derivative of TE with respect to λ , i.e., $\frac{d(TE)}{d\lambda}$ also exhibits local minima for the development stages around the distance $\lambda = 360 \mu\text{m}$ for images b_1 to b_2 , and around the distance $\lambda = 560 \mu\text{m}$ for images c_1 to c_2 , which may be an indication of the possible spatial scale of interaction at these time points of wave progression (Fig. 5.7(b), orange and red, respectively). However, similar to the TE , the $\frac{d(TE)}{d\lambda}$ also does not show any clue for the images at the early stage of wave formation (Fig. 5.7(b), blue). Another important observation is that the inferred spatial scale of interaction changes dynamically over time. The intuitive explanation is as follows: during the early stage of wave formation, a few cells emit cAMP, most cells have low cAMP intensities that may not be sufficient to respond to the cAMP signals of nearby cells. Consequently, cells mostly move randomly, and TE decreases monotonically over λ without showing any clue of the spatial scale of interaction. In contrast, when wave development stages progress over time, more cells emit cAMP signals because the cAMP intensities increased. At these stages, the intensities may become sufficient for cells to respond to the cAMP signals of neighboring cells, leading to a collective wave of cAMP

signals in their movements. Therefore, TE decreases over λ involving a plateau (clue) at a certain value of λ that may be the expected spatial scale of interaction, since a similar indication was also observed at the ground truth of the interaction distance (R) in the simulation data of Basak et al. [76]. Additionally, since the number of cAMP pulsing cells varies as the wave development stages progress over time, it is reasonable to obtain the different spatial scales of interaction over time.

5.4 Concluding Remarks

This chapter describes the inference of the interaction distance R between *D. discoideum* cells. Here, TE vs cutoff distance λ and its derivative, i.e., $\frac{d(TE)}{d\lambda}$, are estimated for the consecutive image pairs obtained at three different stages (such as early phase, intermediary phase, and fully developed phase) of the cAMP wave formation. For the images of the early stage, it is observed that neither TE vs λ nor its derivative shows any clear indication of the spatial scale of interaction. However, as wave development progresses over time, both show a kick at a specific value of λ , which likely corresponds to the expected spatial scale of interaction. Furthermore, since the number of cAMP pulsing cells varies over time, it is also reasonable to obtain different spatial scales of interaction over time.

Chapter 6

General conclusions

In this study, a new scheme has been proposed to predict direct/indirect interactions between a pair of agents solely from their pairwise time series, while keeping the remaining agents of the system hidden from the analysis. The working hypothesis of this study is that, under the assumption of stationary, the modified transfer entropy (*MT*)—which is upper-bounded by $H(Y_{t+\tau}|Y_{t+\tau-1})$ independent of the time delay τ —monotonically decreases as time delay τ increases when agents interact directly with each other. The feasibility of this hypothesis has been demonstrated by analyzing the time series data of agents simulated using the modified Vicsek model (VM) and the Langevin dynamics (LD) model under four schematic interaction networks including unidirectional and bidirectional effects. It was found that the working hypothesis works for different conditions of both model systems varying their parameter values, including some deviations found at small noise levels with very strong coupling strengths.

In this study, one key observation is that the interaction timescale τ_0 —that is, the time delay (or time lag) at which the motion of one agent affects the motions of other agents in a system—is predefined in the case of modified VM (i.e., $\tau_0 = \text{simulation time step}(\Delta t) = 1$). So, in this model, the proposed scheme can be applied in a simple manner to distinguish direct and indirect interactions between a pair of agents as a function of the time delay τ in units of the simulation time step ($\Delta t = 1$).

In contrast, in the LD model—which is more representative of real-world systems such as cell dynamics where the timescale is unknown—the proposed scheme generally requires a two-steps approach. Firstly, one needs to determine the interaction timescale τ_0 of agents in a system. Since the simulation time step Δt does not necessarily correspond

to the interaction timescale τ_0 of agents in this model. This is because the simulation time step may not be the appropriate time delay for an agent to feel any interaction from another agent. Secondly, the estimation of MT values for each pair of agents over time delay τ in units of the estimated interaction timescale τ_0 to predict their interactions —direct or indirect —following the pattern of MT values over time delay τ . A heuristic method such as the autocorrelation function (ACF) is used to estimate the timescale of interaction τ_0 from time series of agents. Here, the decay rates of the ACF curves of the velocity trajectories of individual agents are determined by fitting an appropriate curve. Then the mean of the timescales of all agents was taken as the interaction timescale τ_0 to measure MT values for each pair of agents. However, this heuristic approach may be less effective in predicting direct and indirect interactions by applying MT in an individual pair of agents in a system, particularly when the interaction timescales of individual agents in a system are more heterogeneous. The proposed scheme may also provide inconsistent prediction of the direct and indirect influences of agents in a system, especially if the common driver effect exists between agents. For example, in an interaction chain such as $X \leftrightarrow Y \leftrightarrow Z$ (where Y serves as a common driver for both X and Z) the scheme can provide inconsistent results when the coupling strengths are very different.

Furthermore, the working hypothesis has also been examined in predicting direct/indirect interactions of agents using the standard transfer entropy (TE) measure, which is upper-bounded by $H(Y_{t+\tau}|Y_t)$ varies over time delay τ . It is observed that TE does not support the working hypothesis at lower noise levels in modified VM, that is, it does not decrease monotonically with time delay τ when agents interact directly. However, it supports the hypothesis at moderate to higher noise levels. In case of the LD model, it is found that TE supports the hypothesis for almost all thermal noise levels. Therefore, the reason for violating the hypothesis at lower noise levels in modified VM is that the variation in the upper bound $H(Y_{t+\tau}|Y_t)$ which is much more prominent over τ in modified VM at lower noise levels, while the variation is less prominent in the LD model. Since the possible variation in the upper bound of TE may lead to the inconsistent inference of direct / indirect interactions, modified transfer entropy (MT)—whose upper bound does not vary over time delay τ —is a more reliable measure for the inference of direct/indirect interactions between agents over time delay τ .

The next subjects are to predict direct and indirect influences between agents from their pairwise time series observed in the systems of many agents involving heterogeneous interactions among agents, multiple hidden agents, and variations in space and interaction over time. To address these challenges using information-theoretic measures, a deeper exploration is required. The proposed scheme offers an approach for predicting both direct and indirect influences among agents in dynamic, time-varying systems, as studied in Ref. [111]. Suppose a network in which mobile agents A1, B1, and C1 are placed at site-1 (e.g., spatial region), and A2, B2, and C2 at site-2. Furthermore, agents A1, B1, A2, and B2 independently switch places and interact with agents they encounter, while C1 and C2 do not. In such a case, the metric MT between agents C1 and C2 may provide a nonmonotonic trend over time delay τ , reflecting their purely indirect interactions through mobile agents. On the other hand, the monotonic behavior of MT between co-located agents may depend on how often and how quickly they switch places.

Also, to apply the proposed scheme to experimental data, for instance, cell dynamics, the question of sampling rate should be addressed. It is expected that the dependency of MT on time delay τ , expressed in units of the interaction timescale τ_0 , may provide a new means to distinguish direct or indirect interactions between agents from trajectory data in a wide range of research domains when the appropriate sampling rate is available.

Bibliography

1. S. Hubbard, P. Babak, S. T. Sigurdsson, and K. G. Magnússon, “A model of the formation of fish schools and migrations of fish,” *Ecol. Modell.*, vol. 174, no. 4, pp. 359–374, 2004.
2. U. Lopez, J. Gautrais, I. D. Couzin, and G. Theraulaz, “From behavioural analyses to models of collective motion in fish schools,” *Interface focus*, vol. 2, no. 6, pp. 693–707, 2012.
3. W. Bialek, A. Cavagna, I. Giardina, T. Mora, E. Silvestri, M. Viale, and A. M. Walczak, “Statistical mechanics for natural flocks of birds,” *Proc. Natl. Acad. Sci. USA.*, vol. 109, no. 13, pp. 4786–4791, 2012.
4. D. H. Morse, “Ecological aspects of some mixed-species foraging flocks of birds,” *Ecol. Monogr.*, vol. 40, no. 1, pp. 119–168, 1970.
5. X. Wang and J. Lu, “Collective behaviors through social interactions in bird flocks,” *IEEE Circuits and Systems Magazine*, vol. 19, no. 3, pp. 6–22, 2019.
6. J. Buhl, D. J. Sumpter, I. D. Couzin, J. J. Hale, E. Despland, E. R. Miller, and S. J. Simpson, “From disorder to order in marching locusts,” *Science*, vol. 312, no. 5778, pp. 1402–1406, 2006.
7. A. Sokolov, I. S. Aranson, J. O. Kessler, and R. E. Goldstein, “Concentration dependence of the collective dynamics of swimming bacteria,” *Phys. Rev. Lett.*, vol. 98, no. 15, p. 158102, 2007.
8. A. Czirók, E. Ben-Jacob, I. Cohen, and T. Vicsek, “Formation of complex bacterial colonies via self-generated vortices,” *Phys. Rev. E*, vol. 54, no. 2, p. 1791, 1996.

9. K. J. Cheung, E. Gabrielson, Z. Werb, and A. J. Ewald, “Collective invasion in breast cancer requires a conserved basal epithelial program,” *Cell*, vol. 155, no. 7, pp. 1639–1651, 2013.
10. Y. Yang, N. Jamilpour, B. Yao, Z. S. Dean, R. Riahi, and P. K. Wong, “Probing leader cells in endothelial collective migration by plasma lithography geometric confinement,” *Sci. Rep.*, vol. 6, no. 1, p. 22707, 2016.
11. T. Vicsek and A. Zafeiris, “Collective motion,” *Phys. Rep.*, vol. 517, no. 3-4, pp. 71–140, 2012.
12. T. Vicsek, “Universal patterns of collective motion from minimal models of flocking,” in *2008 Second IEEE International Conference on Self-Adaptive and Self-Organizing Systems*, pp. 3–11, IEEE, 2008.
13. N. Kumar, H. Soni, S. Ramaswamy, and A. Sood, “Flocking at a distance in active granular matter,” *Nature communications*, vol. 5, no. 1, p. 4688, 2014.
14. T. Sanchez, D. T. Chen, S. J. DeCamp, M. Heymann, and Z. Dogic, “Spontaneous motion in hierarchically assembled active matter,” *Nature*, vol. 491, no. 7424, pp. 431–434, 2012.
15. W. Wang, W. Duan, S. Ahmed, A. Sen, and T. E. Mallouk, “From one to many: Dynamic assembly and collective behavior of self-propelled colloidal motors,” *Accounts of chemical research*, vol. 48, no. 7, pp. 1938–1946, 2015.
16. A. Kaiser, A. Snezhko, and I. S. Aranson, “Flocking ferromagnetic colloids,” *Science advances*, vol. 3, no. 2, p. e1601469, 2017.
17. M. Ibele, T. E. Mallouk, and A. Sen, “Schooling behavior of light-powered autonomous micromotors in water,” *Angewandte Chemie*, vol. 121, no. 18, pp. 3358–3362, 2009.
18. J. Elgeti, R. G. Winkler, and G. Gompper, “Physics of microswimmers—single particle motion and collective behavior: a review,” *Reports on progress in physics*, vol. 78, no. 5, p. 056601, 2015.

19. I. D. Couzin, J. Krause, *et al.*, “Self-organization and collective behavior in vertebrates,” *Advances in the Study of Behavior*, vol. 32, no. 1, pp. 10–1016, 2003.
20. J. Gaskell, N. Campioni, J. M. Morales, D. Husmeier, and C. J. Torney, “Inferring the interaction rules of complex systems with graph neural networks and approximate bayesian computation,” *Journal of the Royal Society Interface*, vol. 20, no. 198, p. 20220676, 2023.
21. F. Battiston, E. Amico, A. Barrat, G. Bianconi, G. Ferraz de Arruda, B. Franceschiello, I. Iacopini, S. Kéfi, V. Latora, Y. Moreno, *et al.*, “The physics of higher-order interactions in complex systems,” *Nature Physics*, vol. 17, no. 10, pp. 1093–1098, 2021.
22. C. Szabo, Y. M. Teo, and G. K. Chngleput, “Understanding complex systems: Using interaction as a measure of emergence,” in *Proceedings of the Winter Simulation Conference 2014*, pp. 207–218, IEEE, 2014.
23. S. K. Stavroglou, A. A. Pantelous, H. E. Stanley, and K. M. Zuev, “Unveiling causal interactions in complex systems,” *Proceedings of the National Academy of Sciences*, vol. 117, no. 14, pp. 7599–7605, 2020.
24. A. M. Reynolds, G. E. McIvor, A. Thornton, P. Yang, and N. T. Ouellette, “Stochastic modelling of bird flocks: accounting for the cohesiveness of collective motion,” *Journal of the Royal Society Interface*, vol. 19, no. 189, p. 20210745, 2022.
25. A. K. Mishra, J. P. Campanale, J. A. Mondo, and D. J. Montell, “Cell interactions in collective cell migration,” *Development*, vol. 146, no. 23, p. dev172056, 2019.
26. F. R. Adler, A. R. Anderson, A. Bhushan, P. Bogdan, J. J. Bravo-Cordero, A. Brock, Y. Chen, E. Cukierman, K. E. DelGiorno, G. V. Denis, *et al.*, “Modeling collective cell behavior in cancer: Perspectives from an interdisciplinary conversation,” *Cell systems*, vol. 14, no. 4, pp. 252–257, 2023.
27. U. S. Basak, “Study on identification of leader and follower agents and its interaction domain from trajectories in a collectively moving colony,” *phd thesis*, 2021.

28. C. C. Ioannou and K. L. Laskowski, “A multi-scale review of the dynamics of collective behaviour: from rapid responses to ontogeny and evolution,” *Philosophical transactions of the royal society B*, vol. 378, no. 1874, p. 20220059, 2023.
29. A. E. King and M. S. Turner, “Non-local interactions in collective motion,” *Royal Society open science*, vol. 8, no. 3, p. 201536, 2021.
30. N. T. Ouellette and D. M. Gordon, “Goals and limitations of modeling collective behavior in biological systems,” *Frontiers in Physics*, vol. 9, p. 687823, 2021.
31. M. Ponce C, C. Masoller, and A. C. Martí, “Synchronizability of chaotic logistic maps in delayed complex networks,” *Eur. Phys. J. B*, vol. 67, pp. 83–93, 2009.
32. S. Leng, H. Ma, J. Kurths, Y.-C. Lai, W. Lin, K. Aihara, and L. Chen, “Partial cross mapping eliminates indirect causal influences,” *Nature communications*, vol. 11, no. 1, p. 2632, 2020.
33. M. Aldana and C. Huepe, “Phase transitions in self-driven many-particle systems and related non-equilibrium models: a network approach,” *Journal of Statistical Physics*, vol. 112, pp. 135–153, 2003.
34. A. Cavagna, I. Giardina, and T. S. Grigera, “The physics of flocking: Correlation as a compass from experiments to theory,” *Physics Reports*, vol. 728, pp. 1–62, 2018.
35. T. Walser, X. Cui, J. Yanagawa, J. M. Lee, E. Heinrich, G. Lee, S. Sharma, and S. M. Dubinett, “Smoking and lung cancer: the role of inflammation,” *Proceedings of the American Thoracic Society*, vol. 5, no. 8, pp. 811–815, 2008.
36. G. W. Warren and K. M. Cummings, “Tobacco and lung cancer: risks, trends, and outcomes in patients with cancer,” *American Society of Clinical Oncology Educational Book*, vol. 33, no. 1, pp. 359–364, 2013.
37. V. J. López-Madrona, F. S. Matias, C. R. Mirasso, S. Canals, and E. Pereda, “Inferring correlations associated to causal interactions in brain signals using autoregressive models,” *Scientific reports*, vol. 9, no. 1, p. 17041, 2019.
38. S. L. Bressler and A. K. Seth, “Wiener–granger causality: a well established methodology,” *Neuroimage*, vol. 58, no. 2, pp. 323–329, 2011.

39. S. Z. Chiou-Wei, C.-F. Chen, and Z. Zhu, “Economic growth and energy consumption revisited—evidence from linear and nonlinear granger causality,” *Energy economics*, vol. 30, no. 6, pp. 3063–3076, 2008.
40. R. Horváth, J. Seidler, and L. Weill, “Bank capital and liquidity creation: Granger-causality evidence,” *Journal of Financial Services Research*, vol. 45, pp. 341–361, 2014.
41. L. Keele, “Social capital and the dynamics of trust in government,” *American journal of political science*, vol. 51, no. 2, pp. 241–254, 2007.
42. Y. Chen, G. Rangarajan, J. Feng, and M. Ding, “Analyzing multiple nonlinear time series with extended granger causality,” *Physics letters A*, vol. 324, no. 1, pp. 26–35, 2004.
43. N. D. Mukhopadhyay and S. Chatterjee, “Causality and pathway search in microarray time series experiment,” *Bioinformatics*, vol. 23, no. 4, pp. 442–449, 2007.
44. S. Li, Y. Xiao, D. Zhou, and D. Cai, “Causal inference in nonlinear systems: Granger causality versus time-delayed mutual information,” *Phys. Rev. E*, vol. 97, no. 5, p. 052216, 2018.
45. T. Schreiber, “Measuring information transfer,” *Phys. Rev. Lett.*, vol. 85, no. 2, p. 461, 2000.
46. M. Rubinov and O. Sporns, “Complex network measures of brain connectivity: uses and interpretations,” *Neuroimage*, vol. 52, no. 3, pp. 1059–1069, 2010.
47. R. Vicente, M. Wibral, M. Lindner, and G. Pipa, “Transfer entropy—a model-free measure of effective connectivity for the neurosciences,” *Journal of computational neuroscience*, vol. 30, no. 1, pp. 45–67, 2011.
48. M. Wibral, B. Rahm, M. Rieder, M. Lindner, R. Vicente, and J. Kaiser, “Transfer entropy in magnetoencephalographic data: quantifying information flow in cortical and cerebellar networks,” *Progress in biophysics and molecular biology*, vol. 105, no. 1-2, pp. 80–97, 2011.

49. M. Bauer, J. W. Cox, M. H. Caveness, J. J. Downs, and N. F. Thornhill, “Finding the direction of disturbance propagation in a chemical process using transfer entropy,” *IEEE transactions on control systems technology*, vol. 15, no. 1, pp. 12–21, 2006.
50. S. K. Baek, W.-S. Jung, O. Kwon, and H.-T. Moon, “Transfer entropy analysis of the stock market,” *arXiv preprint physics/0509014*, 2005.
51. R. Marschinski and H. Kantz, “Analysing the information flow between financial time series: An improved estimator for transfer entropy,” *The European Physical Journal B-Condensed Matter and Complex Systems*, vol. 30, pp. 275–281, 2002.
52. C. W. Kulp and D. Schlingmann, “Using mathematica to compose music and analyze music with information theory,” in *International Conference on Mathematics and Computation in Music*, pp. 441–448, Springer, 2007.
53. N. A. Aziz, “Transfer entropy as a tool for inferring causality from observational studies in epidemiology,” *bioRxiv*, p. 149625, 2017.
54. F. Delussu, M. Tizzoni, and L. Gauvin, “The limits of human mobility traces to predict the spread of covid-19: A transfer entropy approach,” *PNAS nexus*, vol. 2, no. 10, p. pgad302, 2023.
55. Y. Chen, S. L. Bressler, and M. Ding, “Frequency decomposition of conditional granger causality and application to multivariate neural field potential data,” *Journal of neuroscience methods*, vol. 150, no. 2, pp. 228–237, 2006.
56. Z. Zhou, Y. Chen, M. Ding, P. Wright, Z. Lu, and Y. Liu, “Analyzing brain networks with pca and conditional granger causality,” *Human brain mapping*, vol. 30, no. 7, pp. 2197–2206, 2009.
57. C. Zou, C. Ladroue, S. Guo, and J. Feng, “Identifying interactions in the time and frequency domains in local and global networks-a granger causality approach,” *BMC bioinformatics*, vol. 11, pp. 1–17, 2010.
58. V. A. Vakorin, O. A. Krakovska, and A. R. McIntosh, “Confounding effects of indirect connections on causality estimation,” *Journal of neuroscience methods*, vol. 184, no. 1, pp. 152–160, 2009.

59. A. Papana, D. Kugiumtzis, and P. G. Larsson, “Detection of direct causal effects and application to epileptic electroencephalogram analysis,” *International Journal of Bifurcation and Chaos*, vol. 22, no. 09, p. 1250222, 2012.
60. P. Duan, F. Yang, T. Chen, and S. L. Shah, “Direct causality detection via the transfer entropy approach,” *IEEE transactions on control systems technology*, vol. 21, no. 6, pp. 2052–2066, 2013.
61. J. Sun and E. M. Bollt, “Causation entropy identifies indirect influences, dominance of neighbors and anticipatory couplings,” *Physica D*, vol. 267, pp. 49–57, 2014.
62. J. Sun, D. Taylor, and E. M. Bollt, “Causal network inference by optimal causation entropy,” *SIAM J. Appl. Dyn. Syst.*, vol. 14, no. 1, pp. 73–106, 2015.
63. S. Roy, “Quantifying interactions among car drivers using information theory,” *Chaos*, vol. 30, no. 11, p. 113125, 2020.
64. R. Sipahi and M. Porfiri, “Improving on transfer entropy-based network reconstruction using time-delays: Approach and validation,” *Chaos: An Interdisciplinary Journal of Nonlinear Science*, vol. 30, no. 2, 2020.
65. M. Wibral, N. Pampu, V. Priesemann, F. Siebenhühner, H. Seiwert, M. Lindner, J. T. Lizier, and R. Vicente, “Measuring information-transfer delays,” *PLoS One*, vol. 8, no. 2, p. e55809, 2013.
66. Y. Shu and J. Zhao, “Data-driven causal inference based on a modified transfer entropy,” *Comput. Chem. Eng.*, vol. 57, pp. 173–180, 2013.
67. S. Sattari, U. S. Basak, R. G. James, L. W. Perrin, J. P. Crutchfield, and T. Komatsuzaki, “Modes of information flow in collective cohesion,” *Sci. Adv.*, vol. 8, no. 6, p. eabj1720, 2022.
68. J. A. Anderson, J. Glaser, and S. C. Glotzer, “Hoomd-blue: A python package for high-performance molecular dynamics and hard particle monte carlo simulations,” *Comput. Mater. Sci.*, vol. 173, p. 109363, 2020.
69. H. Chaté, F. Ginelli, G. Grégoire, F. Peruani, and F. Raynaud, “Modeling collective motion: variations on the vicsek model,” *Eur. Phys. J. B*, vol. 64, pp. 451–456, 2008.

70. H. Serna and W. T. Gózdź, “The influence of obstacles on the collective motion of self-propelled objects,” *Physica A: Statistical Mechanics and its Applications*, vol. 625, p. 129042, 2023.
71. J.-x. Qian and Y.-q. Lu, “The collective motion of self-propelled particles affected by the spatial-dependent noise based on vicsek rules,” *Physica A: Statistical Mechanics and its Applications*, vol. 626, p. 129079, 2023.
72. Z. Kirchner, A. Geohagan, and A. Truszkowska, “A vicsek-type model of confined cancer cells with variable clustering affinities,” *Integrative Biology*, vol. 16, p. zya005, 2024.
73. S. De Karmakar, A. Chugh, and R. Ganesh, “Collective behavior of soft self-propelled disks with rotational inertia,” *Scientific Reports*, vol. 12, no. 1, p. 22563, 2022.
74. R. S. Negi, R. G. Winkler, and G. Gompper, “Emergent collective behavior of active brownian particles with visual perception,” *Soft Matter*, vol. 18, no. 33, pp. 6167–6178, 2022.
75. T. Ichiye and M. Karplus, “Collective motions in proteins: a covariance analysis of atomic fluctuations in molecular dynamics and normal mode simulations,” *Proteins*, vol. 11, no. 3, pp. 205–217, 1991.
76. U. S. Basak, S. Sattari, K. Horikawa, and T. Komatsuzaki, “Inferring domain of interactions among particles from ensemble of trajectories,” *Phys. Rev. E*, vol. 102, no. 1, p. 012404, 2020.
77. M. W. Hounslow, M. Domeier, and A. J. Biggin, “Subduction flux modulates the geomagnetic polarity reversal rate,” *Tectonophysics*, vol. 742, pp. 34–49, 2018.
78. D. Yang, H. Chen, Y. Song, and Z. Gong, “Granger causality for multivariate time series classification,” in *2017 IEEE international conference on big knowledge (ICBK), Hefei, China, 09-10 August*, pp. 103–110, 2017.
79. C. W. Granger, “Investigating causal relations by econometric models and cross-spectral methods,” *Econometrica*, pp. 424–438, 1969.

80. U. S. Basak, S. Sattari, M. Hossain, K. Horikawa, and T. Komatsuzaki, “Transfer entropy dependent on distance among agents in quantifying leader-follower relationships,” *Biophys. Physicobiol.*, vol. 18, pp. 131–144, 2021.
81. T. M. Cover, *Elements of information theory*. John Wiley & Sons, Cham, Switzerland, 1999.
82. T. Bossomaier, L. Barnett, M. Harré, J. T. Lizier, T. Bossomaier, L. Barnett, M. Harré, and J. T. Lizier, *An Introduction to Transfer Entropy*. Springer, Hoboken, New Jersey, 2016.
83. A. Kraskov, H. Stögbauer, and P. Grassberger, “Estimating mutual information,” *Phys. rev. E*, vol. 69, no. 6, p. 066138, 2004.
84. J. Jeong, J. C. Gore, and B. S. Peterson, “Mutual information analysis of the eeg in patients with alzheimer’s disease,” *Clin. Neurophysiol.*, vol. 112, no. 5, pp. 827–835, 2001.
85. S.-H. Jin, Y.-J. Kwon, J.-S. Jeong, S.-W. Kwon, and D.-H. Shin, “Differences in brain information transmission between gifted and normal children during scientific hypothesis generation,” *Brain Cogn.*, vol. 62, no. 3, pp. 191–197, 2006.
86. T. Vicsek, A. Czirók, E. Ben-Jacob, I. Cohen, and O. Shochet, “Novel type of phase transition in a system of self-driven particles,” *Phys. Rev. Lett.*, vol. 75, no. 6, p. 1226, 1995.
87. J. Brown, T. Bossomaier, and L. Barnett, “Information flow in finite flocks,” *Sci. Rep.*, vol. 10, no. 1, p. 3837, 2020.
88. J. M. Brown, T. Bossomaier, and L. Barnett, “Information transfer in finite flocks with topological interactions,” *Journal of Computational Science*, vol. 53, p. 101370, 2021.
89. P. Clusella and R. Pastor-Satorras, “Phase transitions on a class of generalized vicsek-like models of collective motion,” *Chaos: An Interdisciplinary Journal of Nonlinear Science*, vol. 31, no. 4, 2021.

90. L. Sang-Hee, N. Van Thanh, N. A. Viet, *et al.*, “Study on the phase transition behavior of fishes schooling system,” *Communications in Physics*, vol. 23, no. 2, pp. 121–121, 2013.
91. Y. Yang, F. Turci, E. Kague, C. L. Hammond, J. Russo, and C. P. Royall, “Dominating lengthscales of zebrafish collective behaviour,” *PLoS computational biology*, vol. 18, no. 1, p. e1009394, 2022.
92. X. Lu, C. Zhang, and B. Qin, “An improved vicsek model of swarm based on remote neighbors strategy,” *Physica A: Statistical Mechanics and its Applications*, vol. 587, p. 126553, 2022.
93. X. Lu, C. Zhang, C. Huang, and B. Qin, “Research on swarm consistent performance of improved vicsek model with neighbors’ degree,” *Physica A: Statistical Mechanics and its Applications*, vol. 588, p. 126567, 2022.
94. G. Dieck Kattas and M. Small, “Building computational models of swarms from simulated positional data,” in *Advances in Swarm Intelligence: Second International Conference, ICSI 2011, Chongqing, China, June 12-15, 2011, Proceedings, Part I* 2, pp. 9–18, Springer, 2011.
95. B. K. Haddon, “Cycle-sort: a linear sorting method,” *The Computer Journal*, vol. 33, no. 4, pp. 365–367, 1990.
96. J. T. Lizier, “Jidt: An information-theoretic toolkit for studying the dynamics of complex systems,” *Front. Robot. AI*, vol. 1, p. 11, 2014.
97. H. Abarbanel, *Analysis of observed chaotic data*. Springer Science & Business Media, 2012.
98. J. D. Murray, A. Bernacchia, D. J. Freedman, R. Romo, J. D. Wallis, X. Cai, C. Padoa-Schioppa, T. Pasternak, H. Seo, D. Lee, *et al.*, “A hierarchy of intrinsic timescales across primate cortex,” *Nature neuroscience*, vol. 17, no. 12, pp. 1661–1663, 2014.
99. R. Zeraati, T. A. Engel, and A. Levina, “A flexible bayesian framework for unbiased estimation of timescales,” *Nature computational science*, vol. 2, no. 3, pp. 193–204, 2022.

100. F. P. Spitzner, J. Dehning, J. Wilting, A. Hagemann, J. P. Neto, J. Zierenberg, and V. Priesemann, “Mr. estimator, a toolbox to determine intrinsic timescales from subsampled spiking activity,” *PLoS One*, vol. 16, no. 4, p. e0249447, 2021.
101. M. Steinert, “Pathogen–host interactions in dictyostelium, legionella, mycobacterium and other pathogens,” in *Seminars in cell & developmental biology*, vol. 22, pp. 70–76, Elsevier, 2011.
102. O. Lamrabet, T. Jauslin, W. C. Lima, M. Leippe, and P. Cosson, “The multifarious lysozyme arsenal of dictyostelium discoideum,” *Developmental & Comparative Immunology*, vol. 107, p. 103645, 2020.
103. S. D. Rosen, J. A. Kafka, D. L. Simpson, and S. H. Barondes, “Developmentally regulated, carbohydrate-binding protein in dictyostelium discoideum,” *Proceedings of the National Academy of Sciences*, vol. 70, no. 9, pp. 2554–2557, 1973.
104. D. Watts and J. Ashworth, “Growth of myxamoebae of the cellular slime mould dictyostelium discoideum in axenic culture,” *Biochemical Journal*, vol. 119, no. 2, p. 171, 1970.
105. Y. Maeda and J. Chida, “Control of cell differentiation by mitochondria, typically evidenced in dictyostelium development,” *Biomolecules*, vol. 3, no. 4, pp. 943–966, 2013.
106. P. C. Newell, “Cellular communication during aggregation of dictyostelium: The second Fleming lecture:(delivered at the general meeting of the society for general microbiology on 8 september 1977),” *Microbiology*, vol. 104, no. 1, pp. 1–13, 1978.
107. A. R. Kimmel and R. A. Firtel, “Breaking symmetries: regulation of dictyostelium development through chemoattractant and morphogen signal-response,” *Current opinion in genetics & development*, vol. 14, no. 5, pp. 540–549, 2004.
108. U. S. Basak, S. Sattari, M. M. Hossain, K. Horikawa, and T. Komatsuzaki, “An information-theoretic approach to infer the underlying interaction domain among elements from finite length trajectories in a noisy environment,” *J. Chem. Phys.*, vol. 154, no. 3, p. 034901, 2021.

109. J. D. Dunn, C. Bosmani, C. Barisch, L. Raykov, L. H. Lefrançois, E. Cardenal-Muñoz, A. T. López-Jiménez, and T. Soldati, “Eat prey, live: *Dictyostelium discoideum* as a model for cell-autonomous defenses,” *Frontiers in immunology*, vol. 8, p. 1906, 2018.
110. V. Nanjundiah, “The evolution of communication and social behaviour in *dictyostelium discoideum*,” *Proceedings: Animal Sciences*, vol. 94, pp. 639–653, 1985.
111. G. Mikaberidze, S. N. Chowdhury, A. Hastings, and R. M. D’Souza, “Consensus formation among mobile agents in networks of heterogeneous interaction venues,” *Chaos, Solitons & Fractals*, vol. 178, p. 114298, 2024.

Appendix A

Appendix

A.1 Hypothetical statistical test

In this study, to investigate whether the estimated MT (Note that the same hypothetical test can also be applied for TE) values are meaningfully different over consecutive time delays τ (for example, $MT(\tau = 1) - MT(\tau = 2)$, $MT(\tau = 2) - MT(\tau = 3)$, \dots) or not, a hypothetical statistical test is performed [67]. This hypothetical test preserves the statistical properties of MT values at each individual value of τ , while destroying any causal relationships that may exist in the MT values across different time delay τ . In this test, the null hypothesis is assumed that the differences in MT values over consecutive time delays $\tau = \tau_0, 2\tau_0, 3\tau_0$ and $4\tau_0$ are not statistically significant, where τ_0 is the timescale of interaction between agents. Here, initially, a set of K independent observations is performed —each of which contains the trajectories of all agents of a given system— for both the model systems such as modified VM and LD model using the same parameter setting as specified in the main text. Now, assume that m and m' denote the indices of two distinct observations among the total observations K (where m and m' vary from 1 to K), and also assume that i and j represent two different agents within any observation. Then, the MT values from agent i to agent j are calculated for time delays $\tau = \tau_0, 2\tau_0, 3\tau_0$, and $4\tau_0$ as described below:

$$MT_{i \rightarrow j}(\tau) = \frac{1}{K} \sum_{m=1}^K MT_{i_m \rightarrow j_m}(\tau) .$$

Here, i_m and j_m represent the agents i and j observed in the observation m . The difference in MT values for two consecutive time delays τ_a and τ_b is defined as follows:

$$\Delta MT_{i \rightarrow j} := MT_{i \rightarrow j}(\tau_a) - MT_{i \rightarrow j}(\tau_b); \text{ where } \tau_a \in \{\tau_0, 2\tau_0, 3\tau_0\} \text{ and } \tau_b = \tau_a + \tau_0.$$

Subsequently, the surrogate MT values (MT^s) are quantified for time delays $\tau =$

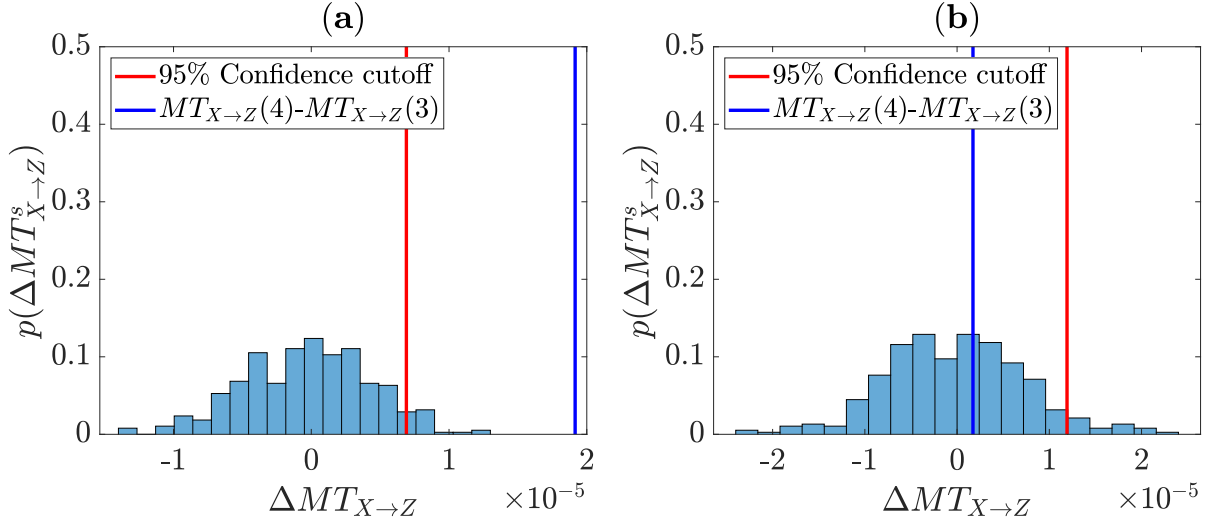


Figure S1. The statistical hypothetical test for the difference between $MT(3)$ and $MT(4)$ (corresponding to time delays $3\tau_0$ and $4\tau_0$, where $\tau_0 = 1$) from agent X to agent Z , as shown in Fig. 3.1(Ba), based on the trajectories simulated using the modified VM. **(a)** The distribution of difference in surrogate MT values $p(\Delta MT_{X \rightarrow Z}^s)$ at noise level $\eta = 0.5\pi$, and coupling strength $w = 0.2$. The red and blue vertical lines denote the locations of 95% confidence level, and difference in MT values $\Delta MT_{X \rightarrow Z}$, respectively. The difference in $MT_{X \rightarrow Z}$ values over consecutive time delays $\tau = 3\tau_0$ and $4\tau_0$ is considered as statistically significant. **(b)** The distribution of difference in surrogate MT values $p(\Delta MT_{X \rightarrow Z}^s)$ at $\eta = 0.7\pi$, and $w = 0.2$. The difference in $MT_{X \rightarrow Z}$ values over consecutive time delays $\tau = 3\tau_0$ and $4\tau_0$ cannot be said “statistically meaningful”.

$\tau_0, 2\tau_0, 3\tau_0$, and $4\tau_0$ as described below:

$$MT_{i \rightarrow j}^s(\tau) = \{MT_{i_m \rightarrow j_{m'}}(\tau) : m, m' \in \{1, 2, \dots, K\} \text{ and } m \neq m'\}$$

where i_m and $j_{m'}$ denote the agents i and j observed in two distinct observations m and m' , respectively. The difference in the MT^s values for two consecutive time delays τ_a and τ_b is defined as follows:

$$\Delta MT_{i \rightarrow j}^s := MT_{i \rightarrow j}^s(\tau_a) - MT_{i \rightarrow j}^s(\tau_b); \text{ where } \tau_a \in \{\tau_0, 2\tau_0, 3\tau_0\} \text{ and } \tau_b = \tau_a + \tau_0.$$

The null hypothesis has been tested for a false positive error rate $\alpha' = 0.05$ in the distribution of difference in surrogate MT values, i.e., $MT^s p(\Delta MT_{i \rightarrow j}^s)$. If the difference of MT value, i.e., $\Delta MT_{i \rightarrow j}$ falls within the domain of $1 - \alpha'$, the null hypothesis – the difference in the values of $MT(\tau)$ during consecutive time delays τ is statistically insignificant – is not considered to be discarded, and the difference in $MT(\tau)$ values over consecutive time delays τ observed in the same observation is not statistically significant. In contrast, if the difference $\Delta MT_{i \rightarrow j}$ falls outside the domain of $1 - \alpha'$, then it is considered statistically significant (see an example in Fig. S1). In the monotonicity metric map, as in Fig. 3.5 in the main text, if any of the differences in the values of $MT_{i \rightarrow j}$ over consecutive time delays τ used in computing the metric d_m falls outside the confidence interval $(1 - \alpha')$, the corresponding value of d_m is assigned as the statistically insignificant case and is highlighted by black color.

A.2 Estimation of the degree of monotonicity

In this study, the monotonicity metric map d_m (see the main text) has been evaluated by counting the number of writes required to transform the sequence of estimated MT (or TE) values of length n in a monotonically decreasing order. Here, to count the number of required writes, the cycle sort algorithm [95] is used, which directly places the values at their exact locations. This algorithm is the most straightforward with a computational complexity of $O(n^2)$, and ensures that the lowest number of required writes is presented to rearrange the original sequence of the MT values into a monotonically decreasing order. In this sorting approach, each element is written exactly once to its proper location if it is initially in the wrong place, and not written at all if it is already in the exact location. Thus, this sorting process guarantees the lowest number of writes required to sort a sequence of estimated MT values into a monotonically decreasing order. Using this method, for example, the monotonicity metric d_m is evaluated for the estimated MT values between a pair of agents during time delays $\tau = 1, 2, 3$, and 4 under different conditions of the modified VM varying noise levels $\eta \in [0.1\pi, 1.9\pi]$ and coupling strengths $w \in [0.1, 1.0]$. Figure S2 illustrates the case of the estimated MT values in the modified VM. Figure S2(a-d) demonstrates the cases in which the number of writes required N_r to transform the estimated MT values into monotonically decreasing order are $0, 2, 3,$

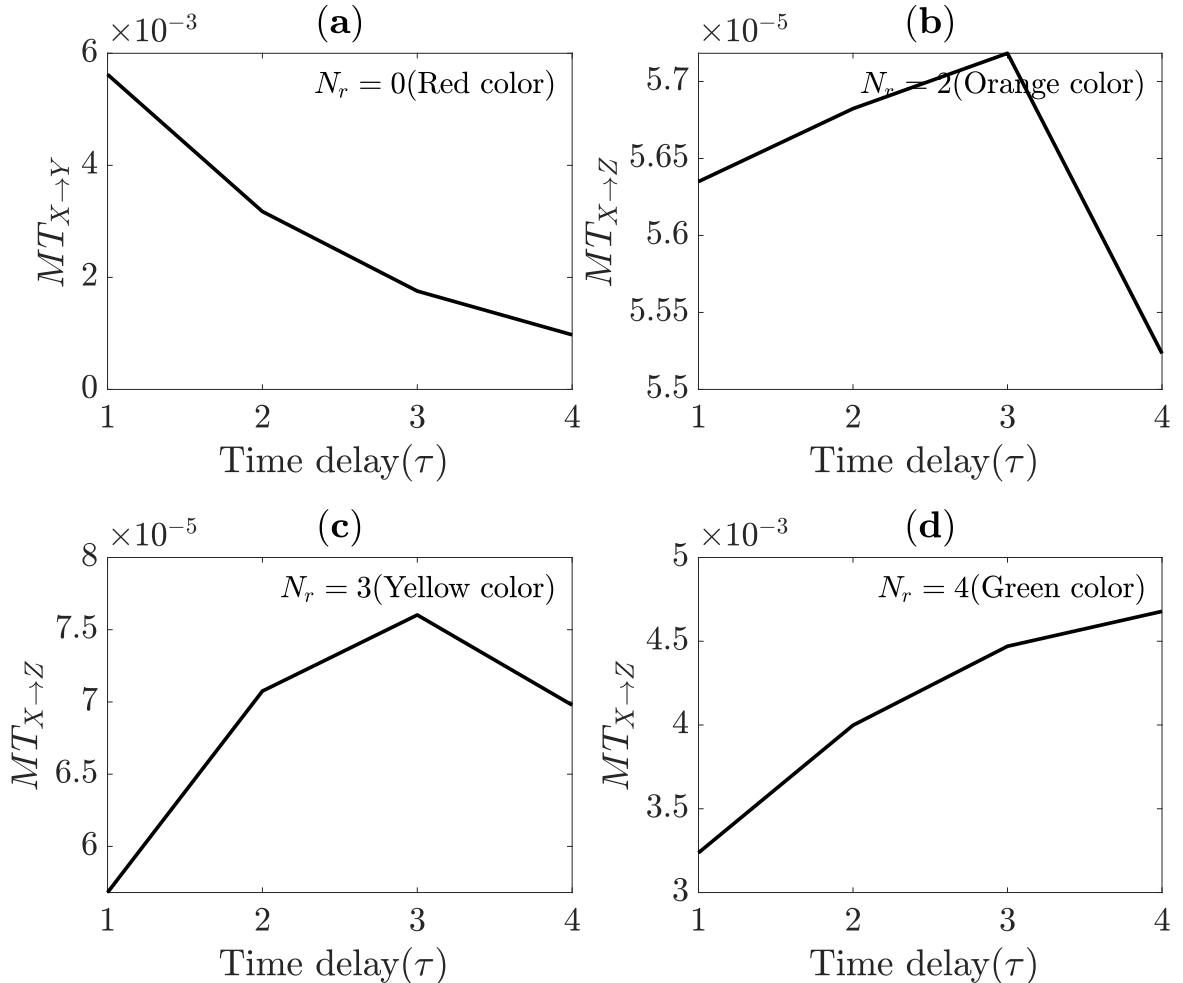


Figure S2. Examples of the sequence of time delay (τ), and the number of required writes N_r for the estimated MT values $MT(\tau)$, shown in Figs. 3.5 and S3, from the trajectories of modified VM. (a) $MT_{X \rightarrow Y}$ at $(\eta, w) = (0.9\pi, 0.3)$. a monotonic decreasing order over time delay τ , i.e., $MT(1) > MT(2) > MT(3) > MT(4)$, where no write is required to transform into a monotonic decreasing order (i.e., $N_r = 0$), and the monotonicity metric is $d_m = 1$. (b) $MT_{X \rightarrow Z}$ at $(\eta, w) = (1.5\pi, 0.3)$. a nonmonotonic decreasing order, i.e., $MT(3) > MT(2) > MT(1) > MT(4)$, where two writes are needed (i.e., $N_r = 2$), and $d_m = 0.5$. (c) $MT_{X \rightarrow Z}$ at $(\eta, w) = (0.9\pi, 0.3)$. a nonmonotonic decreasing order, i.e., $MT(3) > MT(2) > MT(4) > MT(1)$, where three writes are needed (i.e., $N_r = 3$), and $d_m = 0.25$. (d) $MT_{X \rightarrow Z}$ at $(\eta, w) = (0.5\pi, 0.4)$. a nonmonotonic decreasing order, i.e., $MT(4) > MT(3) > MT(2) > MT(1)$, where four writes are needed (i.e., $N_r = 4$), $d_m = 0$.

and 4, respectively.

A.3 Monotonicity metric d_m of $TE(\tau)$ and $MT(\tau)$ values estimated from the trajectories of agents simulated using modified VM under the unidirectional interaction illustrated in Fig. 3.1(Ba)

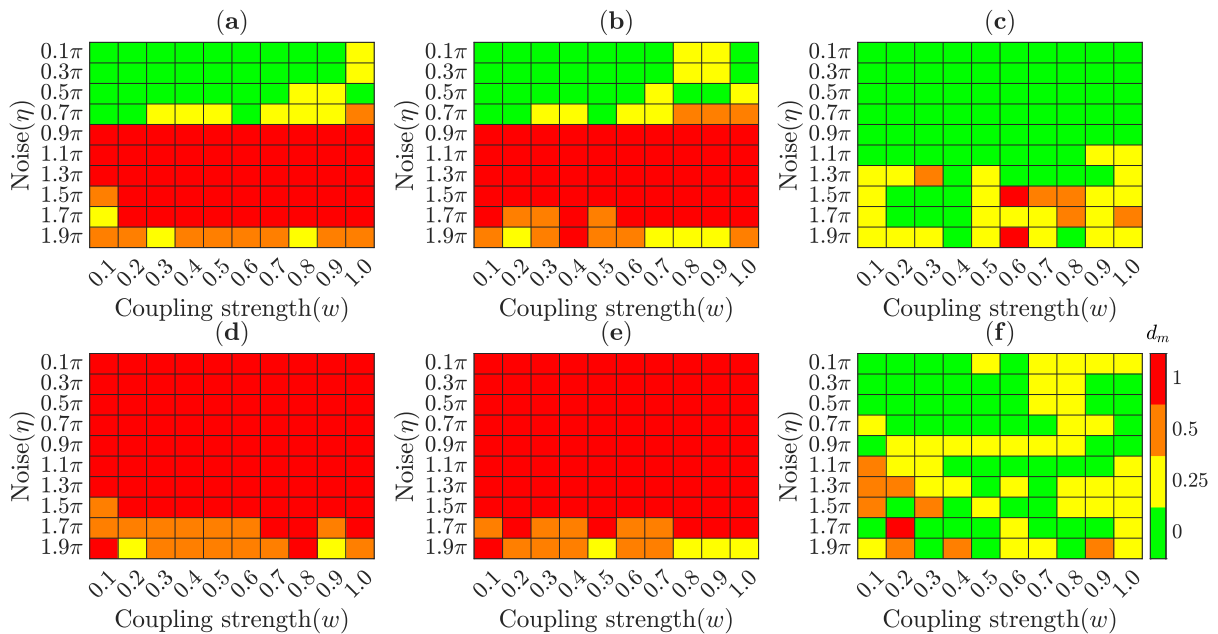


Figure S3. Monotonicity metric map (d_m) of TE and MT values estimated from the trajectories of agents using modified VM varying noise level η and coupling strength w (discussed in the main text Fig. 3.5). Here, each color represents the value of d_m ; The meaning of the colors—red (fully monotonic), orange, yellow, and green—are the same as shown in Fig. 3.5. The only difference from Fig. 3.5 is that the hypothetical test (Appendix A.1) is not employed to the differences of TE (or, MT) values over consecutive time delays $\tau = 1, 2, 3$, and 4. (a)-(c) $T_{X \rightarrow Y}$, $T_{Y \rightarrow Z}$ and $T_{X \rightarrow Z}$ represent TE for pairs $X-Y$, $Y-Z$ and $X-Z$, respectively. (d)-(f) $MT_{X \rightarrow Y}$, $MT_{Y \rightarrow Z}$ and $MT_{X \rightarrow Z}$ represent MT for pairs $X-Y$, $Y-Z$, and $X-Z$, respectively. The exceptions emerged at the higher noise levels—that is, the nonmonotonicity in the directly interacting pairs $X-Y$ and $Y-Z$, and monotonicity in the indirectly interacting pair $X-Z$ —are found to be statistically meaningless by statistical hypothetical test (c.f., Fig. 3.5).

Figure S3 illustrates the monotonic and nonmonotonic decreasing orders of TE (or, MT) values estimated at time delays $\tau = 1, 2, 3$, and 4 from the trajectories of agents shown in Fig. 1(Ba) simulated using the modified VM at different conditions of noise level η

and coupling strength w without applying the statistical hypothetical test for differences of TE (or, MT) values over consecutive time delays τ . In this analysis, the difference in TE values and in MT values over time delays $\tau = 3$ and $\tau = 4$ is found to be statistically insignificant at higher noise levels. The comparison of Fig. S3 and Fig. 3.5 highlights the specific conditions (η, w) at which the differences in TE values and in MT values over all consecutive time delay sequences are not statistically significant, indicated by the black color in Fig. 3.5.

A.4 Monotonicity metric d_m of $MT(\tau)$ values estimated from the trajectories of agents simulated using modified VM under the unidirectional interaction loop illustrated in Fig. 3.1(Bb)

In the unidirectional interaction loop shown in Fig. 3.1(Bb), X affects Y , Y affects Z , and Z affects X , with no effect through the opposite directions ($X \rightarrow Z$, $Z \rightarrow Y$, and $Y \rightarrow X$). The coupling strengths for direct interactions (solid arrows in Fig. 3.1(Bb)) are uniformly varied within the range [0.1,1.0], while the coupling strength is set to zero for the opposite directions (dashed arrows). Here, because of the intermediary roles of Y , X , and Z , indirect effects are expected in opposite directions $X \rightarrow Z$, $Z \rightarrow Y$, and $Y \rightarrow X$, respectively. The monotonically decreasing order in MT values over time delay τ is observed for direct interactions between agents under all conditions of the modified VM varying noise η and coupling strength w (Figs. S4(a)-(c)). In contrast, the nonmonotonic trends are found in MT values for the opposite directions, with some deviations—that is, monotonically decreasing order in MT values (red color) for opposite directions (dashed arrows in Fig. 3.1(Bb)) through which an indirect influence is anticipated—at low noise levels when coupling strength is weak, i.e., $w = 0.1$ and 0.2 (Figs. S4(d)-(f)).

The plausible reason for these deviations could be explained as follows: when the coupling strength is weak, the agents X , Y , and Z are more strongly influenced by the information of their past states, respectively, rather than the information passed from other agents through the edges that lead to them. For example, in estimating $MT_{X \rightarrow Z}$, the information of Z retained in the past states of X (e.g., see the dotted sequence in Fig. S6) may result

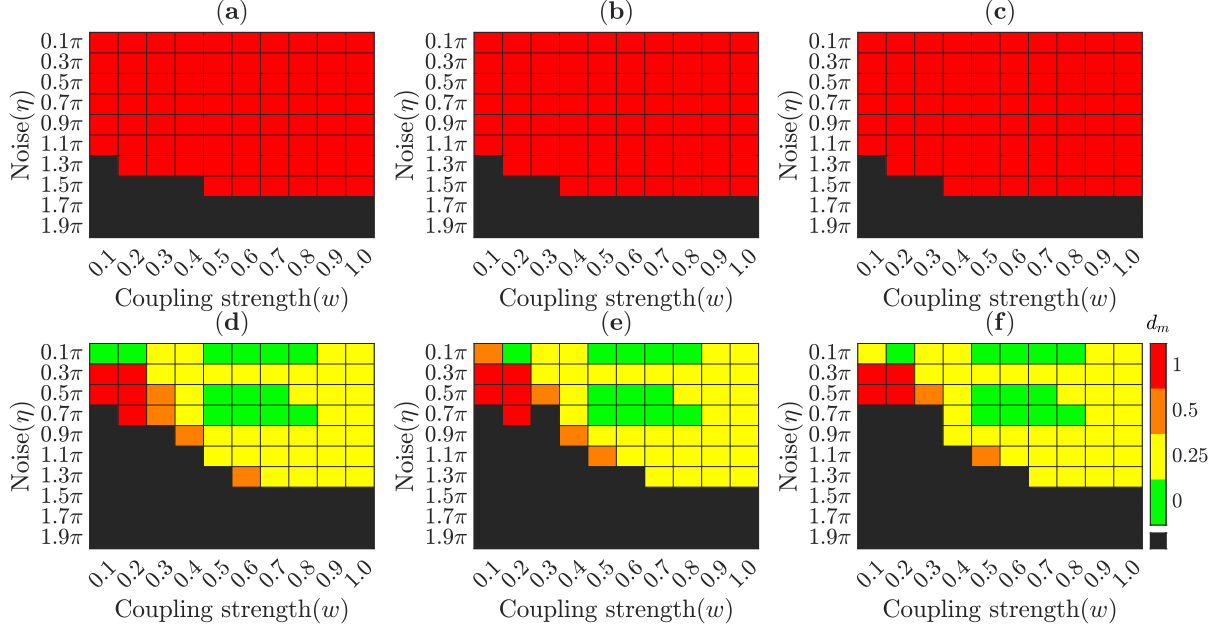


Figure S4. Monotonicity metric map d_m of the MT values between a pair of agents depicted in Fig. 3.1(Bb) at different conditions of the modified VM varying noise (η) and coupling strength (w). (a)-(c) $MT_{X \rightarrow Y}$, $MT_{Y \rightarrow Z}$, and $MT_{Z \rightarrow X}$ represent MT for direct interactions of X with Y , Y with Z and Z with X , respectively. (d)-(f) $MT_{Y \rightarrow X}$, $MT_{Z \rightarrow Y}$ and $MT_{X \rightarrow Z}$ represent MT for indirect interactions from Y to X through mediator Z , Z to Y through mediator X , and X to Z through mediator Y , respectively. MT exhibits a monotonically decreasing order over time delay τ for direct interactions, and nonmonotonic orders for indirect interactions, including some exceptions—that is, the monotonically decreasing order (red color)—at weak coupling strengths $w = 0.1$ and 0.2 .

in this monotonically decreasing order under the weak coupling strength, even though X does not directly affect Z . To ensure this conjecture, one can reduce more the self-effect on the future state of the targeted agent by conditioning on the more past state. Specifically, in estimating $MT_{X \rightarrow Z}$, information about the past state of Z at time $t + \tau - 2\tau_0$, i.e., $Z_{t+\tau-2\tau_0}$, can also be conditioned on. For example, the $MT_{X \rightarrow Z}$ with respect to time delay τ conditioning on the past state $Z_{t+\tau-2\tau_0}$ of Z is defined as follows:

$$\begin{aligned}
 CMT_{X \rightarrow Z|Z_{t+\tau-2\tau_0}}(\tau) &= H(Z_{t+\tau}|Z_{t+\tau-\tau_0}, Z_{t+\tau-2\tau_0}) - H(Z_{t+\tau}|Z_{t+\tau-\tau_0}, Z_{t+\tau-2\tau_0}, X_t) \\
 &= \sum_{Z_{t+\tau}, Z_{t+\tau-\tau_0}, Z_{t+\tau-2\tau_0} \in Z, X_t \in X} p(Z_{t+\tau}, Z_{t+\tau-\tau_0}, Z_{t+\tau-2\tau_0}, X_t) \\
 &\quad \log_2 \frac{p(Z_{t+\tau}, Z_{t+\tau-\tau_0}, Z_{t+\tau-2\tau_0}, X_t)p(Z_{t+\tau-\tau_0}, Z_{t+\tau-2\tau_0})}{p(Z_{t+\tau-\tau_0}, Z_{t+\tau-2\tau_0}, X_t)p(Z_{t+\tau}, Z_{t+\tau-\tau_0}, Z_{t+\tau-2\tau_0})}.
 \end{aligned}$$

Using this equation, it is observed that the CMT values between a pair of agents decrease monotonically over time delay τ when agents interact directly and non-monotonically

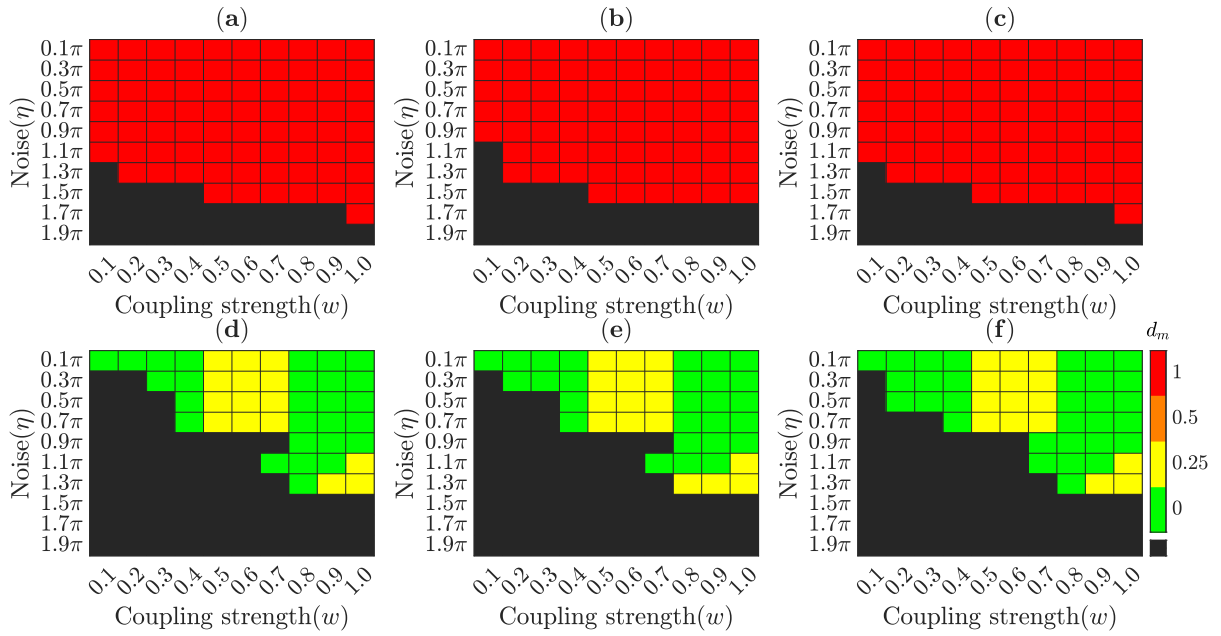


Figure S5. Monotonicity metric map d_m of the CMT values over time delay τ between a pair of agents, illustrated in Fig. 3.1(Bb), at different conditions of modified VM varying noise level η and coupling strength w . **(a)-(c)** $CMT_{X \rightarrow Y|Y_{t+\tau-2\tau_0}}$, $CMT_{Y \rightarrow Z|Z_{t+\tau-2\tau_0}}$ and $CMT_{Z \rightarrow X|X_{t+\tau-2\tau_0}}$ represent CMT for direct interactions of X with Y , Y with Z , and Z with X , respectively. **(d)-(f)** $CMT_{Y \rightarrow X|X_{t+\tau-2\tau_0}}$, $CMT_{Z \rightarrow Y|Y_{t+\tau-2\tau_0}}$ and $CMT_{X \rightarrow Z|Z_{t+\tau-2\tau_0}}$ represent CMT for indirect interactions from Y to X through mediator Z , Z to Y through mediator X , and X to Z through mediator Y , respectively. It is observed that CMT shows a monotonically decreasing order for direct interactions, and nonmonotonic orders for indirect interactions without any deviations, as expected.

decrease for the case of indirect interactions under all conditions of the modified VM, varying noise levels (η) and coupling strengths (w) (Fig. S5).

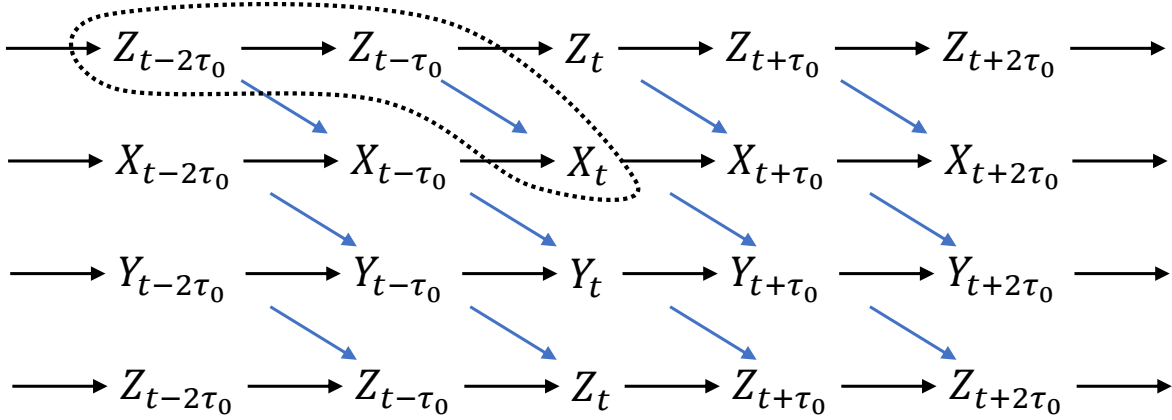


Figure S6. Demonstration of the causal relationship between agents in the unidirectional interaction loop shown in Fig. 3.1(Bb).

A.5 Monotonicity metric d_m of $MT(\tau)$ values estimated from the trajectories of agents simulated using modified VM under the bidirectional interaction illustrated in Fig. 3.1(Ab)

Figure S7 shows the behaviors of MT with respect to time delay τ for directly interacting pairs 1-2, 1-4 and 5-6 and indirectly interacting pairs 1-5, 2-6 and 3-5, estimated from the trajectories of agents, illustrated in Fig. 3.1(Ab), using the modified VM as a function of η and w . For indirectly interacting pairs, the nonmonotonic pattern is observed in MT values with increasing τ at all conditions of the modified VM (Figs. S7(d)-(f)). For directly interacting pairs, the monotonically decreasing order is also observed in MT values with increasing τ at almost all the conditions including some exceptions at the lowest noise levels η when coupling strength w (Figs. S7(a) and (c)).

However, it is noted that the monotonically decreasing order is observed in $MT_{1 \rightarrow 4}$ values with increasing τ even at the conditions of lowest noise levels η and coupling strength w is strong (Fig. S7(b)). The monotonic behavior of $MT_{1 \rightarrow 4}$ values at the lowest noise η with strong coupling strength w is likely observed because of agent 4 interacting with

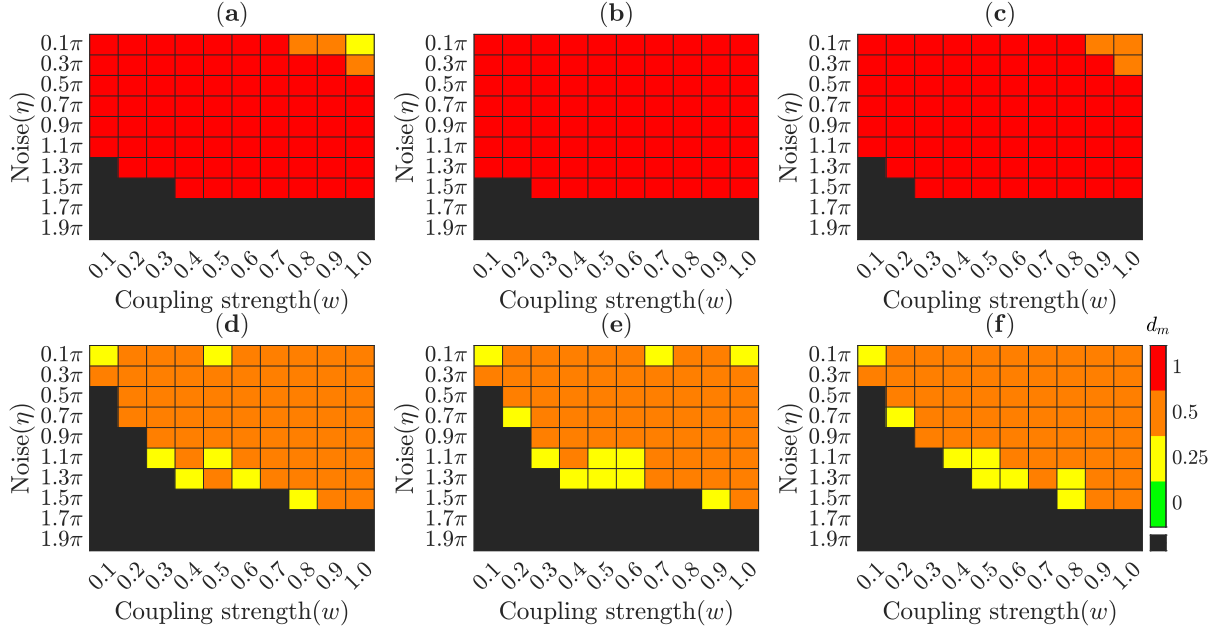


Figure S7. Monotonicity metric map d_m of the MT values with increasing τ for directly interacting pairs 1-2, 1-4 and 5-6, and indirectly interacting pairs 1-5, 2-6 and 3-5, shown in Fig. 3.1(Ab), in the modified VM varying η and w . (a)-(c) $MT_{1 \rightarrow 2}$, $MT_{1 \rightarrow 4}$ and $MT_{5 \rightarrow 6}$ represent MT of directly interacting pairs 1-2, 1-4 and 5-6, respectively. (d)-(f) $MT_{1 \rightarrow 5}$, $MT_{2 \rightarrow 6}$ and $MT_{3 \rightarrow 5}$ represent MT of indirectly interacting pairs 1-5, 2-6 and 3-5, respectively. It is observed that MT monotonically decreases with increasing τ for directly interacting pairs including some deviations in the pairs 1-2 and 5-6 at the lowest noise levels when coupling strength w is strong. However, MT shows the expected nonmonotonic trend with increasing τ for the case of indirectly interacting pairs 1-5, 2-6 and 3-5, respectively.

more agents than the others. These additional interactions may add more informational variability into the dynamics of agent 4 by mitigating its tendency to rely on the single agent, resulting in a consistent monotonically decreasing order over τ in $MT_{1 \rightarrow 4}$ values.

A.6 Monotonicity metric d_m of $MT(\tau)$ values estimated from the trajectories of agents simulated using LD model under the bidirectional interaction illustrated in Fig. 3.1(Ab)

Figure S8 shows the monotonic and nonmonotonic behaviors of TE and MT with respect to τ for directly interacting pairs 1-2 and 1-4, and indirectly interacting pair 1-5, depicted in Fig.3.1(Ab), estimated from the LD-simulated trajectories for $k_B T \in [0.2, 3.8]$ and

A.6 MONOTONICITY METRIC d_m OF MT(τ) VALUES ESTIMATED FROM THE TRAJECTORIES OF AGENTS SIMULATED USING LD MODEL UNDER THE BIDIRECTIONAL INTERACTION ILLUSTRATED IN FIG. 3.1(Ab&B3)

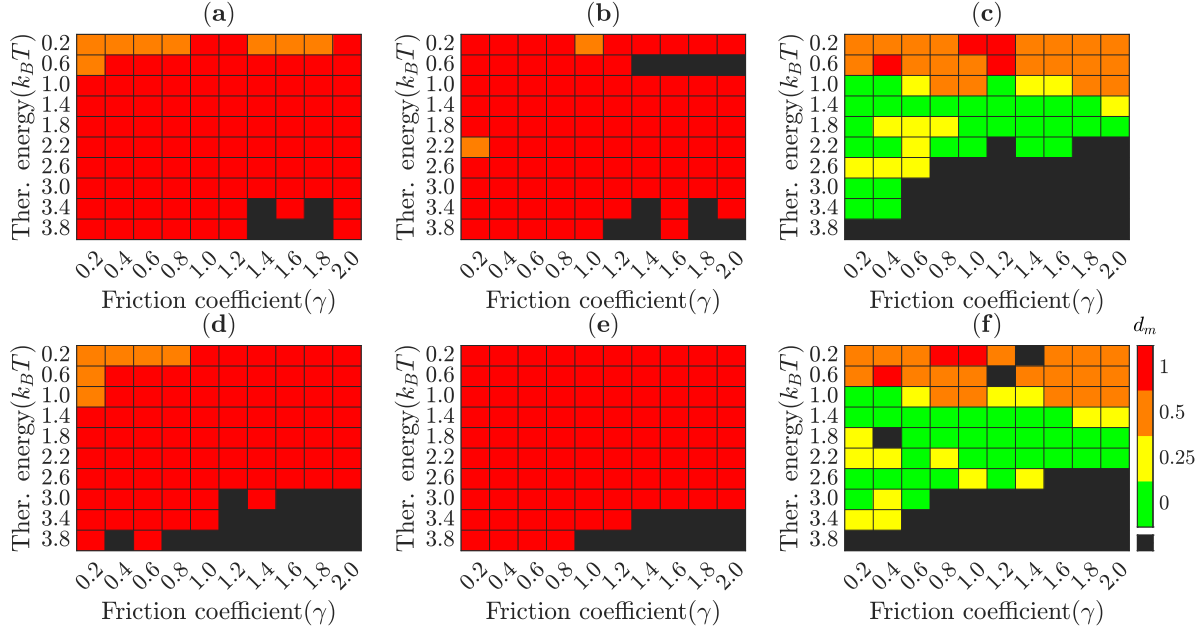


Figure S8. Monotonicity metric map d_m of the TE and MT values for a pair of agents, shown in Fig.1(Ab), at different conditions of the LD model varying thermal noise k_BT and friction coefficient γ . (a)-(b) present the monotonically decreasing behavior of $T_{1 \rightarrow 2}$ and $T_{1 \rightarrow 4}$ with increasing τ for directly interacting pairs 1-2 and 1-4 including some deviations, respectively. In contrast, (d)-(e) display the monotonically decreasing behavior of $MT_{1 \rightarrow 2}$ and $MT_{1 \rightarrow 4}$ with increasing τ including some exceptions only in the pair 1-2 at lower thermal noise levels k_BT , respectively. Figures (c) and (f) show the nonmonotonic trends of $T_{1 \rightarrow 5}$ and $MT_{1 \rightarrow 5}$ for indirectly interacting pair 1-5 including some deviations (that is, monotonically decreasing order (red color)) at lower thermal noise levels k_BT , respectively.

$\gamma \in [0.2, 2]$. The values of TE and MT show the expected monotonically decreasing order over time delay τ for all directly interacting pairs and nonmonotonic order for all indirectly interacting pairs, except some deviations at lower thermal noise levels k_BT . It is observed that, likewise the behavior of MT for the directly interacting pair 1-4 in the modified VM (see Fig. S7(b)), MT also exhibits a monotonically decreasing order with increasing τ for the pair 1-4 at all conditions of LD model varying k_BT and γ (Fig. S8(e)). In contrast, TE exhibit nonmonotonic order at $(k_BT, \gamma) = (0.2, 1.0)$ and $(k_BT, \gamma) = (2.2, 0.2)$ (Fig. S8(b)). Also for pair 1-2 (see Figs. S8(a) and (d)) and pair 1-5 (see Figs. S8(c) and (f)), TE exhibits more deviations than MT . Therefore, as the number of interacting agents increases, it is appeared that MT can capture the influence between a pair of agents more reliably than TE .